

MASTERARBEIT / MASTER'S THESIS

Titel der Masterarbeit / Title of the Master Thesis

”Incohesive fault rocks from the active Mur-Mürz-Fault in the Semmering-region (Austria) formed by a combination of rock pulverization, dilation, and excessive fluid flow?”

verfasst von / submitted by

Sophia Johanna Swaton, BSc

angestrebter akademischer Grad / in partial fulfilment of the requirements for the degree of
Master of Science (MSc)

Wien, 2023 / Vienna, 2023

Studienkennzahl lt. Studienblatt /
degree programme code as it appears on
the student record sheet:

UA 066 815

Studienrichtung lt. Studienblatt /
degree programme as it appears on
the student record sheet:

Masterstudium Erdwissenschaften

Betreut von / Supervisor:

Dr. Kurt Decker

Zusammenfassung

Die vorliegende Arbeit beschreibt spröde, inkohäsive Störungsgesteine der Mur-Mürz-Störung, die im Zuge der Bauarbeiten des Semmering-Basistunnels aufgeschlossen wurden. Karbonatische Störungsbreccien, Dilatationsbreccien und Kataklastite einer horizontalen Kernbohrung aus ca. 600m Tiefe wurden mit optischer Mikroskopie, Kathodenlumineszenz, EBSD und EDX analysiert. Die makroskopisch als karbonatische Störungsbreccien und Dilatationsbreccien mit Korngößen bis ca. 6cm klassifizierten Gesteine werden durch Karbonatlösung teilweise in Zellendolomite umgewandelt, die durch angulare Öffnungen (Zellen), von kalzitischen Veins (Septa) getrennt, charakterisiert sind. Entgegen der makroskopischen Aufnahme zeigen die mikroskopischen Untersuchungen, dass das Material keine undeformierten Bruchstücke der Ausgangsgesteine enthält, die größer als etwa 500µm sind.

Ausgangsgestein der Dilatations- und Störungsbreccien ist Dolomit, der in situ in 10-50µm große Partikel zertrümmert wurde. Die Partikel sind polyedrisch-angular und bilden Puzzle-ähnliche Gefüge, in denen (*i*) die Partikel weder zueinander versetzt noch rotiert sind, sodass Sedimentstrukturen erhalten sind („crackle fabric“), oder (*ii*) offene Zwischenräume zwischen bewegten und rotierten Partikeln entstanden sind („mosaique fabric“, „chaotic fabric“). Die Gefüge weisen eine extrem hohe Mikroporosität bis etwa 50% auf. Die Breccie wird von einem Netzwerk von Septa durchschlagen, die Partikel des zertrümmerten Dolomits enthalten, die durch gravitatives Absinken Geopetalaggregate ausbilden.

Cm-große Zellen, die durch die Lösung der Brekzienklasten entstehen, öffnen sich. Die Wände dieser Zellen werden von mehrphasigen euhedralen Kalzitzementen überwachsen. Teilweise enthalten die Zellen Kokarden-ähnliche, rotationssymmetrische, bis ca. 300µm große Strukturen, die aus einem Kern von µm-großen Dolomitpartikeln und in mehreren Phasen gewachsenen Kalzitsäumen und Ringen aus angelagerten Partikeln bestehen. Die Daten der Analysen dieser Arbeit belegen folgende Genese für die tektonischen Breccien: (*i*) Zertrümmerung des Dolomit-Protoliths in 10-50µm große Partikel in Gefüge, die von pulverisierten Gesteinen bekannt sind (*ii*) Dilatation des Gesteins verbunden mit Veining, Lösung und Abschlämmung der zertrümmerten Klasten und Zellenbildung (*iii*) mehrphasige kalzitische Zementation der Zellwände sowie Wachstum der Kokarden-ähnlichen Strukturen unter ausreichend

hohen Fließgeschwindigkeiten des durchströmenden Fluids, um Kokarden in Suspension zu halten. Der teilweise extrem hohe Gehalte an Kalzit, hohe Mikroporosität und das Auftreten von Kokarden-ähnlichen Kalzitkristallen belegen den großen Einfluss von Fluiden auf die Genese der Zellendolomite.

In den Breccien wurden keine Strukturen beobachtet, die signifikante Scherung und Kataklastik andeuten. Die Breccien sind jedoch Ausgangsgesteine für Kataklastite, die sich von den Breccien durch ihre foliierte Matrix, relativ hohe Gehalte an Schichtsilikaten und das Auftreten von kristallinen Gesteinsfragmenten unterscheiden. Dies belegt, dass die Bildung der Breccien einer späteren Störungsbewegung vorangeht.

Basierend auf den gemachten Beobachtungen ist offensichtlich, dass die zellulären Dolomite, die im Bereich des Semmerings als Sedimentgesteine wurden, keineswegs solche sind, sondern Störungsgesteine aus mehreren Deformationsereignissen. Daher ist die bisher als alpin-triassischer stratigraphischer Horizont behandelte Rauhwacke definitiv nicht als ein solcher anwendbar.

Abstract

The present work describes the brittle and incohesive fault rocks of the Mur-Mürz fault, which were exposed during the construction work of the Semmering Base Tunnel. Carbonate fault breccias, dilatation breccias, and cataclasites from a horizontal drilling hole at approximately 600m depth were analyzed using optical microscopy, cathodoluminescence, EBSD, and EDX.

The rocks, macroscopically classified as carbonate fault breccias and dilatation breccias with grain sizes of up to approximately 6 cm, have partially transformed into cellular dolomites due to carbonate dissolution. Cellular dolomites are characterized by angular openings (cells) separated by calcitic veins (septa). Contrary to the macroscopic image, microscopic investigations show that the material does not contain any undeformed fragments of the parent rock larger than approximately 500 μm .

The protolith of the dilatation and fault breccia is dolomite, which in situ fractured into particles ranging from 10-50 μm . The particles have a polyhedral-angular shape and form a puzzle-like fabric where (i) the particles are neither offset nor rotated, preserving sedimentary structures ("crackle fabric"), or (ii) open spaces were created between moving and rotating particles ("mosaique fabric," "chaotic fabric"). The structure exhibits an extremely high microporosity of up to approximately 50%. The breccia is penetrated by a network of septa containing particles of shattered dolomite, some of which form geopetal aggregates. Where clasts between the septa dissolve, cm-sized cells open. The walls of these cells are encrusted with multiphase euhedral calcite cement. The cell fillings contain cockade-like structures with rotational symmetry, measuring up to approximately 300 μm . These structures consist of a core of μm -sized dolomite particles, multiple phases of grown calcite seams, and rims of rock flour particles. The data generated in this study indicate the following genesis for the tectonic breccias: (i) fragmentation of the dolostone protolith into 10-50 μm particles, resembling pulverized rocks, (ii) dilation associated with veining, dissolution, and removal of particles from shattered clasts, leading to cell formation, and (iii) multiphase cementation of septa and cell walls, along with the formation of cockade-like structures under high fluid velocities that are sufficient to keep the cockades suspended.

The presence of extremely high amounts of calcite cement, high microporosity, and the occurrence of cockade-resembling structures are indicative of

the significant influence of fluids on the genesis of the studied rocks.

No structures indicative of significant shearing and cataclasis were observed in the breccias. However, the breccias serve as parent rocks for cataclasites, which differ from breccias in terms of their foliated matrix, relatively high content of layered silicates, and the presence of crystalline rock fragments. This demonstrates that the described formation of the breccia predates a later fault movement.

Based on the observations made, it is evident that the fabric of the occurring cellular dolomite in the Semmering area is no primary sedimentary fabric, but the result of multiple breakage events and leaching of comminuted host rock remains. Thus, the Rauhwanke, which until now has been dealt as an Alpine Triassic-stratigraphic horizon, is definitely not applicable as such.

Contents

Abstract	1
1 Introduction	7
1.1 Research history	7
1.2 Regional Geology	8
1.3 Tectonic evolution of the study area	11
1.4 Study site	13
2 Fault rocks	17
2.1 Cataclasite	17
2.2 Fault gouge	18
2.3 Fault breccia	19
2.4 Dilation breccia	19
2.5 Cockade breccia	22
2.6 Cellular dolomite	23
2.7 Pulverized rock, rock flour	25
2.8 Terminology used in this study	27
3 Methods	29
4 Results	31
4.1 SFK1m22-90	31
4.2 SFK1m23-10	44
4.3 SFK1m20-40A-E	50
4.4 SFK1m18-40A, B	67

4.5	SFK1m19-50A, B	73
4.6	SFK1m18-30	78
4.7	SFK1m17-80	82
4.8	SFK1m23-70A, B	89
4.9	SFK1m27-40A, B; SFK1m27-50A, B	96
5	Discussion	102
5.1	Grain size reduction via pore fluid pressure or mechanical processes? .	102
5.2	Did rock pulverization occur along the Grasberg-Schlagl-fault zone? .	105
5.3	Growth of calcite-dolomite-aggregates as initial cockade-cores?	107
5.4	The problem with „cellular dolomite“ in the area of the intermediate access Göstritz	110
5.5	Fault rocks of the Grasberg-Schlagl-fault zone	115
6	Conclusion	116
	References	118
	List of figures	127
A	Borelogs	i
B	Drillcores	xi

Chapter 1

Introduction

1.1 Research history

Earliest research activity began in the 1850's in course of the construction work of the first Semmering-tunnel. At first, geologists believed sedimentary rocks in the area (especially carbonates) to be of Devonian age (comp. Toula, 1876). In 1877, Toula recognized his mistake and identified the carbonates to be "supposedly" of Triassic age (Toula, 1877).

In the early 20th century, Termier established his nappe-theory when working in the Tauern window (Termier, 1904). Mohr, 1910, 1912 and Kober, 1912 did earliest research of the tectonic activity in the Semmering unit. Dispute, if the units were of penninic or austroalpine origin, carried on. Kober, 1923, 1925 parallelized the Semmering-unit with Carpathian units in eastern Europe and placed them into the Lower Austroalpine.

It took decades to resolve the complex tectonic setting in the area. Cornelius, 1936 published the 1:75000 "Mürzzuschlag" map that contains excellently detailed observations from his field work. When exploration for the second Semmering-tunnel started, Mohr, 1950, 1951 described intensely fractured rocks ("Trümmergesteine") but was not able to explain their exact significance.

By the end of the decade, Tollmann, 1959 discovered the similarities between the Semmering-sedimentary succession and the metamorphosed sedimentary rocks from the Radstädter-Tauern that constitute the Tauern window's frame at its east-

ern border. In 1963, he published his well-recognized synthesis on the Eastern alps, attempting to explain the complex folding- and tectonic history in the Lower Austroalpine (Tollmann, 1963).

1.2 Regional Geology

The rocks sampled for this thesis are tectonized sedimentary rocks, deriving from units of the “Lower Austroalpine” (LAA) in the Eastern alps. The LAA is a nappe stack that represents the base of the “Upper Austroalpine”. It consists of shallow- to deep-water shelf sediments, deposited on the south-eastern margin of the Penninic ocean in Permo-mesozoic times. During the lifetime of the ocean, the rocks repeatedly suffered intense metamorphic and structural overprint, with higher-grade metamorphism in the western part than in the eastern parts (Schuster, 2022).

The differentiation into oceanic Penninic and continent-derived LAA-sediments is complicated, often primary facies-boundaries are not clearly developed or are preserved in a bad state by Neogene nappe-stacking. Schuster, 2022 solely counts units without oceanic-sedimentary-imprint or signs of oceanic magmatism to the domain of the LAA. Furthermore, only nappes that were subducted during late cretaceous times (around 85 Ma) are counted to the LAA, but never reached higher-grade metamorphism conditions.

Today, following units are considered to be part the LAA: Semmering-Wechsel-unit, Wechsel-nappe as well as Mürz-Tachenberg-nappe at the margin of the Eastern alps (Equivalentents that frame the Tauern-window are the Radstadt-nappe system, Hippold-nappe and slivers on the window’s southern margin) and the easternmost parts being in the "Kriznanappe" in the western Carpathians (Häusler et al., 1993. Further in the west, the “Subsilvrettide-slices” frame the Unterengadiner-window (Oberhauser, 1980).

Several slivers of the LAA exist as outcrops on the westernmost border of the Eastern alps. Examples are the Err-Bernina-nappe system, the Walser-sliver, Schwarzhorn-sliver, and more. (Schuster, 2022, Tollmann, 1977). It is apparent that the LAA is mostly preserved as thin slivers, often in complex associations with Penninic- and UAA-units. Therefore, reconstructing the sub-units’ original relative

positions turns out to be complicated.

The following sedimentary succession is characteristic for the LAA (from footwall to hanging wall):

Crystalline basement The variscan event led to metamorphism of greenschist- to amphibolite-facies of the basement rocks:

- Pre-variscan-paragneisses of Ordovician age, i.e. the “Innsbrucker-Quarzphyllit”, “Radstädter-Quarzphyllit” (Rockenschaub, 2003)
- Carboniferous variscan intrusions, known as “Grobgneis” in the Semmering-Wechsel-nappe system (Schuster, 2022, Schuster and Stüwe, 2008)

Permomesozoic succession From the lowermost to the uppermost stratum, the succession reads as follows (comp. Piller et al., 2004)

- “Alpiner Verrucano”, a mixture of Permian siliciclastic conglomerates with layers of volcanic material, deposited in the dry, arid climates of the continent Pangea that experienced rifting in Permian times (Schuster et al., 2001, Schuster and Stüwe, 2008).

Today, this stratum appears as a greenish or purplish rock with distinct schistosity, its color derived from phengite and sericite on foliation planes. Verrucano is interlayered with breccias, porphyric material and arcotic sandstones. (Kellermann, 2008 after Tollmann, 1977)

- “Semmering Quarzite”, fine-grained, greenish quartzite of lowermost triassic age, sometimes interlayered with quartz-conglomerates. Its color is derived from detrital (?)retrograde overprinted chlorite (Kellermann, 2008 after Tollmann, 1977, Schuster, 2022). This unit can also be found in the Tauern-window with the local name “Lantschfeldquarzit” and in several other locations in Austria and Switzerland.
- Sedimentary “Rauhacke”, cellular dolomite with yellowish appearance of assumed sedimentary origin (Leine, 1969). It is debated to which extent “cellular

dolomite”, as this rock type is referred to in older literature, is indeed of sedimentary origin. In this rocktype, the more soluble components (e.g. gypsum) are leached out of the host rock by fluids. The residual less soluble material (calcite or dolomite) points out in the shape of planar “bridges” and angular pores remain between. There is no definite consensus on the genesis of this rock type.

- “Gutenstein-” and “Reifling”-formation. Dark, grey limestones with dolomite layers and sedimentary breccias in it. Formation occurred in a shallow water shelf environment during reoccurring anoxic events (Tollmann, 1977)
- Thinly-bedded limestones with radiolarite-layers and chert nodules. Echinoderm fossils prove Anisian-Ladinian age.
- “Wettersteindolomit”: Brightly appearing dolomite, deposited in the Ladinian in a shallow-water environment.
- “Keuperschiefer”: Shists in Keuper-facies with evaporites, e.g. bed-concordant gypsum. Locally, fossil-rich layers occur. The characteristic sandstone is not abundant, but there are excellently preserved outcrops: The type locality Lunz am See in lower Austria contains coal deposits, of up to 120m thickness with well-preserved fossil flora (Schuster and Stüwe, 2008).
- Norian ?“Bunter Keuper” consists of purplish and greenish sericite-schists with layers of quartzite, dolomite lenses and bands of cellular dolomite.
- “Rhätkeuper” contains characteristic, thinly-bedded shales ("Rhät-shales"), intercalated with massive bedded limestones in Keuper-facies and fossil-rich layers of uppermost Triassic age (Kellermann, 2008, Kristan-Tollmann and Tollmann, 1963).
- “Hauptdolomit” and “Kössen”-formation, limestone or dolostone.

Sedimentation stopped or is not yet recorded in the eastern part of the LAA. In the Tarntaler Mountains, a more western equivalent to the succession in the Semmering-Area, sedimentation stopped after deposition of breccias (“Tarntaler Brekzie”) and schists (Kristan-Tollmann and Tollmann, 1963).

The breccias show the opening of the penninic oceans in the lower Jurassic. Above this unit, chert deposits follow, that indicate deepening of the sedimentation realm. In the western parts of the LAA, sedimentation ends in the middle of the Cretaceous (Schuster, 2022).

Lithologies in the context of Paleogeography The Permian event initiated rifting, leading to the breakup of Pangea (Schuster and Stüwe, 2008).

Alpine Verrucano is the product of volcanic activity caused by rifting. In spreading zones, upwelling magma caused an anomalous heat flow in the upper part of the crust. Temperature-imprinted metamorphism followed.

The warm and arid climate during the Permomesozoic led to the deposition of thick layers of evaporites in deposited in sabkhas, an environment, suitable for the formation of sedimentary rauhwacken.

Depository material mainly was supplied from the hinterland of the Adriatic continent. In the middle Triassic, biogenic activity caused precipitation of pelagic limestones and dolostones (“Gutenstein-limestone”, “Reifling-formation”, “Wettersteindolomite”). In the middle Triassic, Tethys-regression led to deposition of evaporites and delta-sediments on top of the sedimentary succession (“Rhätkeuper”). In the uppermost Triassic, the sea transgressed again. Shallow-marine sedimentation in a neritic environment is dominant in this period (“Hauptdolomite”).

In the cause of the opening of the Penninic oceans in the Middle Jurassic, rift-related sedimentary breccias were deposited. This type of sedimentary breccias can be found everywhere where Jurassic rocks of the LAA are preserved, (Schmid et al., 2013). They reflect the onset of the tearing of the continent Pangea e.g. in the Radstädter Tauern, Tarntaler Mountains (Blattmann, 1937) or Western Tatrídes (Häusler et al., 1993).

1.3 Tectonic evolution of the study area

Nappe-stacking of the Upper-Austroalpine nappes began during the deposition of the latest sedimentary units in the middle Jurassic, with the Upper-Austro-Alpine unit Silvretta-Seckau nappe system as hanging wall. By the uppermost Cretaceous (ca. 85 Ma), ongoing northward-directed movement of the Adriatic plate occurred

and caused the subduction of Penninic ocean and the European plate (Handy et al., 2010).

Permomesozoic units experienced greenschist- to blueschist-facies-prograde metamorphism when the UAA-nappe-stack was thrust on top of the LAA and the Penninic units (ophiolites and overlying deep-sea sediments). The peak metamorphism occurred around 50-80 Ma in the east (Liu et al., 2001). After peak metamorphism, buoyancy of the less dense rocks caused obduction. The subsequent faulting was initiated by the NW-directed movement of the Adriatic plate towards the Helvetic unit, whereas vertical compression in the Eastern Alps was compensated through lateral eastward extension of the Alps into the Carpathian realm (Ratschbacher, Merle, Davy and Cobbold, 1991):

Tectonic evolution since the Oligocene Since the Oligocene, the nappe stacks' lateral extrusion into the East is traceable: A combination of N-S-directed shortening and gravitational collapse of the thickened crust is responsible (Ratschbacher, Merle, Davy and Cobbold, 1991). The units' boundaries are the dextral Periadriatic Lineament strike-slip-fault in the south, and the sinistral Salzach-Ennstal-Mariazell-Puchberg-fault (SEMP) in the north.

Nappe-stacking continued until the early Miocene. The LAA's crystalline basement experienced retrograde deformation, i.e. the phyllonites of the Katschbergzone, when lateral eastward extrusion of the eastern Alps set in (Schmid et al., 2013).

Several east-directed normal faults and linked pairs of dextral and sinistral strike-slip faults are branches of the SEMP and transfer portions of the units' eastern movement into the foreland (Ratschbacher, Frisch and Linzer, 1991, Decker et al., 1994, Linzer et al., 2002 hold a detailed review). These faults overall strike in NE direction. Important examples of these balancing faults are the sinistral Vienna-Basin-transform fault (VBF) and the corresponding dextral Lavanttal fault (LA) (Decker et al., 2005).

Faulting is active since at least the Lower Badenian/Karpatian, when syn-tectonic sedimentation in pull-apart- and subsidence basins in the Mur-Mürz-valley is recorded (lower Miocene, 17 Ma): The sinistral Mur-Mürz-fault (MU) is accountable. The Mur-Mürz-Vienna-Basin (MMVB) is opened between the Fohnsdorfbasin in the SW and the Viennese Basin in the NE, and extends over a length of

130km (Frisch et al., 2000). One interruption of seismicity from the uppermost Pannon to the lowermost pleistocene is known (Peresson and Decker, 1997).

1.4 Study site

The study site is located in a branch of the sinistral MU-fault in the SE of the Vienna basin. The sinistral Grasberg-Schlagl fault zone is kinematically linked to the MU-fault (Fig. 1.1).

Samples derive from drill cores of the intermediate access Göstritz of the Semmering-Base tunnel in Lower Austria. Drilling revealed carbonatic rocks of the Grasberg (limestone) and Otter-mountain (dolomite, rauhacken, breccias), belonging to the Semmering unit. The Grasberg-Schlagl fault zone led to faulting and partly karstification of the rocks. Bodies of mountain water are abundant (as the Hirschquelle, Palkaquelle in the valley of Schottwien as well as along the northern border of the Grasberg-unit: Auequellen and Duftquellen, in the area of the Sonnwendstein: Göstritzquelle) (SBT-Baulos, 2010).

Rarely, slivers of sheared mica-shists of the Semmering-crystalline are chipped into the carbonatic rocks (SBT-Baulos, 2010).

The permomesozoic in the area Göstritz is dominated by rocks in “Keuper” facies: Schists, sericite-phyllites and greenish-greyish layered quartzites, all partly heavily comminuted. Slivers of “Alpine Verrucano” are sheared into the Keuper-units: Supposedly, the primary rocks were sandstones and arcose rocks. Additionally, sulfatic rocks (gypsum and anhydrite) with thicknesses of several 10’s of meters are embedded within the main unit in the east of the Göstritz-river. Gypsum was mined in the south of Schottwien up until the 1960’s, the gypsum-containing layers are layer-concordant, or occur as diapirs. Only carbonatic rocks in the area are relevant as mountain water aquifers. Bodies of water are locally restricted because of sealing slivers of crystalline rocks bordering the carbonatic units.

The intermediate access is located on Map 105 “Neunkirchen”, nearside the mountain Semmering, and the tunnel crosses the Grasberg-Schlagl fault zone that is kinematically linked to the MU- fault (SBT-Baulos, 2010). The fault system divides the Tattermann-sliver that derives from the Semmering-crystalline unit from the middle-Triassic Wettersteindolomite (Kristan-Tollmann and Tollmann, 1963).

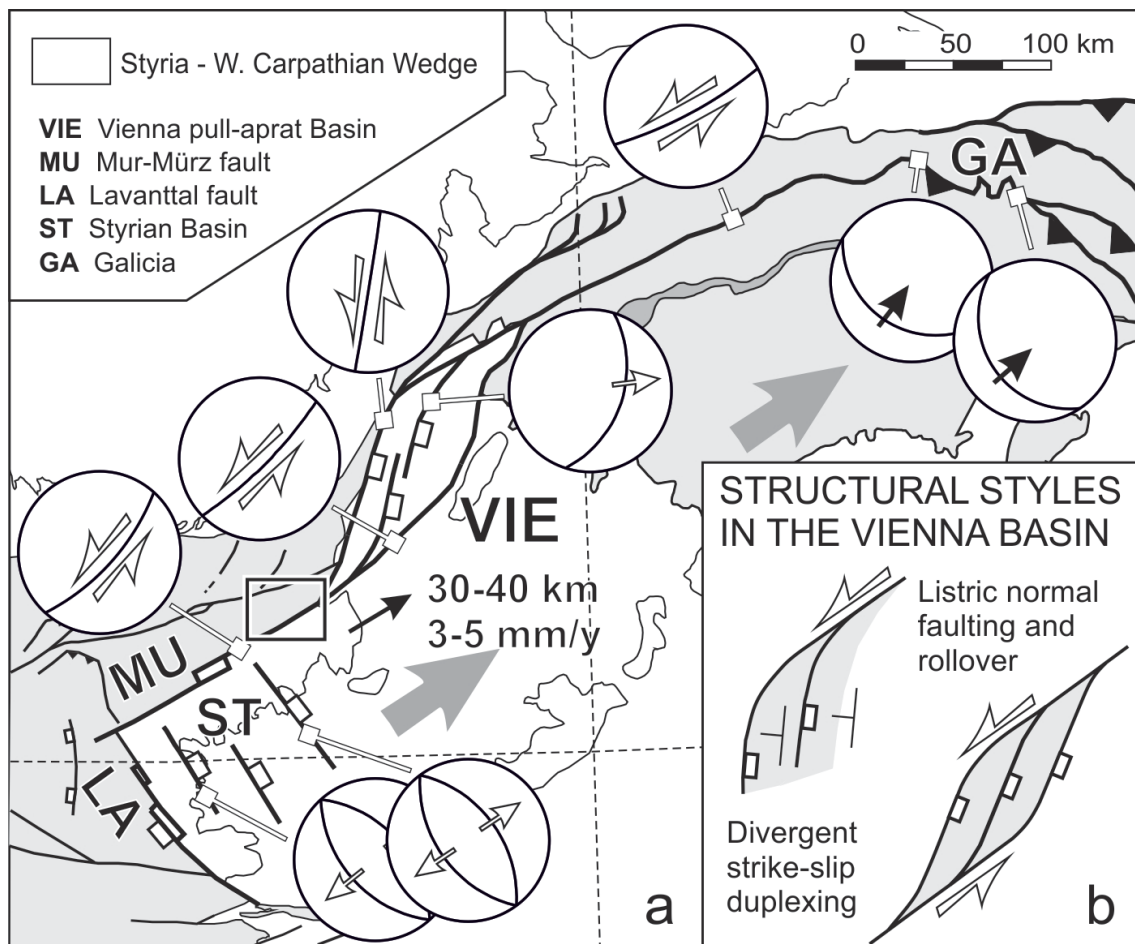


Figure 1.1 – A tectonic map of the study area. In the NE, one can see the Vienna Basin, in the SW Styrian basin, bordered by the Lavanttal fault and MU-fault. The rectangle marks the area of Göstritz, where the intermediate access Göstritz of the Semmering-tunnel is located. After Decker et al., 2005.

The main strike of the fault is NNE-SSW oriented. Slivers of rocks belonging to the Semmering-unit are sheared into the carbonatic Permomesozoic units. On the surface, as well as the subsurface and in drill cores, sericite-phyllites are reported. The phyllites are entirely tectonized, folded, and appear as cataclasites and fault gouges with remaining intact rock fragments of max. dm-size. The phyllites crop out at the eponymous Grasberg as deformed mica shists (SBT-Baulos, 2010).

The examined drill cores overall consist of cellular dolomite, dolomite and tectonic breccias that belong to the carbonates of the Otter-unit (in older literature "Otterstock"). Dolostone is bedded or solid, partly rich on limestone or contains dolomite-breccias. Partly, low-grade metamorphosis led to recrystallization of dolomite (pers. communication Robert Holzer). Via fragmented and karstified rocks, drainage of mountain waters takes place underground. The basement of the Otter-unit consists of permomesozoic rocks of the Semmering-unit, that represent the hanging-wall towards the underlying Wechsel-Unit (Herrmann et al., 1992). The boundary between the units is tectonically overprinted by strike-slip faulting (SBT-Baulos, 2010).

The borehole RKB-SFK1 is horizontal in NW direction and 120m long. The diameter of the cores is 10cm. The studied core interval is m14-32, the detailed core log is attached in appendix A.

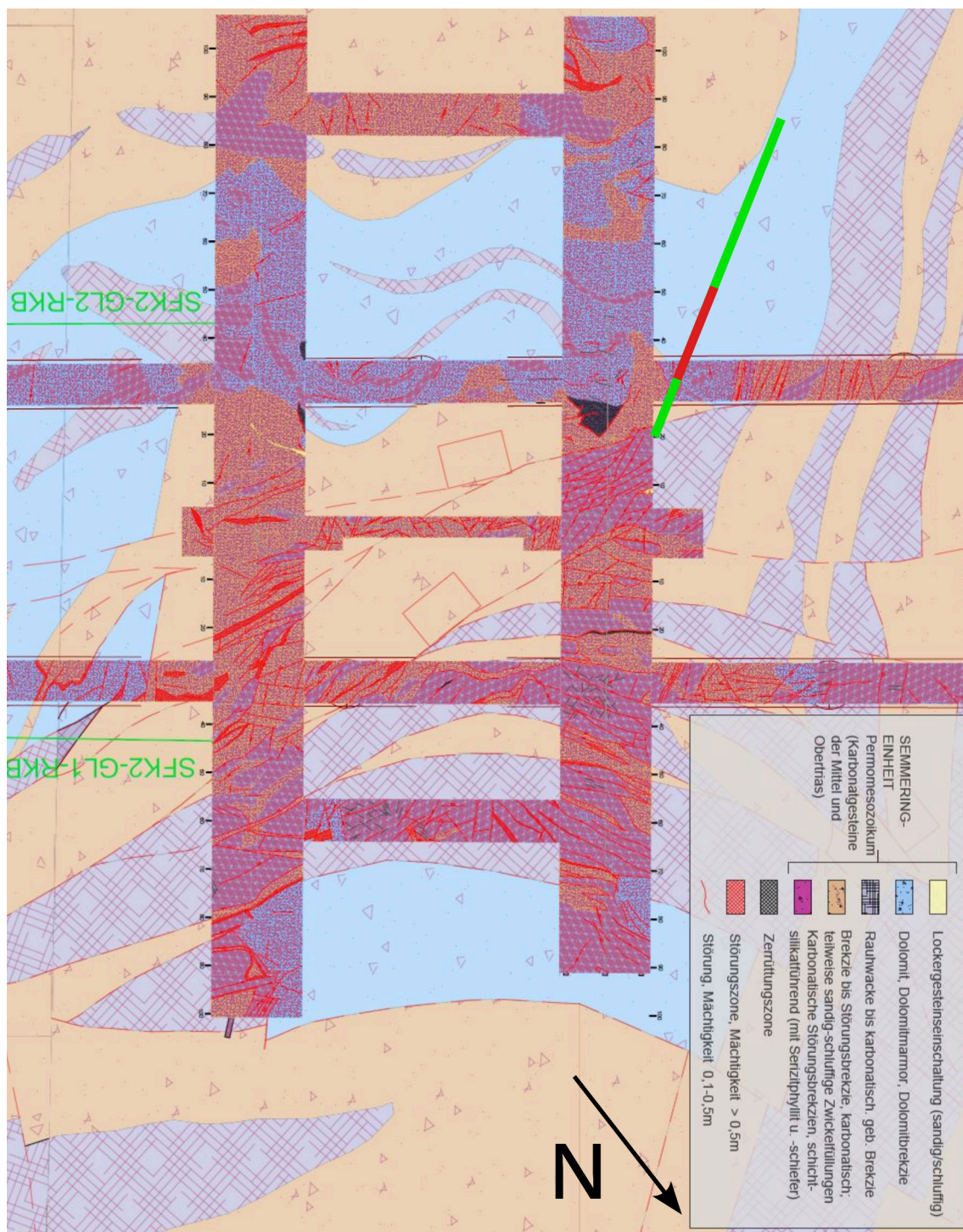


Figure 1.2 – Sample site. The samples derive from a drillcore in the course of an exploratory drilling. The green line marks the borehole of RKB2-SFK1, the red line the studied segment between meters 14-30. Modified figure from Robert Holzer, pers. communication.

Chapter 2

Fault rocks

Considering regional geology and deformation conditions, one can expect different types of fault rocks. Following rock types are presented as products of deformation:

2.1 Cataclasite

Cataclasites in a strict sense do have to meet several specific parameters. In the literature, the name “Cataclasite” often is used in a more general manner for any rocks with subrounded clasts and a fine-grained matrix. Not all fault rocks that suffered shearing, or shattering of its components into smaller fragments fulfil the needed preconditions. The author decides to stay close to Fossens’ definition (Fossen, 2016).

Cataclasites are the product of high-strain shear in the brittle deformation regime. They are restricted to zones near a main fault plane, and to a minor extent, to secondary fault planes. The process responsible for the genesis is called cataclasis: It involves grain size reduction through comminution or intragranular extension fracturing (Billi, 2010), shear fracturing or frictional sliding, and chipping/flaking or spalling. (Bauer et al., 2016, Fossen, 2016).

Intragranular extension fracturing leads to the complete destruction of the original grain’s shape. The shape of the resulting fragments is angular. With ongoing shear along the fault plane, fragmented clasts in the host rock suffer from rolling (rigid body rotation in agreement with the overall shearing direction) and chipping. Rotation of the rock fragments causes abrasion of flakes of the grain’s edges, causing

rounding of the grain (Bauer et al., 2016). Contrasting with the generated fragments of extensional fracturing, fragments affected by abrasion are magnitudes smaller in size.

The matrix is built up by abrasion material (Billi, 2010). Shear fracturing instead produces angular, elongated fragments. With ongoing cataclasis, the portion of fragment comminution gets dominated by shear deformation.

Less mature cataclasites show more heterogeneous grain size distribution with fine-grained matrix and abundant host rock fragments. Here, rock fabric is clast-supported. Generally, one can assume that with the degree of maturation, porosity and permeability decrease, and the smaller grain-size portion increases, practically generating impermeable rocks (Agosta et al., 2007, Bauer et al., 2016). Fluid-migration along transgranular fractures in the fault rock and eventually cementation leads to the sealing of the rock that therefore acts as a fluid barrier. Dissolution of minerals, especially in limestone, can reduce pore space too. The process of cataclasis seems to occur in depths between 5-10km, here, incohesive rocks can be modified into more cohesive rocks through recrystallization and the influence of fluids abundant in the crust. In higher crustal levels, shearing and brittle deformation of rocks often lead to the formation of less consolidated fault rock.

2.2 Fault gouge

Woodcock and Mort, 2008 use the term “fault gouge” for incohesive fault rocks, that can be destroyed when practising slight pressure. According to their introduced classification, fault gouge consists of less than 30% fragments $> 2\text{mm}$ in diameter and can be foliated. As in cataclasis, strain localizes along the fault plane in a narrow zone. In opposite to cataclasites, fault gouge forms in the uppermost crust under near-surface conditions (Fossen, 2016).

Fault gouge mainly consists of phyllosilicates that can be easily smeared with the fingers. The grinding of fragments causing grain size reduction enhances chemical reactions, that lead to the decomposition of mica and feldspar to clay minerals in the host rock. Water influx, higher pressure and higher temperature act as catalysts to these reactions (Sibson, 1977). As in cataclasites, the permeability in fault gouge is reduced by orders of magnitudes (Bauer et al., 2016).

2.3 Fault breccia

The most detailed insight on fault breccias is described in the Tarasewicz et al., 2005 paper. Fault breccias can be cohesive or incohesive, with fractures between clasts filled with cement or released fine-grained rock. They appear in the damage zone of faults in carbonatic or crystalline rocks (Woodcock and Mort, 2008).

Depending on the preservation state of mesoscopic textures of fault breccia, one can differentiate between fault breccia, fault gouge, foliated and non-foliated/random-fabric, and in deeper crustal levels between cataclasites or mylonites (Sibson, 1977) or after the revised classification of Woodcock and Mort, 2008, between foliated or non-foliated breccias as well as cataclasites (unfoliated) and mylonites (foliated). Both classifications have their weaknesses, as fault breccias and gouge after Sibson, 1977 can be foliated as well. Woodcock and Mort, 2008, improved the first model, but still differentiate between non-foliated cataclasites and foliated mylonites, whereas examples of (weakly) foliated cataclasites indeed do exist (Passchier and Trouw, 2005).

The author still chooses the descriptive classification after Woodcock and Mort, 2008, since it is useful for describing brittle fault rocks. Fault breccias in uppermost crustal levels contain more than 30% large clasts of $> 2\text{mm}$ in diameter and can be cohesive or incohesive. The authors introduce the terms crackle, mosaic and chaotic breccia, depending on the orientation and portion of clasts in matrix or cement.

2.4 Dilation breccia

Dilation breccias occur in releasing or dilational jogs in faults that create open space during a seismic event (Sibson, 1986a). Sibson, 1986a uses the term *implosion breccia*, referring to rapid collapse of rock into open fractures, therefore, implosion breccia is a genetic name. Tarasewicz et al., 2005 instead prefer the non-genetic name *dilation breccia*.

Features of dilation breccias are net-volume increase and heavy cementation of fragmented host rock, producing cohesive fault rock. Depending on the shape of grown cement single-crystals into fractures, it probably can be differentiated between fast opening of fractures (with vein-filling blocky cements) or slow opening of voids in

		non-foliated	foliated	
>30% large clasts >2 mm	75-100% large clasts (>2 mm)	fault breccia	crackle breccia	
	60-75% large clasts (>2 mm)		mosaic breccia	
	30-60% large clasts (>2 mm)		chaotic breccia	
<30% large clasts >2 mm	incohesive ¹		fault gouge	
	cohesive	glass or devitrified glass	pseudotachylyte	
		0-50% matrix (<0.1 mm)	protocataclasite	protomylonite
		50-90% matrix (<0.1 mm)	(meso)cataclasite	(meso)mylonite
		90-100% matrix (<0.1 mm)	ultracataclasite	ultramylonite
		pronounced grain growth		blastomylonite²

Figure 2.1 – The classification scheme of Woodcock and Mort, 2008. Despite the weaknesses concerning the differentiation between mylonite and cataclasite, the classification allows great differentiation possibilities of fault breccias.

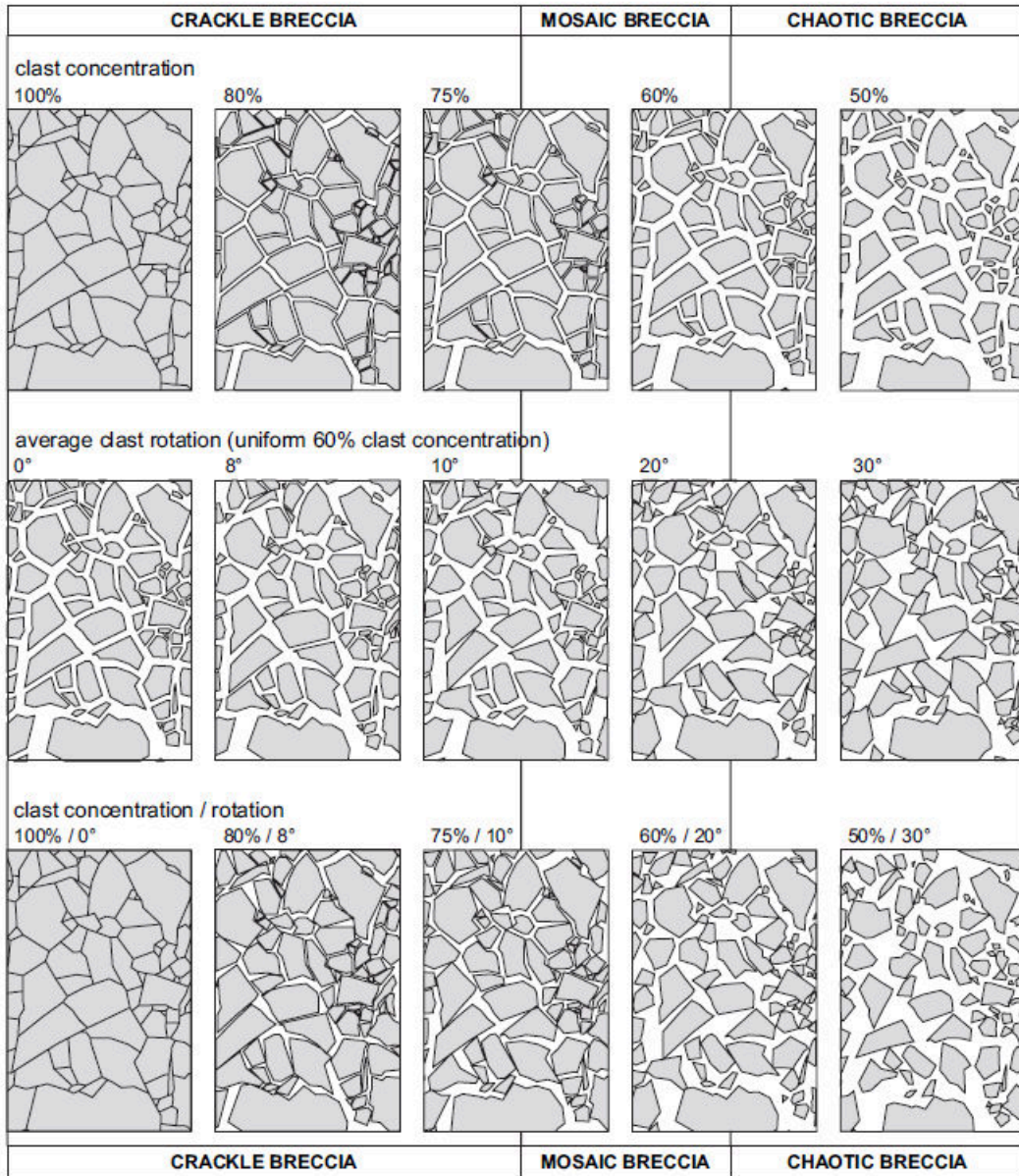


Figure 2.2 – The classification of fault breccias of Mort and Woodcock, 2008. From left to right: Increase of the rocks' net volume due to dilation of the rock. From top to bottom: Increase of the clasts' rotation produces a chaotic fabric of the rock.

the host rock (fibrous or acicular developed crystals) (Sibson, 1986*b*). Vein-cement can consist of quartz, calcite, dolomite, siderite or ore-minerals (Tarasewicz et al., 2005, comp. Masoch et al., 2019, this study).

2.5 Cockade breccia

In transtensional or dilational faults, "cockade breccias," "cockade ores," or "cockade textures" are known (Berger and Herwegh, 2019, see Frenzel and Woodcock, 2014 for further reading). Cockades consist of a core composed of wallrock clasts and are surrounded by cement rings of different growth generations, forming approximately concentric aggregates ranging from cm to dm in size. (Frenzel and Woodcock, 2014, Masoch et al., 2019). These breccias can be used for the potential reconstruction of syntectonic mineralization sequences of veins in fault systems (Genna et al., 1996). The formation temperatures of these structures are estimated to be between 50°C - 350°C in near-surface hydrothermal systems. The mineralogy of these aggregates varies, with cement rings consisting of quartz, galena, calcite, or haematite (Frenzel and Woodcock, 2014).

Several mechanisms for the formation of cockade breccias have been proposed, with the main focus on two mechanisms considered to be the most likely:

1. Suspension in Fluid: Clasts of wall rock are suspended in fluid. The suspension must either be
 - 1.1. highly viscous (Dill and Weber, 2010) or
 - 1.2. have low viscosity but high flow energies to keep clasts suspended in the observed size ranges (Jobson et al., 1994, Eichhubl and Boles, 2000).
2. Repeated rotation and accretion of clasts ("Rotation-accretion-hypothesis"): A partially cemented breccia is fractured between the sutures of individual clasts. Layers of new cement grow around the clast when it is in suspension (Genna et al., 1996), caused by "fluid jets" in a seismic rupture (Berger and Herwegh, 2019). Indicators for gravitational settling in interseismic periods in the form of geopetal aggregates exist.

Frenzel and Woodcock, 2014 note that the term "cockade" is often misused in the literature, where aggregates of wall rock clasts with only *one* cement ring are also referred to as "cockades". While I support the idea that the precise use of terminology is essential for comprehensible work, I want to discuss in the discussion part of this thesis, if in certain cases this definition could not be used more generally.

2.6 Cellular dolomite

In older German literature, this type of rock is known as "Rauhwanke" and is mainly cited as a sedimentary rock. Cellular dolomite is a common rock type of the Alpine Triassic, believed to be deposited in sabkhas (Brückner, 1941, and occurs in the study area (SBT-Baulos, 2010).

This fault rock type is characterized by its angular "cells". Yellowish-ochre coloured bridges ("septum") delimit these pores that can be encrusted with crystals with euhedral faces (Fig. 2.3). In theory, sedimentary Rauhwancken therefore are a product of weathering: differently shaped evaporitic fragments of gypsum or anhydrite are leached out of the rock by fluids and create the characteristic openings in a matrix of dolomite.

In the Semmering area, rocks of similar appearance but unfitting chemistry can be found: Bridges between pores are made of calcite, residual grains in pores consist of dolomite. These rocks are fault rocks, as they occur in intensely tectonized areas along fault planes and even cross sedimentary horizons (Kellermann, 2008). Leine, 1969, already recognized that angular pores, completely free of evaporites, weather out of rocks and questions the sedimentary origin of Rauhwancken in the Swiss Alps critically.

In this work, the author does not exclude the possibility of a sedimentary origin of Rauhwancken, but states, that the sampled rocks of this study indeed are of tectonic origin. The genesis of this rock type will be traced microscopically.

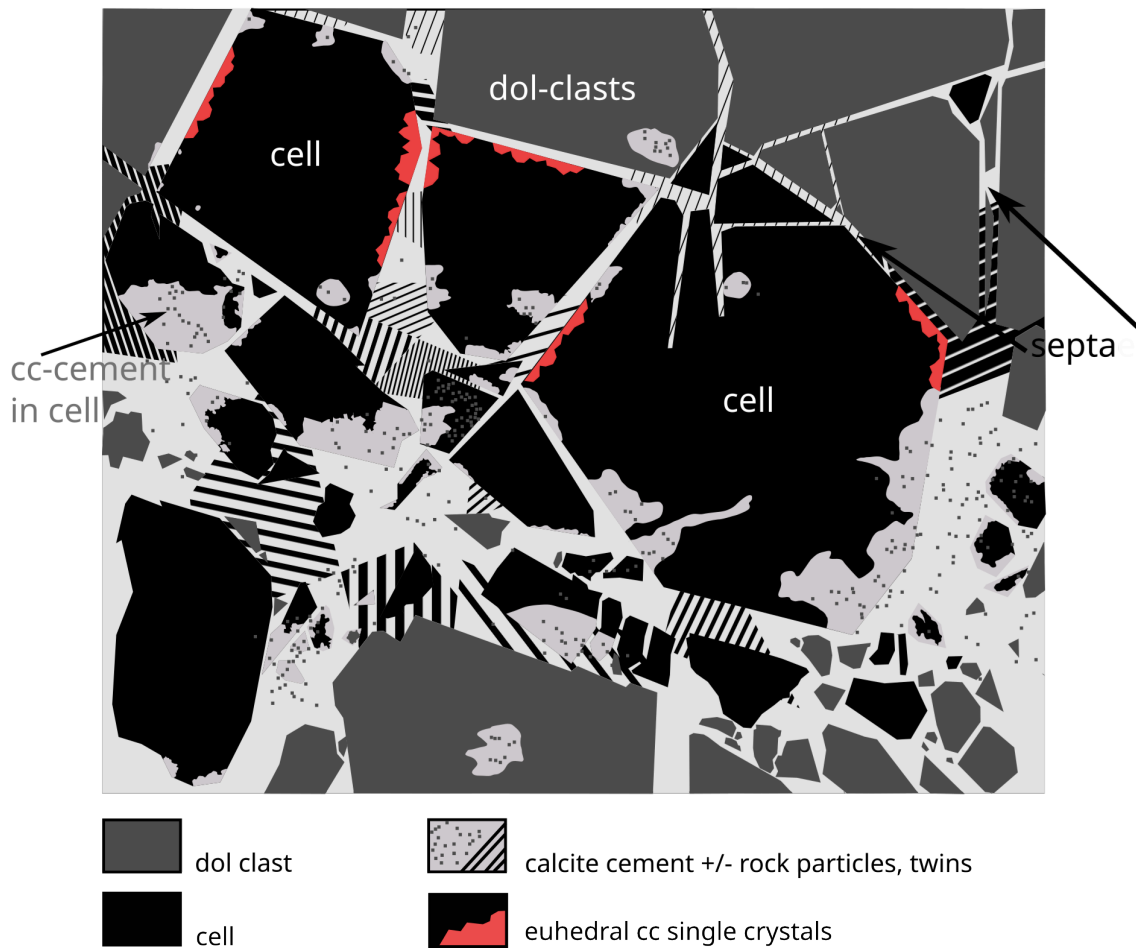


Figure 2.3 – Schematic scetch of a cellular dolomite. Dol clasts in grey, cells in black. The septum consist of cc-vein cement that is intensily twinned. The red colour indicates euhedral cc-crystals that encrust the cells' walls.

2.7 Pulverized rock, rock flour

Pulverized rocks are incohesive, heavily fragmented rocks that can be destroyed with the help of a knife or even by hand. The host rock is crumbled into μm -sized, polyhedral fragments along intergranular fractures. No or merely little shearing contributes to disintegration of the rock, so sedimentary features or magmatic-texture features survive (Dor et al., 2006). Products of chemical alteration often are lacking and therefore cannot serve as an explanation for the intense comminution of the rock volume (Rockwell et al., 2009, Doan and d'Hour, 2012).

In three scenarios, enough energy for high differential stresses; essential for breaking great rock volumes into micron- to sub-micron sized particles can be provided. The processes are:

- "Dynamic unloading" (Brune, 2001)
- "Rock burst" (Gibowicz, 2009)
- "Impact crater shattering" (Key and Schultz, 2011)

The last process will not be further discussed in this chapter, since no indicators for an impact event are known in the study area. "Dynamic unloading" is the preferred term in the seismotectonic community, "rockburst" is the more generic term, preferred in literature concerning topics of mining. The products of both processes are "pulverized rock" or "rock flour" (Dor et al., 2001, Gibowicz, 2009). This heavily fragmented rock type is mainly found in major strike-slip zones.

The arguably best examined and well known area where pulverized rock occurs is the San-Andreas fault, California (Dor et al., 2006, 2008, Doan and Gary, 2009, Reches and Dewers, 2005, Rempe et al., 2013). Other examples are the Arima-Takatsuki Tectonic Line, Japan (Mitchell et al., 2011) and possibly the thrust-Venere-fault zone, Italy (Agosta and Aydin, 2006, Agosta et al., 2007). The width of the zone consisting of "rock flour" (which will be used as the more unspecific term) can range between only few centimetres (Dagbreek fault in the Matjhabeng Mine, South Africa; Dor et al., 2001, Gibowicz, 2009, Bosman fault in South Africa; Reches and Dewers, 2005), and several hundreds of meters (Mojave section of the San-Andreas fault; Dor et al., 2006, Doan and Gary, 2009).

The distribution of the heavily fragmented fault rock along a fault is asymmetric: for example, along the San-Andreas fault 70% of the rock-flour-outcrops exist on the NE-side of the slip zone (Rempe et al., 2013). It appears that the mechanically “stiffer” rocks like granite or dolostone can accommodate less strain before breakage comparing to rheologically weaker limestones in the Mojave Section of the San Andreas fault (Doan and d’Hour, 2012 after Dor et al., 2006, Mitchell et al., 2011).

Although single earthquakes are able to produce volumes of “pulverized” rock (i.e. the 1997 earthquake that created a new fault in the Hartebeestfontein mine, Klerksdorp, see Dor et al., 2001) reoccurring earthquakes seem to be required to produce tens- to hundreds of m-wide zones of pulverized rock. Today there is overall consensus that coseismic shock waves with strain rates of at least 150/s during supershear seismic events are just feasible to create the wide zones of comminuted rock known in pre-damaged rock (Doan and Gary, 2009, Aben et al., 2016). Strain rates of $> 250/s$ are required to shatter intact rock (Yuan et al., 2011, Doan and d’Hour, 2012). The great volumes of pulverized rocks in damage zones can therefore be explained as product of many successive earthquakes (Doan and d’Hour, 2012). Interestingly, no noteworthy transition phase between single fracturing of rocks and fully developed pulverized rock could be reproduced in experiments (Doan and d’Hour, 2012).

Doan and Gary, 2009 suspect the process of “dynamic loading” for being responsible for producing evenly distributed fractures in damage zone rocks far away from fault cores. Dynamic loading prevents strain from being localized along a single or major fracture, instead, many fine fractures develop: large amounts of strain energy released during supershear ruptures cannot be accommodated by the rock volume at once. To this day, estimates of the dimensions of energy dissipation in rocks are imprecise (compare Rockwell et al., 2009 and Wilson et al., 2005).

2.8 Terminology used in this study

In this study, the term "cellular dolomite" is preferred over "Rauhacken". Existing literature can be confusing and often terminology is not used consistently. To avoid confusion or misunderstanding in the reader, these important terms will be defined as follows:

Protolith Fragmented dolostone will be referred to as protolith. Usually, dolostone is brecciated to angular clasts approx. $> 500\mu\text{m}$ in size. Shattered dolostone-protolith serves as *source rock* for rock flour during cc-crystal-growth. In the study area, the prevalent type of dolomite is "Wetterstein"-dolostone (comp. Chapter 1).

Source rock Other source rocks than dolostone can be crystalline magmatic- and metamorphic rocks where heavy minerals (accessories), quartz-grains and phyllosilicates derive from.

Fault rock Fault rocks are any types of rock that suffered from brittle or plastic deformation.

Fault breccia Fault breccias are fault rocks that consist of clasts, either angular or subrounded/rounded, and variable portions of matrix. Breccias in this study can be matrix- or clast-supported.

Cellular dolomite This type of fault rock has a distinctive highly-porous appearance. The name derives from protruding planar walls and dolomite clasts between that when dissolved, leave angular pores, i. e. "cells" behind.

Clast, fragment Here, clast will be used for any fragment in breccias approx. $> 100\mu\text{m}$ size.

Septum, vein Protruding calcite veins in cellular dolomites penetrate the rock volume. In comparison to the fragmented dolomite clasts, the veins are less soluble and often better preserved.

Cell Is the material that constitutes the clasts of dilation breccia not preserved, a cell is left behind.

Pore Pores will be referred to any openings in a lithic fragment (carbonatic or crystalline) that are not enclosed by cements.

Shattering The process leading to the intense fragmentation/disintegration of protolith, especially dolomite in this study. This term will be used, due to it being more general and a non-genetic term.

Rock flour Rock flour is the generic term for intensely shattered rock. Rock flour consists of particles with average sizes between 10 - 50 μm that serve as nuclei for calcite-crystal growth. In this study, if not stated differently, "rock flour" unexceptionally relates to shattered dolomite. Synonymously, "shattered dol"/"shattered rock" will be used.

Particle Shattered dolomite is broken down to fragments of approx. 10-50 μm in size. For easier readability and to distinguish them from clasts of any kind (lithic fragments, recemented carbonatic clasts), these fragments will be strictly referred to as "particles", after Berger and Herwegh, 2019.

Recemented carbonatic-rock In this study, dolomitic rock flour can be densely cemented by calcite and dm-sized calcite-dolomite-aggregates grow. This rock type is interpreted as a type of fault rock or product of faulting activity with differing portions of dol rock flour and calcite cement. Partly, less than 10% of dolomitic rock flour particles constitute this rock type. Fragments of this rock type will be referred to as "carbonatic clasts".

Chapter 3

Methods

In the course of construction work of the Semmering-Base-tunnel, Lower Austria/Styria, 18m of drillcores deriving from exploratory drilling were macroscopically examined for following characteristics: color, proportion, and grain size of clasts in brecciated sections and identification of the undeformed protolith, if determinable.

Additionally, kinematic indicators and the extent of rock fragmentation were recorded in a drill core profile.

Optical microscopy 26 representative samples were selected and processed into thin sections at the Thin Section Preparation Laboratory of the University of Vienna, Josef-Holaubek Platz 2, 1090 Vienna, UZA2. In preparation for cutting, the pieces had to be soaked with resin due to their overall incohesiveness. Blue epoxy-resin was used to mark open pore space.

The polished thin sections were examined using the Leica DM4500P transmitted light microscope at magnifications 2.5x, 4x, 10x, and 20x, pictures were captured with the corresponding Leica DMC4500 camera. Due to small grain sizes, the clear differentiation between calcite and dolomite was not possible in all cases.

Polished thin sections were coated with the Leica-EM-SCD-500 carbon coater (using a double carbon thread) for examination under the scanning electron microscope and cathodoluminescence-optical microscope.

Cathodoluminescence Cathodoluminescence provides an opportunity to uncover differences in material chemistry that are too small to be solvable through techniques

like EBSD-mapping. To make calcite (and occasionally dolomite) growth rims observable, the coated thin sections were investigated with the LUMIC HC5-LM hot-cathodoluminescence microscope at the Department of Lithospheric Research, University of Vienna. CL-Images were captured using a Kappa DX40C digital system and Kappa CameraControl software.

The color-contributing trace elements in carbonate-petrography predominantly are Mn^{2+} as well as rare earth metals (Richter et al., 2003). Depending on the concentration of Fe^{2+} - and Mn^{2+} -ions in the sample, the cations act as a luminescence contributor or inhibitor (Boggs and Kirsinsley, 2009).

This method can reveal cement-growth-sequences and aids in distinguishing different deformation as well as cementation events (Richter et al., 2003).

EBSD- and EDX-analysis Back-scattered electron (BSE) images were obtained through scanning electron microscopy (SEM) using the FEI-Inspect-S50 instrument. Rock fragments that were too small for high resolution using optical methods could be visualized, and calcite could be clearly differentiated from dolomite. Semi-qualitative examination of the mineralogy of components was performed using energy-dispersive X-ray spectroscopy (EDX). Image acquisition was done using the xT Microscope Server software, while EDX analysis was conducted using the EDAX Genesis software. The working distance was 10mm with an applied accelerating voltage of 10-15kV.

Estimates on cement-portions In an attempt to estimate the approximate portion of dol-rock flour encrusted by cc-cement in recemented carbonatic-rocks, Shvetsov, 1954's scheme was used.

Chapter 4

Results

4.1 SFK1m22-90

Between a net of strikingly planar septae of cc, dol host rock is dissolved and cells open. Partly, angular clasts of dol-protolith are preserved with sizes ranging from 1mm - 10mm (Fig. 4.1). Euhedral, mm-sized cc-crystals encrust the cells' walls (Fig. 2.3). The hand specimen is cohesive, but the leftover material in the cells easily gets dissolved when the rock is in contact with water. The rock can be referred to as highly porous dilation breccia/cellular dolomite, but easily mistaken for sedimentary "Rauhwacke" (Fig. 4.1). The sedimentary nature of the rock can be definitely ruled out. The mineralogy does not fit with the typical composition of sedimentary "rauhwacken" (containing gypsum, anhydrite in a matrix of dol), so the sample will be referred to as "cellular dolomite".

Optical microscopy The breccia clasts are entirely made of dol. The clasts are heavily disintegrated into rock flour of μm -size, but preserve the sedimentary fabric (S0) of the former protolith. The bedding can be traced from the upper right hand to the lower left hand corner (Fig. 4.2). Only small amounts of rotation and dilation of the breccia clasts occur, but the fitting fabric, from top to bottom, progressively disintegrates to mosaic fabric and chaotic fabric (Fig. 4.2). Septae in the hand specimen can be confirmed as cc-veins, cross-cutting the breccia clasts. Cross-cutting relationships are observable where enough host rock is preserved (Fig.

4.2, upper left hand side). Cells are encrusted by euhedral cc-crystals.

It can be roughly differentiated between three types of cc-cement:

- Septae-building cement or fracture-filling cement. Cc grows between the breccia clasts, encrusts their walls and partially solidifies the remains of the shattered dol, which creates cells with sharp boundaries against the veins. The cement manages to partly encrust the inner walls of empty cells, where cc can develop regular crystal faces (Fig. 4.10, comp. Fig. 4.3B).
- Fluid can intrude half-empty cells or cells with complete infill. Here, cc precipitates in μm -wide fractures between particles of rock flour and partly solidifies mentioned rock flour. The appearance of this cement type can be referred to as "cloudy" (Fig. 4.10, comp. Fig. 4.3A).
- Where cells and pores are big enough, euhedral cc-crystals can grow. The crystals show extraordinarily well developed crystal faces, can incorporate a core, one ring or more rings of dol-rock flour and grow to sizes of approx. 300 μm . The cc-crystals are loosely packed and touch each other - if at all - via grain-point contacts.

The conditions that need to be met to allow the growth of this cement type will be discussed.

The fine-grained or micro-crystalline nature of dol could be interpreted to be derived from micritic-sparitic algae mats.

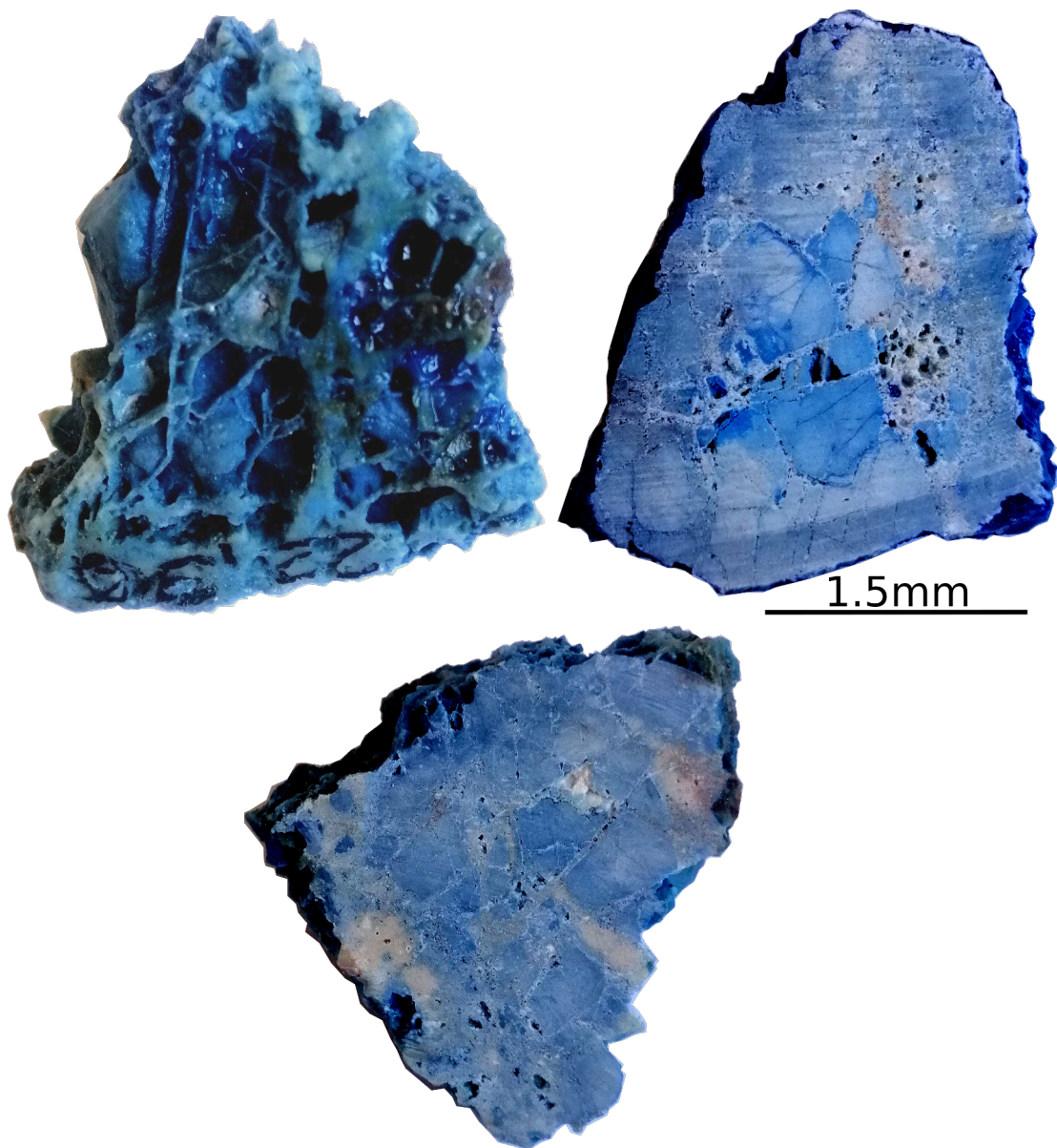


Figure 4.1 – SFK1m22-90. Sample preparation included treatment with resin due to the incohesiveness of dol-clasts that could be easily destroyed by performing slight pressure or simply holding it under water. Dol-breccia clasts are arranged to a fitting fabric.

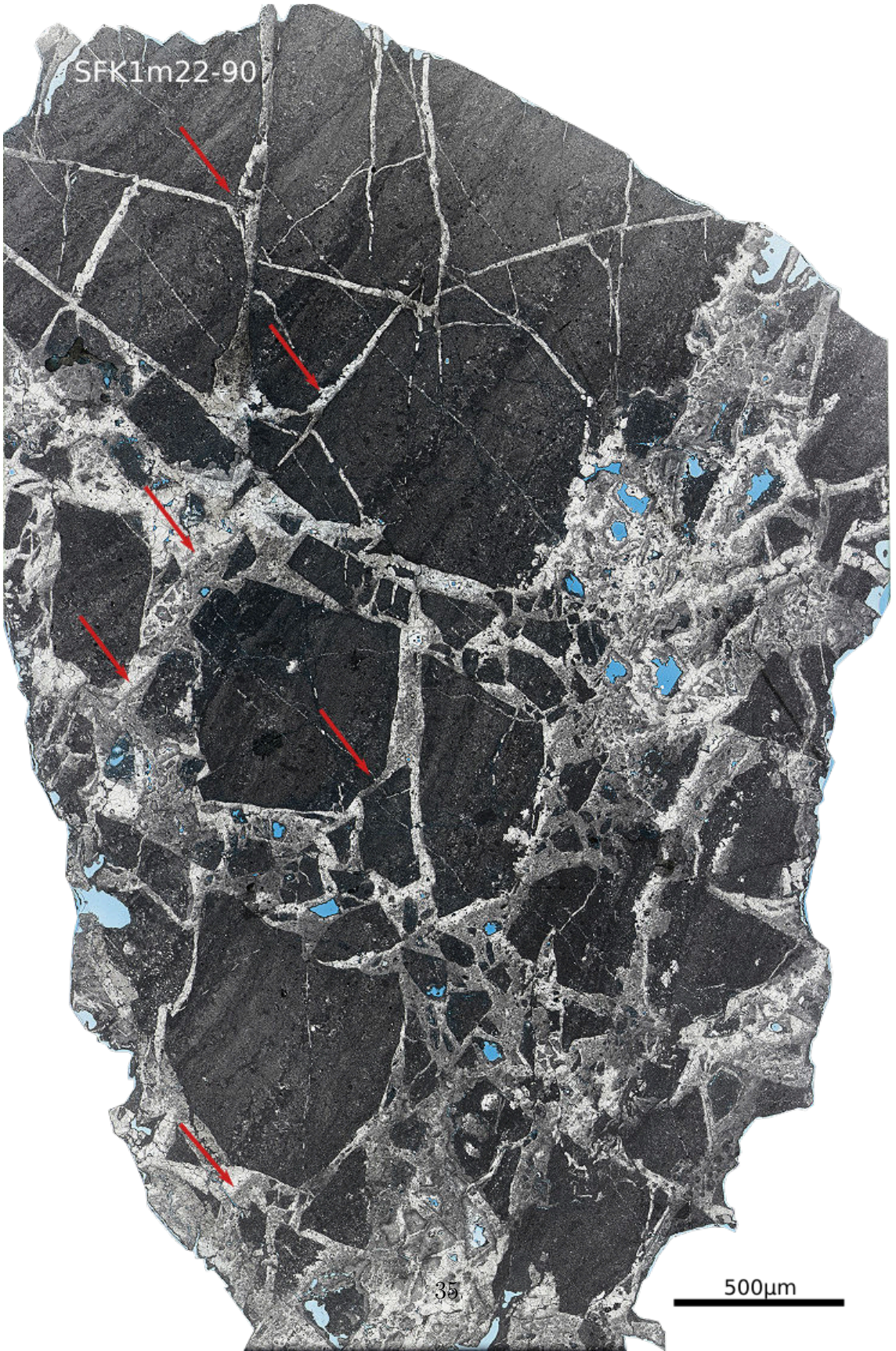
Further structural features can be observed:

- Septae/veins exclusively are made of cc. In the septae, dol-rock flour is ce-

mented. The particles supposedly derive from shattered dol, but this cannot be definitely verified by the means of optical (TL or PL) methods.

- Euhedral cc-crystals encrusting cell-walls are rarely twinned.
- Shattered (disintegrated) dol-clasts are either not cemented at all (Fig. 4.3A) or well encrusted by euhedral growing cc-crystals (Fig. 4.3B, C). Blue stain marks open porespace. Cc-cement growing into permeable leftover-dol-clasts develops no crystal faces (Fig. 4.3A, C).
- Septae-building cc is intensely twinned. Up to 35 μ m-broad cc-twins are bent (Fig. 4.4). According to Passchier and Trouw, 2005, the growth of broad twins could be the result of deformation at slightly elevated temperatures from 200°C to 250°C. Septae-cc develops anhedral crystal faces (Fig. 4.3A, B).
- Thin twins of < 10 μ m width are not deformed. Twins do not generally cross crystals, but taper out (Fig. 4.4A, B, D).
- The preservation state of disintegrated dol-clasts varies: Some of the clasts still preserve all of their primary infill, others only are recognizable through the presence of "ghostly" rings of dol-rock flour, preserving the former clast shape but not their infill.
- Dol-rock flour in fluid-filled fractures sinks and forms geopetal aggregates.
- Contrasting to other samples in this study (comp. SFK1m18-40A, B and SFK1m19-50A, B), the shape of the dol breccia-clasts is preserved extraordinarily well. This sample displays the transition from disintegrated dol-clasts encrusted by cc-crystals to completely dissolved clasts without any remaining infill.

SFK1m22-90



35

500µm

Figure 4.2 – SFK1m22-90. Thinsection-scan. Sedimentary bedding (S0) is still recognizable. Geopetalaggregates are deposited in cc-veins (red arrows). Dilation of the protolith and partial solution of dol-clasts create the "Rauhdecken"-resembling appearance. Clasts are angular. From top to bottom, the fabric disintegrates towards a progressively more chaotic fabric.

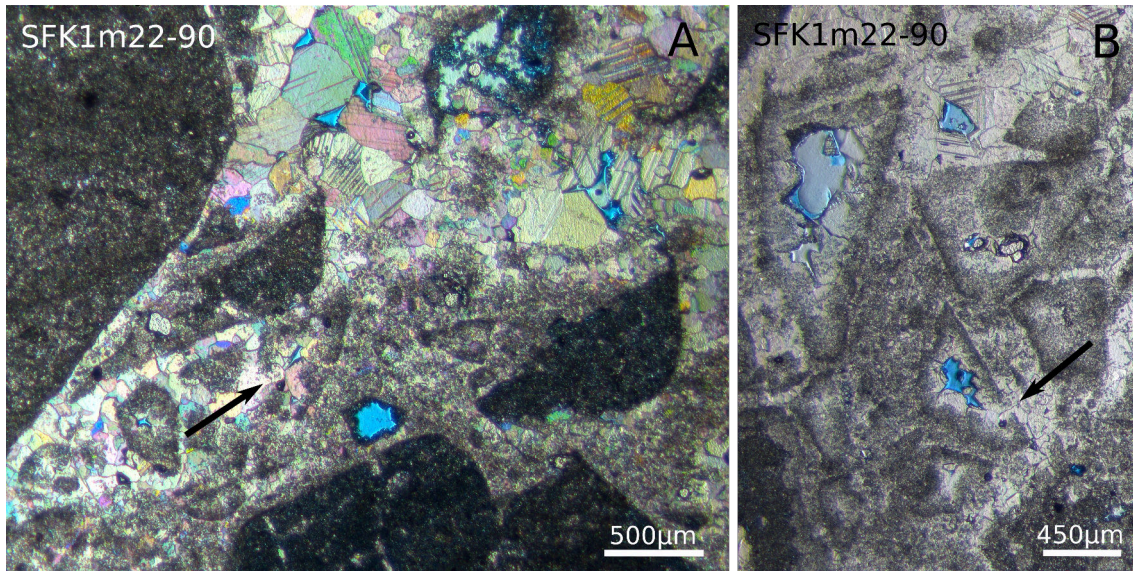


Figure 4.3 – SFK1m22-90 A: Twinned cc grows in fractures. Gravitational sinking of the rock flour in suspension creates geopetalaggregates (in the picture recognizable as grey spots, deposited in sub-horizontal direction). Cc-bearing fluid penetrates protolith and encrusts its clast so the rock is protected of further dissolution (black arrow). B: No protolith in cells is left. Cc in cells develops euhedral crystal faces. Note the perfectly preserved shape of former breccia clasts, now only indicated by attached rock flour. Arrow pointing to a cavity, through which fluids could infiltrate the clasts.

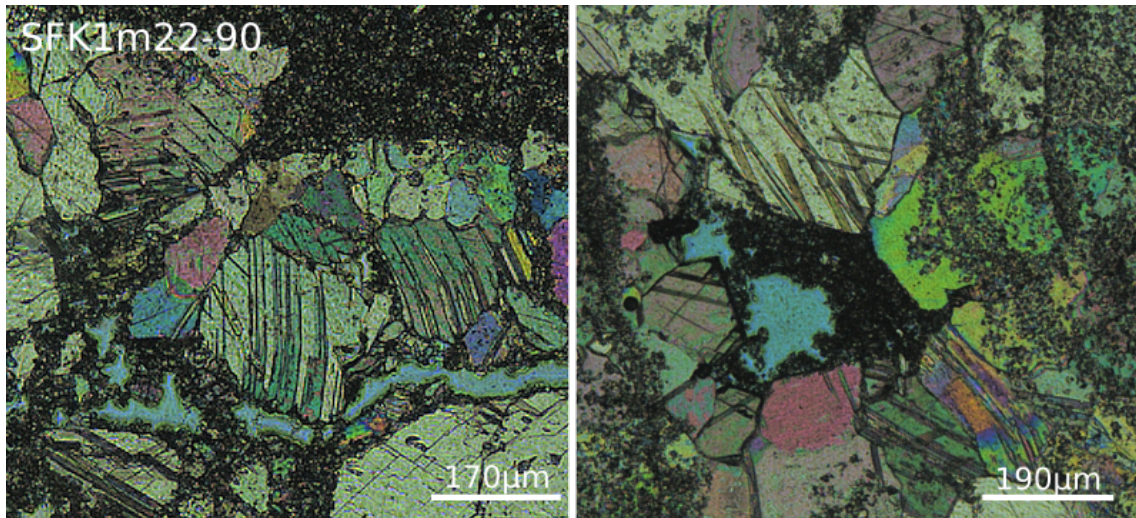


Figure 4.4 – SFK1m22-90. Cc in fractures is intensely twinned. Twins are up to 35µm wide and bent. This indicates elevated temperatures during crystal growth. Note fractured cc crystals, fractures in the crystal follow cc-cleavage.

Cathodoluminescence Different generations of cement can be distinguished. Cement encrusts and solidifies the walls of breccia-clasts and cements the fractures in the rock. The vein cement stands out as the macroscopically visible, planar septae cutting through dol-clasts (comp. Fig. 4.1).

CL-exposure times range from 15 to 23s. The cementation-sequence is developed as follows:

1. Dol-veins penetrate the orange-luminescing dol protolith. The veins are up to 1 mm wide and luminesce in bright red. Intensely bright luminescent lines in dol follow the cleavage of dol-single crystals. Here, the veins are fractured preferentially (Fig. 4.5A).
2. Cc-saturated fluids permeate the orange luminescing rock and dol-veins. The fluid provides enough energy to bring particles of rock flour into suspension and transport them. The shattered dol eventually sinks and geopetal aggregates develop (Fig. 4.3A, Fig. 4.7).
3. If shattered dol clasts are fully dissolved, angular cells open. The shape of breccia clasts are preserved perfectly. Into these cells, non-luminescing cc-

cement can grow. One or several generations of brownish-dark-luminescing cc-cement growing into the cells follow. (Fig. 4.5B, D). Scarcely, if cells provide enough space, bright-orange-red luminescing cement can grow. These seams are broad and its rims diffuse (Fig. 4.5C). Cc-cement develops euhedral crystal faces.

4. Rarely, zoned cc-cement seams grow in the septae (Fig. 4.5C).
5. Anhedral cc-crystals grow into cells that contain remaining protolith: The cc-saturated fluid-front eventually creeps into the porous breccia clasts and cannot develop euhedral crystal faces. Here, non-luminescing cement is followed by broad seams of bright-red cc-cement. Cementation in cells with preserved infill is terminated by cement growth of non-luminescing cc-cement (Fig. 4.3A).
6. Fragments of zoned cc-cements, that cannot be subsumed into the reconstruction of the cementation sequence, are overgrown by non-luminescing cc-cement (Fig. 4.5C). Supposedly, these cements are the result of previous fluid flow events that were incorporated into the current rock volume after fragmentation, transport by fluids and following encrusting.

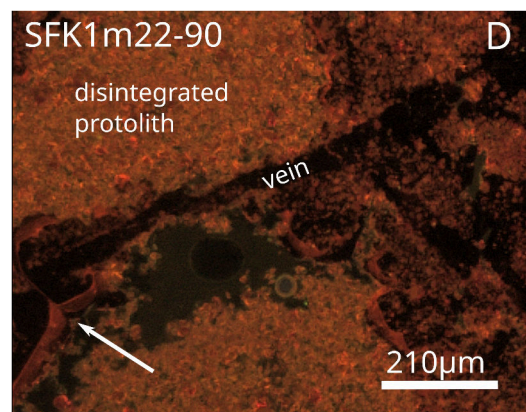
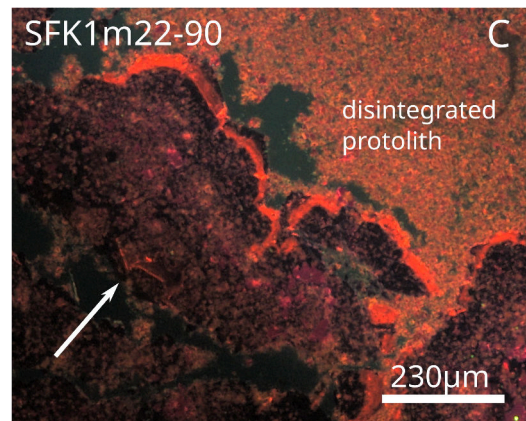
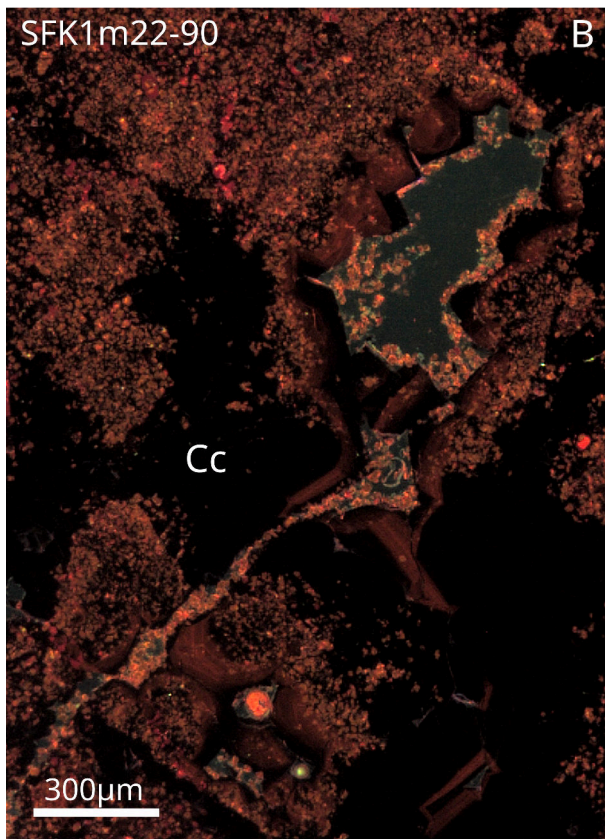
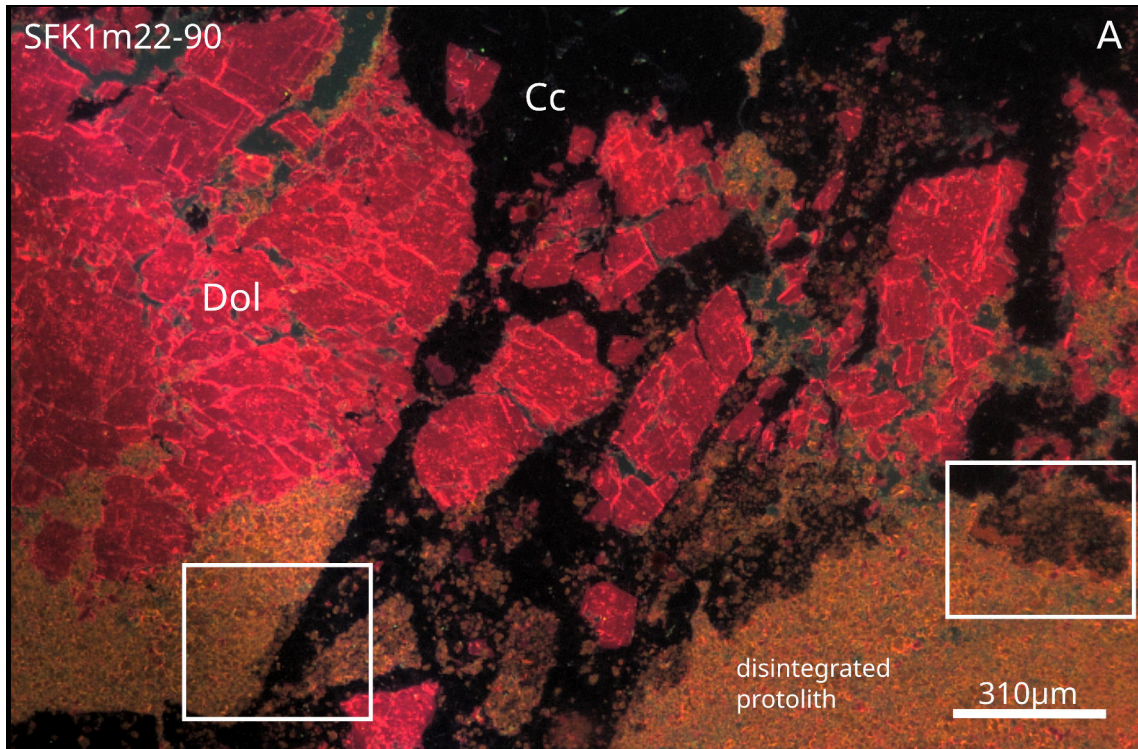


Figure 4.5 – SFK1m22-90: Cementation succession. A: Shattered protolith (orange) is penetrated by dol-vein. Dol-veins are subsequently fractured by non-luminescing cc-cement. Cc-bearing fluid creeps into the clasts, growth of anhedral crystal faces follows (rectangles). Orange-luminescing cement seams follow. B: Non-luminescing cc-cement partially encrusts clasts and preserves their former shape. Where cc-saturated fluid enters the cells, protolith is dissolved and euhedral cc-crystals can grow. A succession of broad, diffuse brown cement seams grow into cells. C: Brightly-luminescing crystals grow in a cell with little preserved protolith. A fragment of zoned cc-cement is overgrown by cc-cement that cannot be definitely subsumed into the cement-growth succession (arrow). D: Vein intruding the porous protolith, zoned cc-cement manages to grow from the vein into open cells (arrow).

EBSD- and EDX-semiquantitative analysis EBSD- and EDX-analysis confirm the rock to be exclusively carbonatic.

The shape of protolith clasts and their high degree of disintegration is apparent (Fig. 4.6). Fractures in clasts are almost planar and the clasts are arranged in a fitting fabric. The sizes of components range from approximately 5 - 500 μ m. The porosity in clasts ranges from 20-50% (values estimated according to Shvetsov, 1954). In well preserved clasts, one can see phase separation of dol to cc (Fig. 4.6).

In one single clast, the fabric of particles can range from fitting fabric to chaotic fabric (Fig. 4.6). Cc dissolves dol and grows into the clasts, the walls of the clasts are sutured. Fluid is not only oversaturated with cc, but also transports rock flour particles that accumulate in geopetal aggregates (Fig. 4.6, Fig. 4.7).

1. Mm-cm-sized clasts of the dilation breccia are angular and arranged into a fitting- to mosaic-fabric. The clasts are cementated by in multiple phases grown cc-cement.
2. The clasts are shattered into μ m-sized particles of rock flour, the particles preserving a fitting- to chaotic-fabric. Cc-cement can creep into the highly fractured clasts and disturb the shape of the breccia clasts.
3. Fractures are almost completely sealed by cc-cement. Few pores in the veins are less than 500 μ m in size.

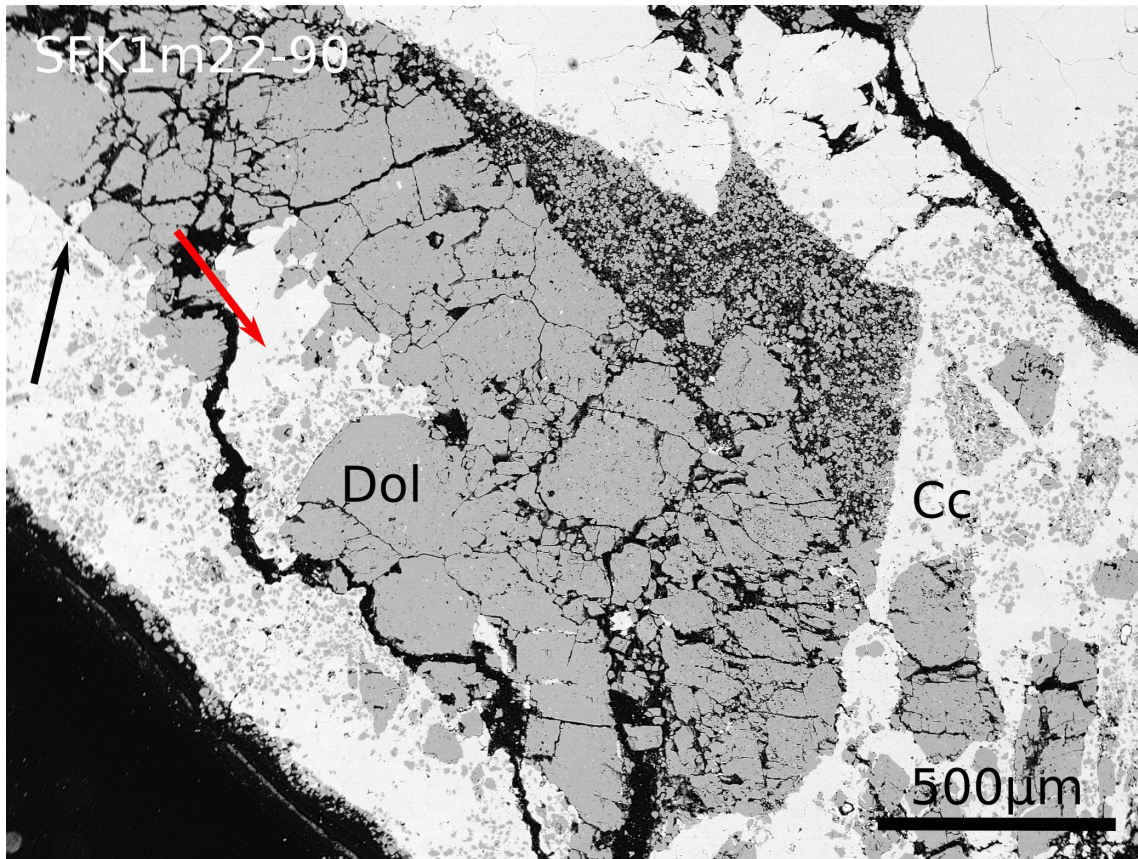


Figure 4.6 – SFK1m22-90. Protolith, comminuted into rock flour, disintegrates into μm -sized fragments. Fractures tend to follow the cleavage planes of dol. Partly, porous breccia clasts get dissolved, the secondary porosity reaches $> 50\%$. Rock flour particles are encrusted in vein cement between clasts. The particles start to sink and geopetal aggregates accumulate (red arrow).

In Fig. 4.7A, veins with well developed geopetal aggregates are shown: Along the boundary clast-veins, great amounts of disintegrated dol-clasts are dissolved and transported by fluid. The porosity along these boundaries reaches 50%. In veins, clasts of dol protolith are abundant but except their encrusted walls, almost no infill is preserved. The former clasts serve as surfaces, where particles of rock flour can be deposited as geopetal aggregates.

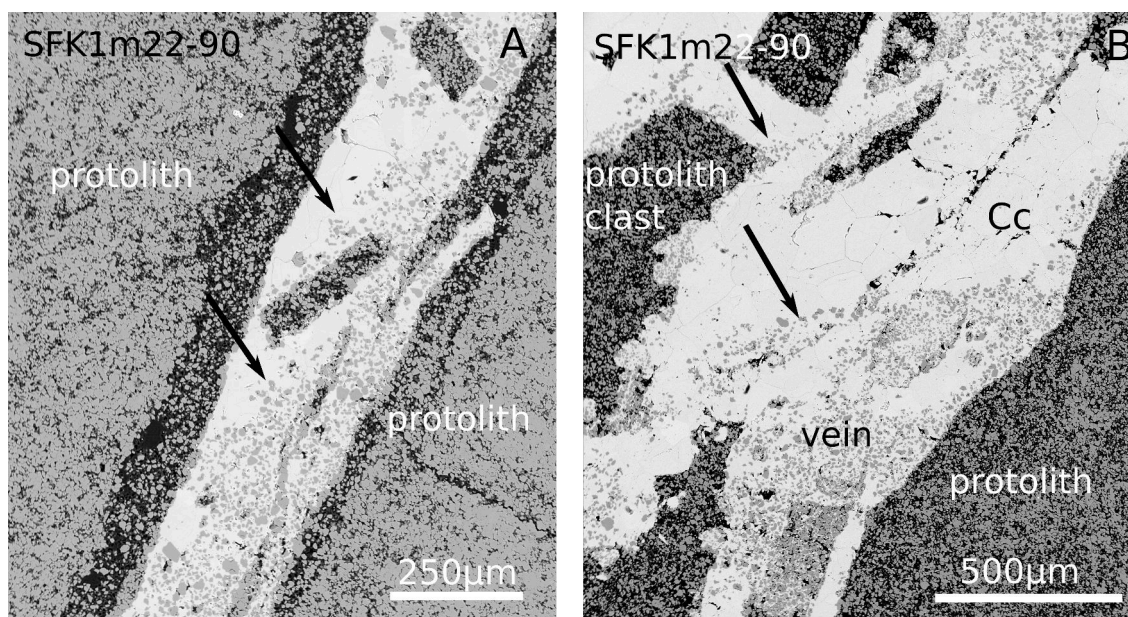


Figure 4.7 – SFK1m22-90. A, B: Arrows pointing towards the upper surface of geopetal aggregates. The disintegrated dol is highly porous and clasts are arranged in a fitting fabric. Remains of protolith-clasts are not cemented, only the walls of the clast are solidified by vein cement. Vein-cc has anhedral crystal faces. The solidified surfaces of the former clasts serve as a plane, where the aggregates can be deposited. B: Note the almost completely decomposed protolith clasts, with porosities > 50%.

Interpretation The protolith experiences several phases of deformation and subsequent cementation by cc-saturated fluids. The following event succession is proposed:

1. Protolith is dilated and develops a fitting- to mosaic fabric. Clasts that appear cohesive turn out to be disintegrated into rock flour and highly porous.
2. Cc-veins penetrate the rock volume in at least two phases, indicated by cross-cutting relationships. Eventually, the chaotic fabric of the protolith clasts developed during fluid influx.
3. Particles of rock flour in suspension presumably originate from shattered clasts of the dilation breccia. Solution of the shattered rock leads to the leaching of cells and early encrusting of cell walls that preserve the clasts' former shape.

4. Ongoing fluid influx in cells either dissolves the remaining protolith or preserves it by cc cementation. This can go on until the walls of the former clasts are completely encrusted by cc and they are protected against further dissolution.

Despite disintegration of the protolith and brecciation through dilation, the sedimentary features of the protolith are still observable.

The sample shows a complete transition from fitting- to chaotic fabric of its clasts. High fluid flow could not destroy the former sedimentary fabric of the protolith: Precipitation of cc healed cracks before dissolution could destroy the deformed rock. Where the fabric is more chaotic, one can trace the ongoing disintegration from intact clasts to partly dissolved clasts with little preserved infill and porosities of up to 50% (comp. Fig. 4.3). Partly, only the walls of the dissolved clasts are remnant as ghostly "rims".

Data indicate, that all of the samples containing cells, bordered by diffuse rims encrusted with cc-crystals and cemented septae separating the cells, are heavily overprinted former dilation breccias. The dol-rock flour that is an important constituent in all samples eventually derives from shattered dol-protolith clasts. After dissolution, empty cells are left, creating the porous, cellular appearance of "Rauhacken", respectively cellular dolomite.

Construction of the Semmering tunnel showed that the Grasberg-Schlagl-fault zone where the drill cores derive is characterized by steady, immense flow of mountain water, highly saturated in cc. This fluid could be saturated enough in cc to provide the material needed for cement-precipitation to that considerable extent.

4.2 SFK1m23-10

Between sample SFK1m22-90 to SFK1m23-10, the transition of rock types in hand specimen ranges from

- Highly fractured rock with angular clasts between protruding septae to a rock of more cellular appearance with subrounded cells as well as a manifestation with
- no remaining dol infill in cells, less even walls and broader septae. Sample SFK1m22-90 can be referred to as dilation breccia, SFK1m23-10 as "cellular dolomite". In the cells of this sample, cc-crystals of up to 1 mm grow and develop euhedral crystal faces.



Figure 4.8 – SFK1m23-10. Cell-diameters range from mm - cm are and angular to subrounded. Euhedral cc-crystals encrust the cells. No protruding clasts between the septae are preserved.

Optical microscopy The sample entirely consists of cc and dol. Neither qtz-grains, nor lithic fragments are incorporated. Cells in the rock are angular. Cc-crystals encrust the cell-walls. Particles of rock flour serve as core of euhedral cc-crystals growing in the cells.

The cell-walls are sharp and well distinguishable from the septae. The sample is highly porous: Cc-crystals touch each other at point contacts and seem to grow

around particles of rock flour in steady suspension. Estimates on the portions of rock flour solidified by cc-cement are hard to make, due to the heterogeneous distribution of the dol-particles in the sample, but are low and range between approx. 10-30%. Two cells preserve shattered-clast infill. Here, cc-bearing fluid can penetrate the fractured rock, cc precipitates and irregular-shaped cc-cement partially encrusts the remaining infill of the clast (Fig. 4.9).

Cathodoluminescence The sample contains all of the cement types observed in SFK1m22-90. The fragmented and recemented, intensely luminescing cement-seams allow the reconstruction of the deformation history:

1. Shattering of the rock into rock flour, eventually before brecciation and the development of a mosaic fabric (comp. SFK1m22-90 Fig. 4.2, Fig. 4.6).
2. Fluid infiltrates the sample. Rock flour is solidified by non-luminescing cc (Fig. 4.11E). Partly, dol breccia clasts are dissolved, where cement cannot encrust the shattered dol in time. The shape of clast boundaries is preserved by early cementation.
3. Growth of non-luminescing, euhedral cc-cement in the open cells (cement-seam II) (Fig. 4.11A, E).
4. Growth of brownish, few- μm thick cement-seams (cement-seam III) (Fig. 4.11E). Non-luminescing cc-cement growth terminates the cementation succession.
5. Influx of dol-rock flour-bearing fluid into unsealed cells (Fig. 4.11A).
6. The walls of the cells are encrusted by μm -thick seams of cc. The luminescence-signal of this cement-type is diverse, the approximate cementation succession is as follows: 1) Orange-non luminescing-orange seams, followed by 2) broad, diffuse brown-cement seams. The cc-crystals at the wall of the cells, as well as in suspension grown cc-single crystals, show the same succession. It is terminated by non-luminescing, euhedral cc (cement-seam IV)
7. Cc-cement is fractured (Fig. 4.11A, C).

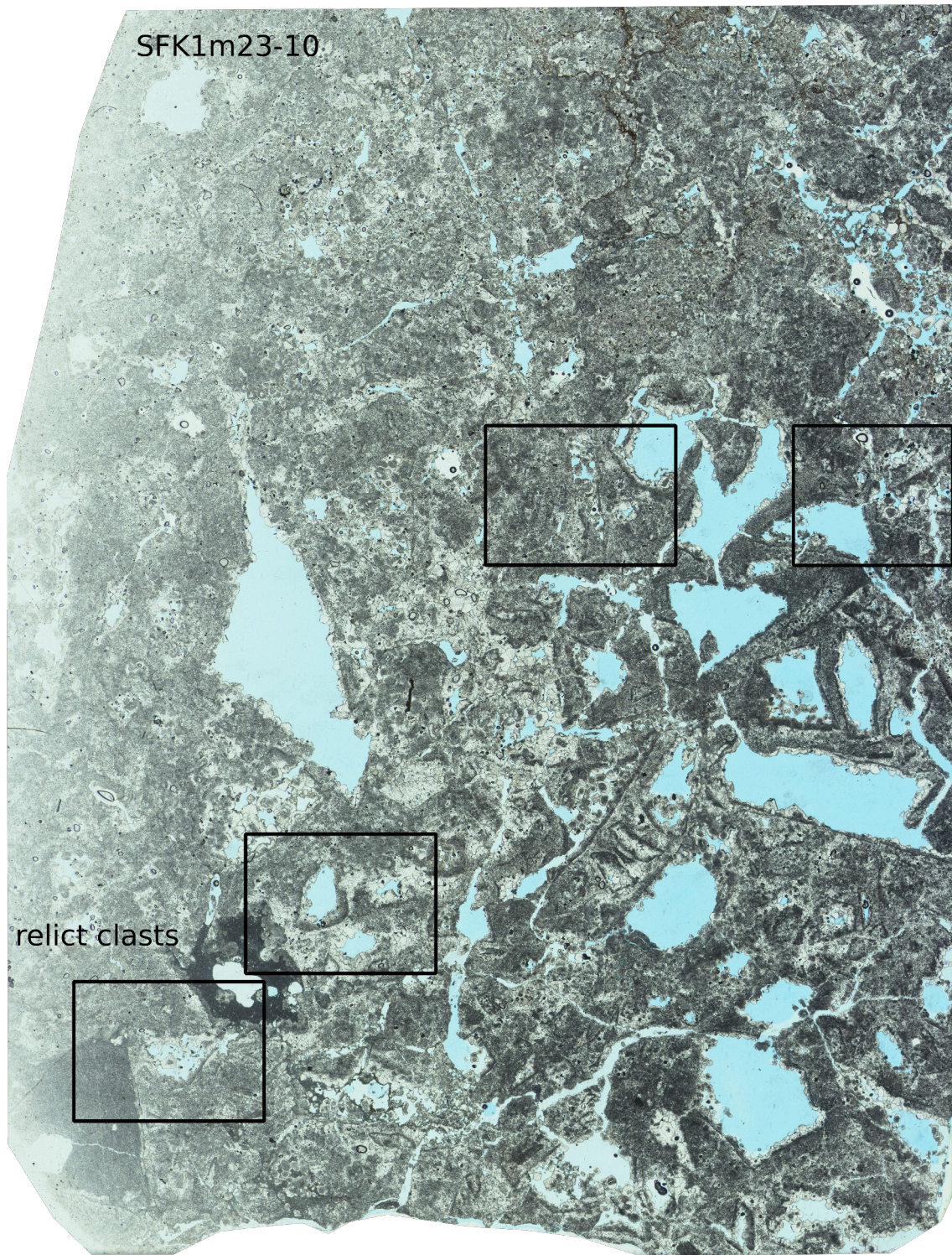


Figure 4.9 – SFK1m23-10. Thinsection scan. The rectangles mark the spots of the CL pictures. Note the missing protolith in former clasts and high amounts of young cc-cement in cells and along septae. The septae break easily and get recemented.

8. Fractured pieces of cement are transported by fluids and encrusted on established rock (Fig. 4.11C) (cement-seam V).
9. Termination of cementation occurs through growth of non-luminescing, euhedral cc-cement (cement-seam VI) (Fig. 4.11C).

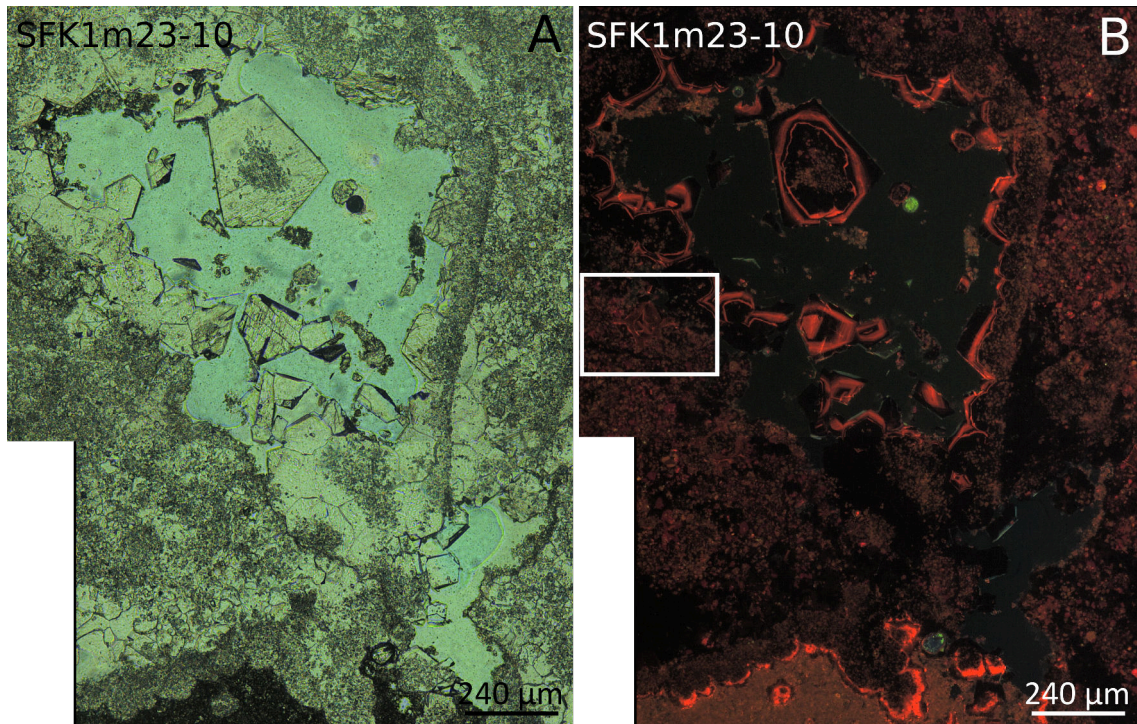


Figure 4.10 – SFK1m23-10. The left rim of the cell is overprinted by pressure solution seams. A: Cement-seams of two different generations next to each other. B: Supposedly older cement-piece luminesces brownish (rectangle). The single cc-crystals in the cell incorporate particles of rock flour. Two bright seams surround non-luminescing cc-cement. The inner seam is irregular, the outer one is broad and diffuse and follows the habit of cc. The CL-signal of cc in the cell and the cement encrusting the cell-walls is identical.

From dilation breccia to cellular dolomite The combination of observations made in SFK1m22-90 and SFK1m23-10 allow to reconstruct the complicated evolution from dilation breccia to cellular dolomite:

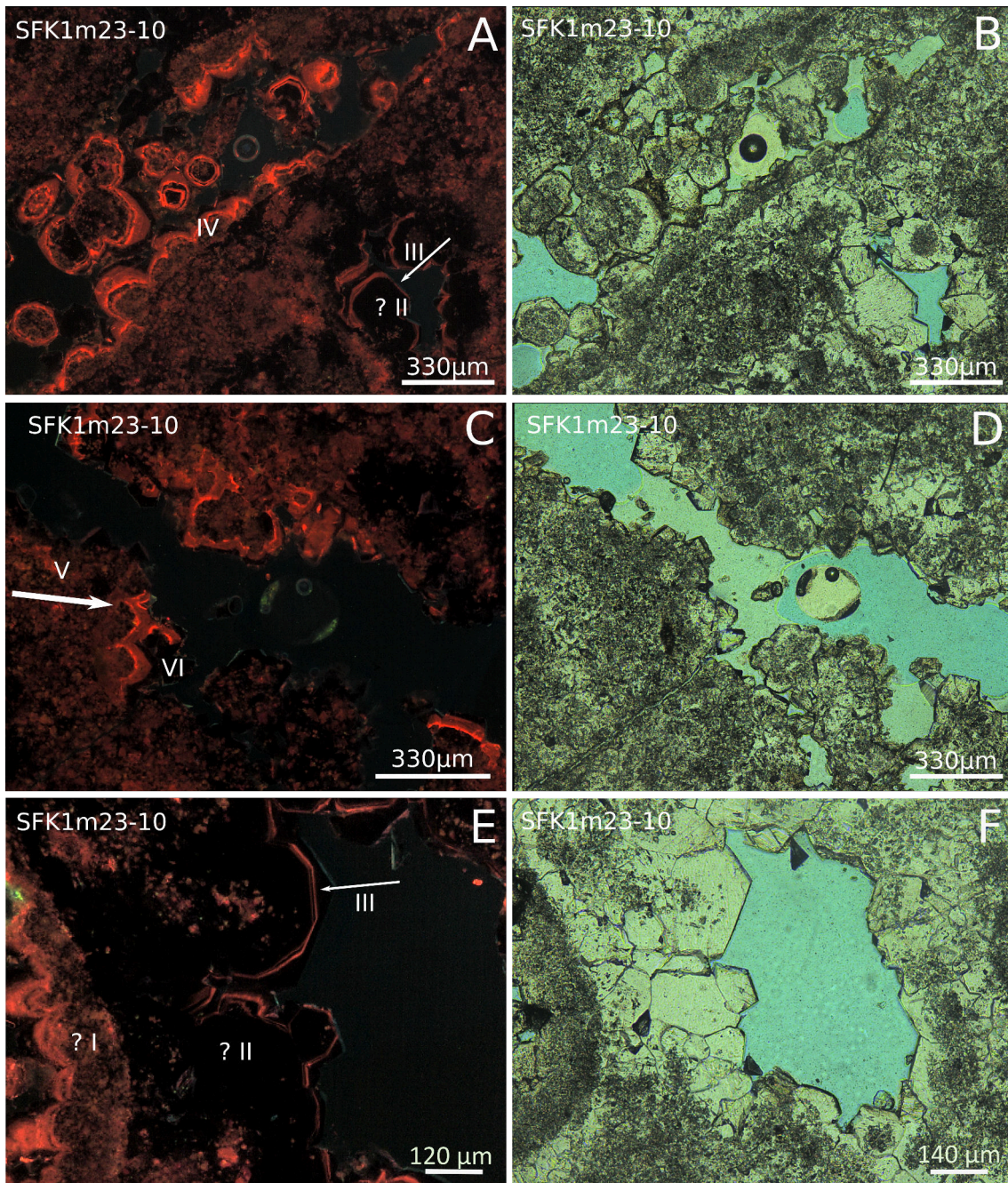


Figure 4.11 – SFK1m23-10. A, B: Cell encrusted with brightly luminescing cc and filled with euhedral cc-crystals. Note the brownish cement next to the specific cell. C, D: A piece of the same, brightly luminescing cement is incorporated elsewhere in the rock. The arrow points towards the wall of the cement-fragment. In TL, the clast is barely visible. E, F: Supposedly the oldest cement types. Rom. I and rom. II are marked with question marks, since it is non-excludible that these cements were formed prior to the main cementation forming the main current rock volume.

1. The dolostone protolith is shattered and its volume enlarged: A dilation breccia developed. The breccia clasts are internally comminuted.
2. Cc-rich fluid infiltrates the fractures. Partly, the fluid front cannot penetrate the breccia clasts. Only the walls of the clasts get cemented.

The further evolution can occur in two ways:

- Case I: Particles of shattered breccia clasts are enclosed by cement and protected of further fluid-influx. (Fig. 4.10B). Cc-cement encrusts the rock flour but cannot develop euhedral crystal faces. The resulting cement seams are irregular (Fig. 4.10B, Fig. 4.11E).
- Case II: Particles of shattered breccia clasts are dissolved by fluids and cc cannot encrust the clast completely. Euhedral cc-crystals can grow in now "empty" cells without preserved infill (Fig. 4.10B).

The variety of different cement-types indicates that the current rock experienced several events of breakage and and subsequent cementation. Pieces of fractured dilation breccias with matchable cement growth can be observed in several samples (comp. Fig. 4.21, Fig. 4.22D, E, Fig. 4.23B, D, Fig. 4.26B, Fig. 4.15).

4.3 SFK1m20-40A-E

Hand specimen The rock consists of mm-dm-sized subangular, cellular carbonatic clasts in brownish, slightly weathered matrix and can be referred to as tectonic breccia with a substantial amount of pressure solution, indicated by striking pressure solution seams (Fig. 4.12). The specimen is cohesive. Pressure solution seams develop along the boundary clasts-matrix.

Cells in carbonatic clasts are rounded and encrusted with small-sized cc-crystals but are in a worse preservation state than cc-crystals in cells of samples SFK1m22-90 and SFK1m23-10. The colour of the clasts is greyish-blue. When applying HCl, the rock does not react, therefore seems to be mainly dolomitic.

The matrix is highly porous and reacts to the HCl-test. It can be comminuted under slight pressure. The rock is matrix supported.

Little, non-carbonatic lithic fragments are incorporated. Macroscopically, they cannot be further determined.



Figure 4.12 – SFK1m20-40A. Clasts in the matrix range between mm-dm in size. Cells in the greyish-blueish components are rounded and chaotically arranged. Cell-diameters range from few mm to > 1.5 cm. Towards the matrix, clasts are bordered by thin pressure solution seams (black arrow). Even though the sample is heavily weathered, it is cohesive.

20-40A

Optical microscopy Clasts that appear dense in hand specimen turn out to be highly porous, indicated by blue resin in the stained thin section ($> 40\%$ porosity) (Fig. 4.13). They consist of anhedral cc-crystals with incorporated rock flour particles. Between single crystals, the average pores are $< 1\text{mm}$. Only a low amount of lithic fragments other than carbonate-clasts are observable.

The highly porous clast is well rounded and surrounded by an even higher-porous matrix: Cc-crystals in the matrix are euhedral and up to approx. $400\mu\text{m}$ in size. Here, crystals are supported by point-contacts and preserve porosities of $> 60\%$ (Fig. 4.13). The matrix contains "micro-clasts" of recemented carbonatic-rocks.

Interestingly, the clasts' fabric strongly resembles the matrix in its constituents and grain-sizes of single crystals.

The more densely packed clast seems to sink into the porous, slush-like matrix of unsolidified cc-single crystals. Along the boundary clast-matrix, anhedral cc crystals grow and different types of dol- and lithic-fragments occur. The "soft" matrix bends around the clast, and cc-crystals in the matrix are rather dissolved, than breaking through the exerted pressure.

In the seams, residual mica-grains are weathered and cannot be optically resolved. They are responsible for the seams' dark colour (Fig. 4.13).

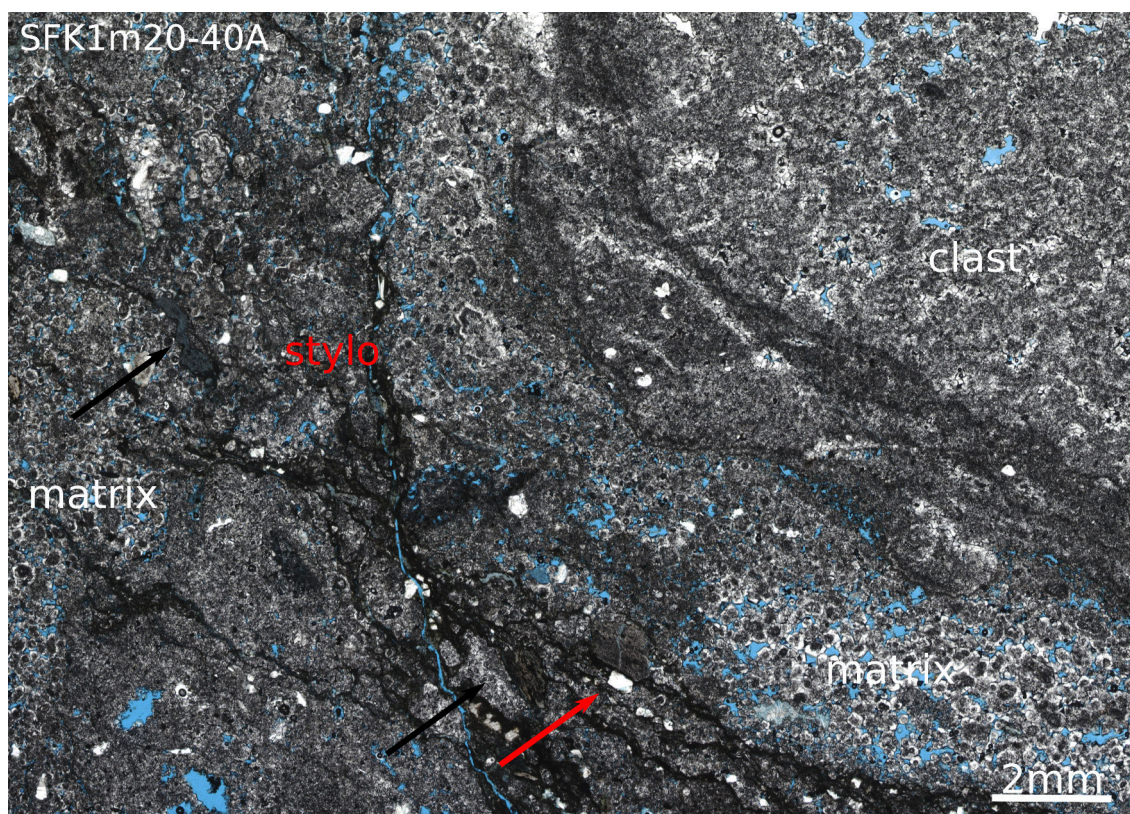


Figure 4.13 – SFK1m20-40A. Porous clast in even more highly porous matrix. Pressure-solution seams with lithic fragments and qtz-grains (red arrows) are enriched in weathered mica-grains. The clast is pressed into the matrix, but cc-crystals do not break or develop pressure-induced twins. instead, they are dissolved. The lithic fragments are altered by weathering (black arrow) and develop porosity.

The rock shows evidence of carbonate-solution along the pressure solution seams, the dissolution affects clasts and micro-clasts in the matrix.

Accessory-minerals in lithic fragments are intensely weathered and appear red with diffuse boundaries (Fig. 4.14A, B). Further determination by optical methods is impossible. Qtz-grains with undulose extinction are dissolved by cc. This creates sutured grain-boundaries in qtz. Cc-crystals growing at the extent of qtz are few μm in size (Fig. 4.14C).

Eventually, lithic fragments are of magmatic origin. Acicular-shaped fsp in the fragments (greyish-yellow interference colours) is typical for rocks of volcanic origin (Fig. 4.14B).

Lithic fragments showing a metamorphic foliation are weathered and develop sec-

ondary porosity (Fig. 4.15A).

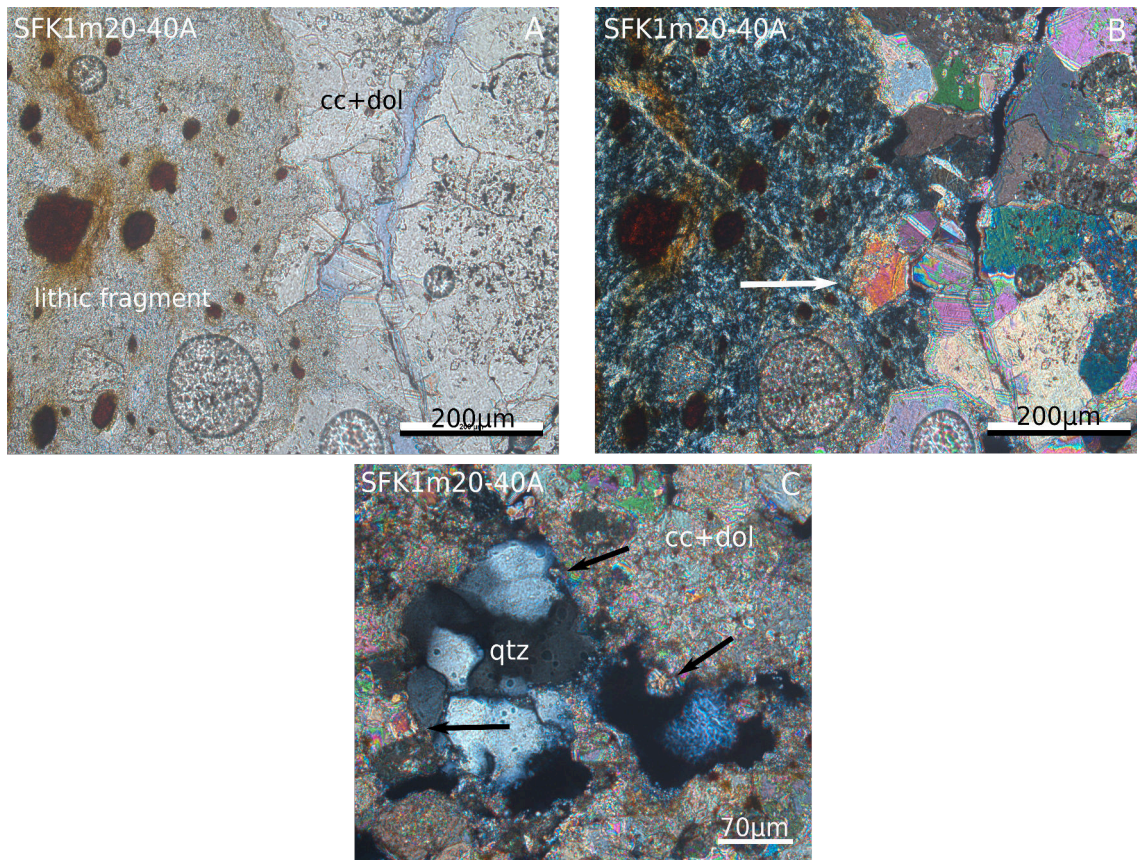


Figure 4.14 – SFK1m20-40A. A, B: Lithic fragment, replaced by cc. Cc grows into grains, creating sutured grain boundaries. Red spots are weathered accessory-minerals. C: Polycrystalline qtz-grain with undulose extinction. Arrows point towards areas of advanced chemical alteration.

Lithic fragments, documenting preceding brittle deformation are abundant. Fragments of heavily reworked dilation breccias/cellular dolomite are recemented (Fig. 4.15). Former contacts between the boundaries of the clasts towards the matrix are overprinted by stylolites, so the clast is only distinguishable by the different appearance of cc-crystals compared to the cc-crystals building the matrix:

- Rock flour is solidified by cc-cement and distributed evenly. This is different to the concentrated particles of rock flour in cores of single-crystals that constitute the matrix (comp. Fig. 4.25A, B).

- Cc-septae/-veins cross the clast: Planar veins cut through the clast (Fig. 4.15A, C). In comparison, the matrix is not penetrated by veins (comp. Fig. 4.12).
- Remains of angular cells with ghostly appearing walls are preserved. They show similar features like the cells in samples SFK1m18-40A, B and SFK1m19-50A, B (comp. Fig. 4.21, Fig. 4.25). Here, euhedral cc-crystals grow from the walls of the cells into the open cells (Fig. 4.15B, C).

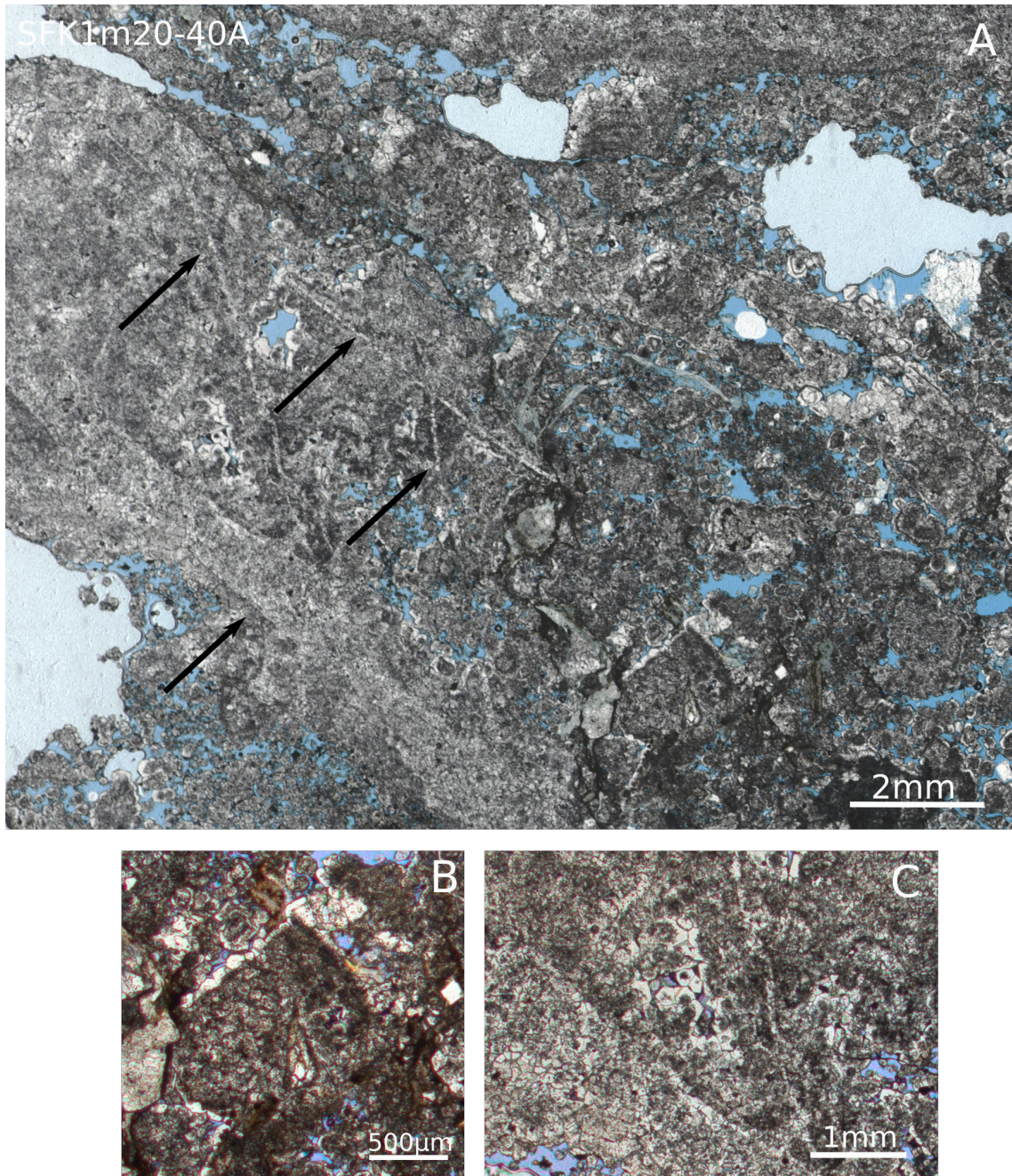


Figure 4.15 – SFK1m20-40A. A fragment of heavily overprinted dilation breccia/cellular dolomite. A: Arrows pointing towards perfectly planar veins. Cc-crystals with euhedral crystal faces encrust the septae of fragments of cellular dolomite (black arrows). Note the concentrated particles of rock flour in the cc-crystals. B: Close-up view of a cellular dolomite fragment. C: Close-up view of euhedral cc-crystals growing into a pore, their cores eventually consisting of rock flour.

In this thin section, no indicators for shear-deformation are observable.

20-40B

SFK1m20-40B derives from the same fault breccia, but is more matrix-rich and porous compared to 20-40A. The main constituent of the rock is dol-rock flour, solidified by cc-cement. Additionally, mica-grains, polycrystalline qtz and lithic fragments from varying protoliths are incorporated. Stylolites overprint the boundary clast-matrix as well as clast-clast (Fig. 4.16).

Optical microscopy In thin section, it can be differentiated between clast and matrix:

- I: Clast in matrix. Rock flour in cc-cement is distributed heterogeneously and accumulates in cloud-like aggregates. This clast type is overgrown by cc-crystals with perfectly developed crystal faces. In parts, the cement encrusts a max. 100µm-wide seam of particles of shattered dol (Fig. 4.16).

The porosity (approx. < 10%) in the clast is lower than in the matrix. The few pores have diameters of up to 1.5mm.

Pressure solution seams in the densely packed clasts are thin. They cross clasts and taper out in the matrix.

- II: High porosity-matrix (approx. 40%), supported by point contacts between grains. The matrix is characterized by euhedral cc-crystals of max. 1 mm with shattered dol in the cores and a ring of shattered dol attached to the single crystals (Fig. 4.17B, C, D). Cc of the matrix gets dissolved against the clast along stylolites. Broad pressure solution seams cross the matrix. Lithic fragments, qtz- and mica-grains generally constitute the matrix.

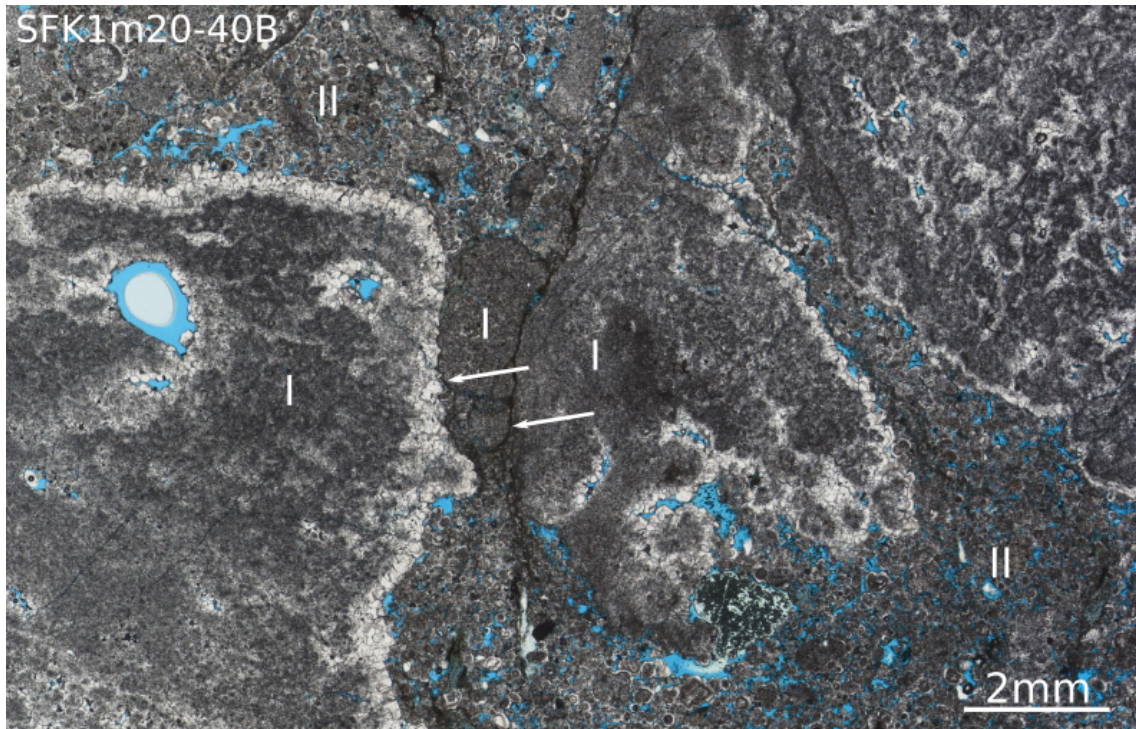


Figure 4.16 – SFK1m20-40B. I: Clasts in matrix. Cc encrusts the heterogeneously distributed dol particles. The porosity in the clasts is low. Pores in the clast are round and scarce. Pressure solution seams cross the densely packed clast. II: Euhehedral cc-crystals with dol particles as nuclei. Note the high porosity between the single-crystals.

20-40D

Optical microscopy As in SFK1m20-40A, the rounded clasts in the matrix consist of homogeneously distributed rock flour in cc-cement (comp. Fig. 4.12). Euhehedral, pure cc-crystals overgrow the clast. As in samples 20-40A and 20-40B, a thin rim of rock flour is incorporated in the cement (Fig. 4.17C, comp. Fig. 4.17A, Fig. 4.16). In the clasts, little porosity (10%) is preserved.

The boundary clast-matrix is overprinted by pressure solution, cc overgrowing the clast is partly dissolved (Fig. 4.17A).

The matrix is grain-supported by well developed cc-crystals and concentric rings of rock flour incorporated (Fig. 4.17B, C). Single-crystals grow up to 500µm in size, porespace of approx. 50% is preserved. Late cementation leads to the growth of irregularly shaped cc-aggregates (Fig. 4.17A, C, vgl. Fig. 4.26 A-D). The aggregates

can eventually be referred to as cockades, too.

Additionally, lithic fragments are part of the matrix. The fragments derive from different protoliths with magmatic and metamorphic fabric. Qtz can be polycrystalline, monocrystalline or recrystallized (Fig. 4.17B, E). Clay minerals in pores are foliated and not overgrown by cc. Weathering of the fragments creates high secondary porosity, indicated by blue colour of the stained thin sections (Fig. 4.17A, D).

Remaining pores between single crystals have diameters of max. 200 μ m.

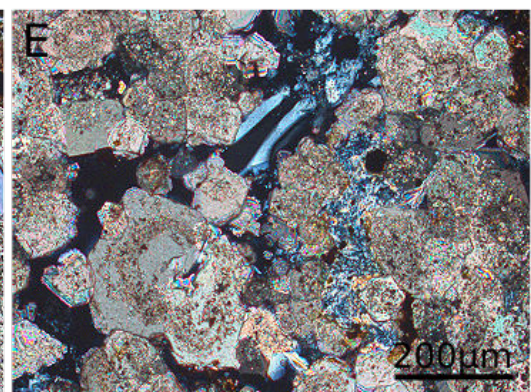
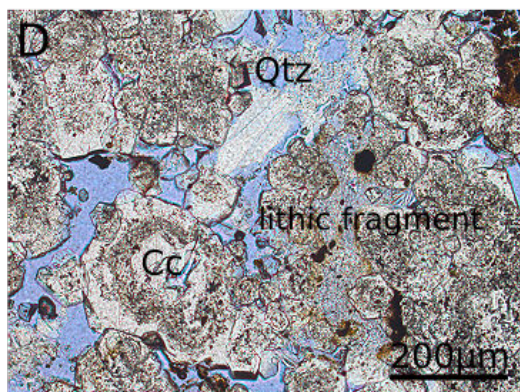
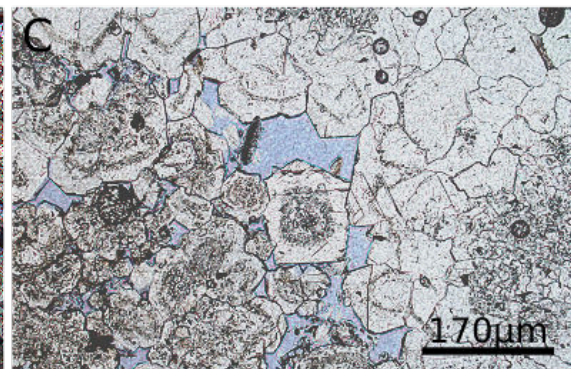
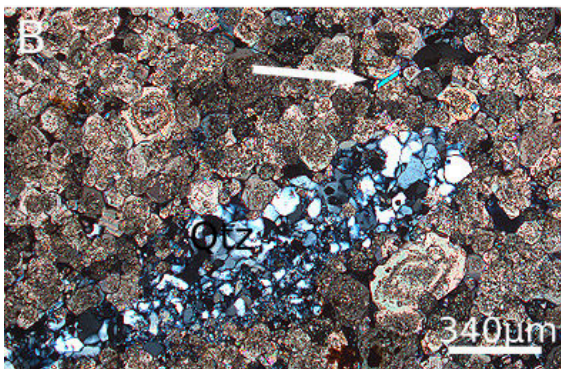
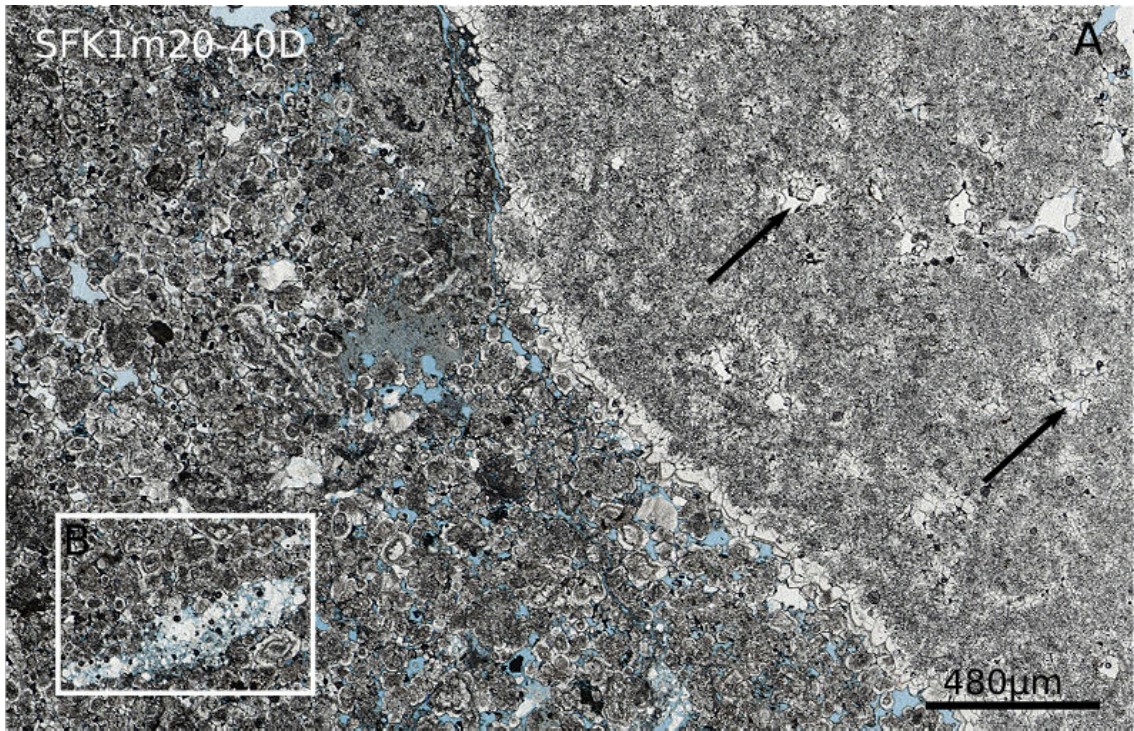


Figure 4.17 – SFK1m20-40D. A: Right hand side: A rounded clast is overgrown by a white seam of cc-cement, that contain a thin line of rock flour. The clast is dense with little left porosity (black arrows). The heterogeneous matrix consists of carbonate- as well as crystalline rock components. B: Polycrystalline qtz, highly recrystallized. Cc-single crystals grew in several phases, indicated by rings of rock flour in them. White arrow: A undeformed, unaltered mica-grain. C: Examples of euhedral cc-crystals with a core and concentric rings of dol particles. This type of cc-crystals is interpreted to have grown in suspension with enough supply of rock flour. D, E: Dissolved, deformed and poorly recrystallized qtz-grain in TL and PL. Fsp in lithic fragments is altered (ochre-colours). The needle-shaped qtz-grains in the fragments point towards a magmatic origin of the source rock.

20-40E

Optical microscopy Loose, heterogeneous matrix incorporates cc- and dol-fragments as well as lithic fragments. In this text, only lithic fragments of >1mm in size will be referred to as clasts: This differentiation is somewhat arbitrary, but necessary for the readability and understanding of the text.

It can be differentiated between following clast types:

- Clast-type I appears bright. Rock flour in cc-cement is evenly distributed. This clast-type is massive and densely cemented, scarce pores in cement are only of few μm and make up approx. 5 - 10%. Thin pressure seams overprint the border clast-matrix. Clasts are overgrown by a thin cc-cement-seam with incorporated rings of rock flour (Fig. 4.18A, B, comp. Fig. 4.17A, C).
- Clast-type II: Shattered cc and dol (rock flour) are not evenly distributed in cc-cement which creates a cloud-resembling appearance (Fig. 4.18C). Subangular pores of several mm in size are overgrown with cc-cement. Rarely, stylolites occur.

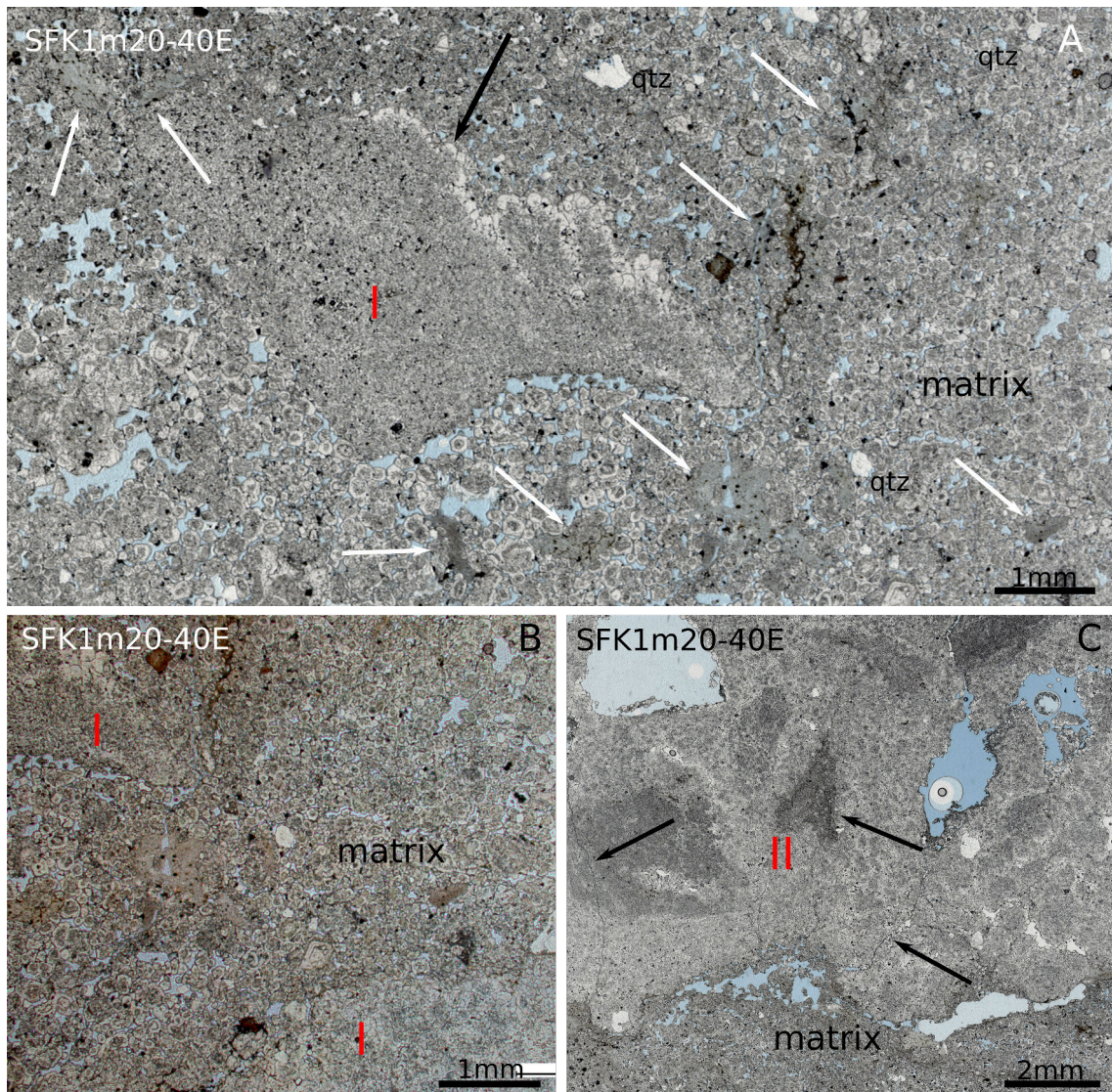


Figure 4.18 – SFK1m20-40E. A: Clast-type I: Black arrow pointing towards the cement-seam, encrusting the clast. Here, the cement-seam contains thin rims of rock flour. White arrows point to lithic fragments in matrix. Brownish colour: A pressure solution seam; poorly solvable lithic fragments are concentrated. B: The highly porous matrix mainly consists from euhedral multiphase-grown cc-crystals. Clast-type II has pores with irregular boundaries.

The matrix consists of euhedral cc-crystals that overgrow rock flour. Lithic fragments range between 10 μm to several mm. In this sample, these types of lithic fragments can be distinguished:

- Euhedral cc-crystals, surrounded by concentric rings of rock flour. Cc-crystals are not twinned. Diameters of the single crystals range from 30 μ m to 500 μ m.
- Carbonate-clasts with homogeneously distributed rock flour in cc-cement and ?accessory-minerals (brown spots) (Fig. 4.18A).
- Non-carbonatic lithic fragments with diameters < 200 μ m - several mm (Fig. 4.19B, D). Partially, the lithic fragments show metamorphic foliation and qtz-grains are recrystallized to different extents. The clasts contain altered accessory minerals that cannot be further determined (Fig. 4.19 A).
- Lithic fragments of supposedly magmatic origin (Fig. 4.19E).
- Polycrystalline qtz-grains with dulose extinction and lobate grain boundaries. Size and shape as well as extinction patterns point towards complete recrystallization of the crystal lattice (Fig. 4.19C, D).
- Single-grain-qtz with dulose extinction and fluid inclusions (black spots). (Fig. 4.19E). Both poly- and monocrystalline qtz-grains are dissolved by fluids enriched in cc (Fig. 4.19C, D, E).

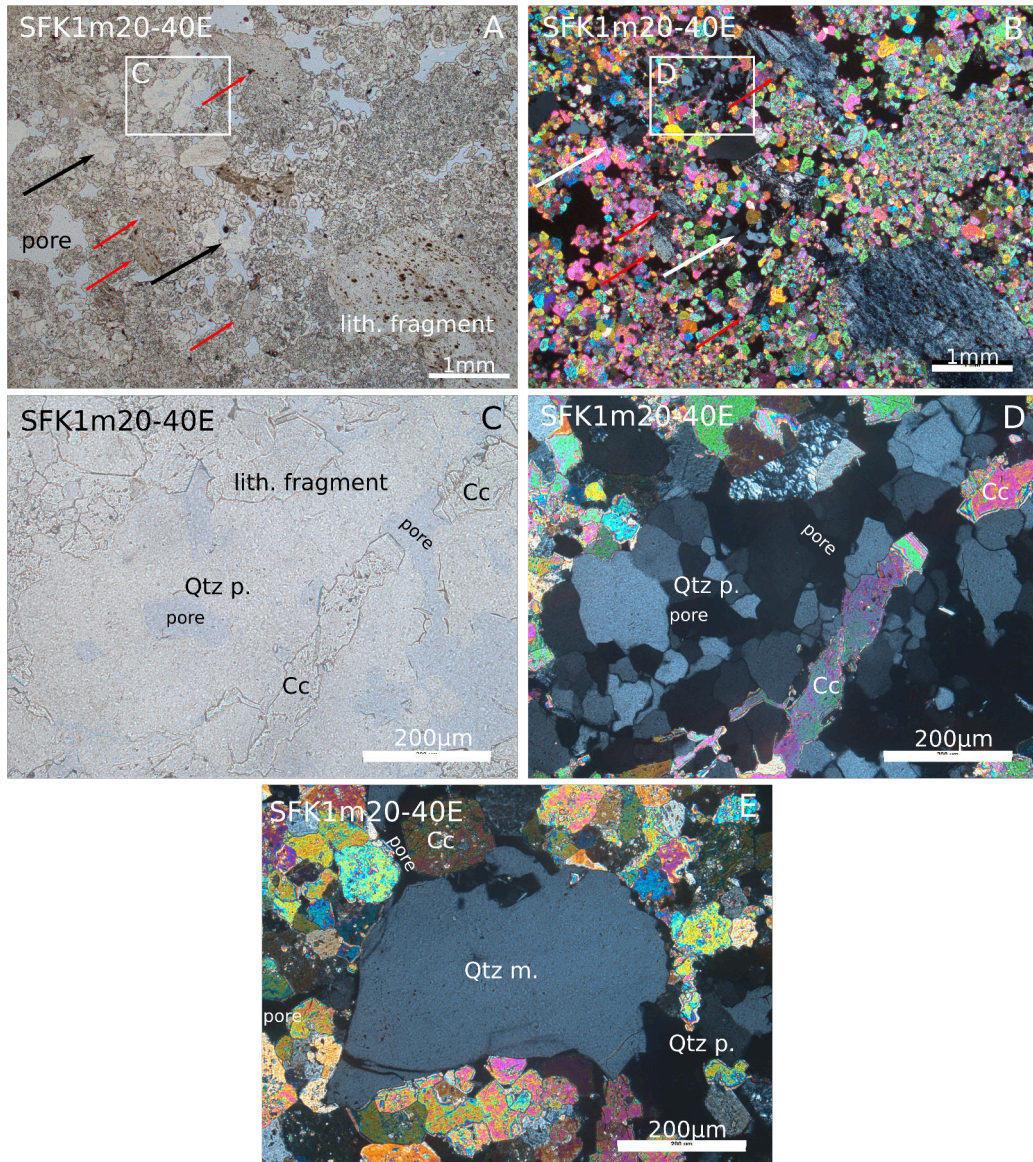


Figure 4.19 – SFK1m20-40E. Material in the matrix. A, B: Lithic fragment with metamorphic foliation and weathered accessory minerals. Black arrows pointing towards Qtz-grains, red arrows pointing towards strongly altered lithic fragments with sutured boundaries. Rectangle: See C, D: Qtz-grain is dissolved by fluids and a secondary porosity develops. Lithic fragment consisting of Qtz and fsp, but without any accessories. E: Dulose single-grain Qtz with fluid inclusions (black spots). Cc dissolves this grain, too. Pores between euhedral Cc-crystals remain.

EBSD-analysis The thin rims of rock flour in cc-cement overgrowing clast-type I can be observed in sections 20-40B, D and E. The average fragment size of shattered rock corresponds with the size of rock flour fragments of other samples (approx. 5 - 30 μ m). Rims do not only contain cc- and dol-rock flour but few accessory minerals as well are overgrown by the cement (Ti-oxides and Fe-oxides) (Fig 4.20B, D).

The thin seams of the carbonate-clasts are relatively even (Fig. 4.20A). Cc-single crystals get encrusted to the clast on top of the overgrowing cement (Fig. 4.20A).

In pressure solution seams, fsp is completely broken down to phyllosilicates. Lithic fragments in undeformed matrix are less weathered.

EBSD reveals that cc-cement of carbonate clasts incorporates different amounts of rock flour particles; the portion of dol-rock flour ranging from 5 - 15%. It appears that combined with the different portions of particles in carbonate clasts, sizes of the particles differ, too (see Fig. 4.20A, B).

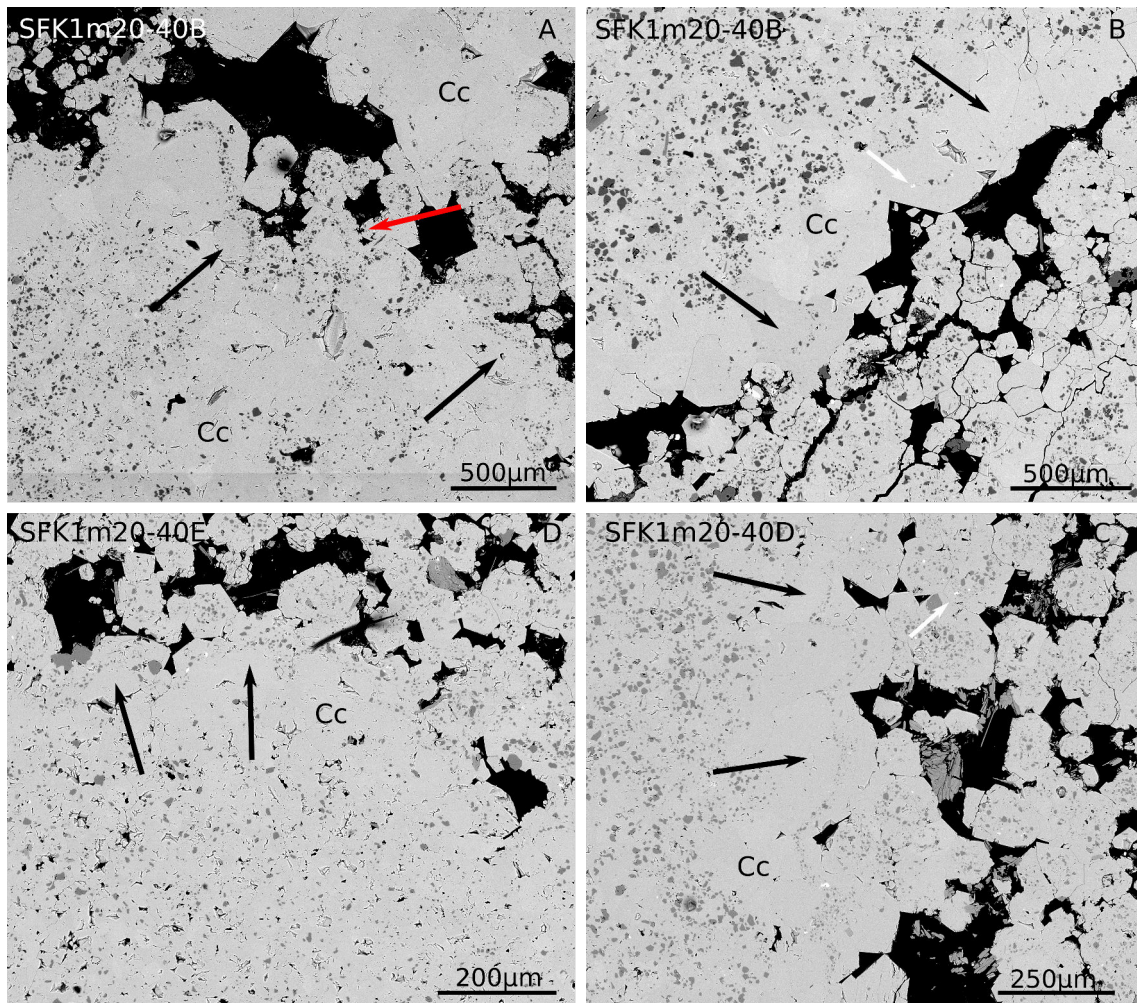


Figure 4.20 – SFK1m20-40B, D, E. Particles of rock flour incorporated in the clast-overgrowing rims of cc-cement. A: Cc-single crystal is encrusted on a carbonate clast by euhedral cc-cement and a rim of rock flour (red arrow). B, C, D: Cc-rims around clasts (black arrows). Heavy minerals are part of the aggregates, too (white arrows).

Estimating the amount of rock flour particles enclosed by cc-cement in carbonate clasts yields 5 - 15%.

Interpretation Indicators of shear deformation are not observable. Pressure-resolution leads to the formation of stylolites and dissolution of non-carbonatic fragments by cc-bearing fluids.

Seams of cc-cement, developing euhedral crystal faces and overgrowing carbonate

clasts appear in every thin section. In none of the sections, non-carbonate lithic fragments are overgrown by this cc-generation. This leads to the assumption, that the growth of this cc-generation did not occur in situ, but in an earlier event. So, the incorporation of the lithic fragments could have only taken place after the growth of the cc-cement with encrusted rock flour rings.

The younger cc-crystals building the matrix, supposedly grow in suspension: Fluid-influx transports cc- and dol-rock flour, diverse lithic fragments and qtz. Berger and Herwegh, 2019 postulate the possibility of fluids with high current velocities to bring fine-grained fragments into suspension. Eventually, this fluid is cc-saturated and cement precipitates. Ongoing supply of shattered-fine-grained rock from an outer source allows the growth of rings of rock flour in cc-cement. Several influx events could explain the accretion of more than one ring in euhedral cc-crystals.

In the case of decreasing current velocity, the current energy is too low for suspension of rock fragments as well as the cc-crystals. Thin rims of cc-dol-rock flour around carbonate-clasts and the accretion of cc-crystals could be the result of the components' gravitational sinking.

4.4 SFK1m18-40A, B

Hand specimen The sample will be referred to as a poorly preserved cellular dolomite with a high amount of cc-cement. The cells of this sample are rounded and their walls heavily overgrown by euhedral cc-crystals. The rock is ochre coloured, compact, and cohesive.

SFK1m18-40 and B solely consist of rock flour and cc-cement, with thin pressure solution seams penetrating the sample. Weathering creates mm- to cm-sized subangular cells in the otherwise compact rock. The dense section is distinguishable from the cavernous section, the sections will be referred to as section Rom. I and Rom. II.

Optical Microscopy Thin sections show the transition from firmly cemented rock without cells to highly porous portions:

SFK1m18-40A Rom. I: Main constituent of the rock is cc-cement that creates the homogeneously bright appearance of the sample. Particles of rock flour serve as nuclei for euhedral cc-crystals. Multiphase growth of cc-crystals is indicated by concentric rings of incorporated rock flour. The habitus of cc is scalenohedral. Microscopy reveals pores with diameters of $< 100\mu\text{m}$ (Fig. 4.21 B, D). The porosity of carbonate-type I measures approx. 5%. Rare, thin pressure solution seams penetrate the sample (Fig. 4.21A, B).

Isolated lithic fragments and qtz-grains occur.

Along pressure solution seams, cc is dissolved and crystals develop irregular boundaries (Fig. 4.21B).

Rom. II: Cc-crystals in the cavernous sections grow to 2mm in size. Perfect-euhedral crystal faces indicate in situ, stable cement-growth conditions. Walls and septae between cells break and are recemented in a later cementation event (Fig. 4.21A, D). Dol is concentrated in the cores of cc-crystals. The porosity in this rock-type is hard to estimate, but definitely $> 30\%$.

SFK1m18-40B Irregular pores are up to 1 cm in diameter and are encrusted with cc-crystals. As in 18-40A, these crystals incorporate concentrated rock flour

in their cores (Fig. 4.21D, Fig. 4.23C, D). One cell contains preserved, uncemented shattered dol (Fig. 4.21C).

Material from other protoliths is abundant in cells, too (Fig. 4.21D).

Examples of fragmented septae, encrusted with cc-cement occur. The overgrowing cc-cement develops euhedral crystal faces that indicate steady fluid flow during growth (Fig. 4.21D).

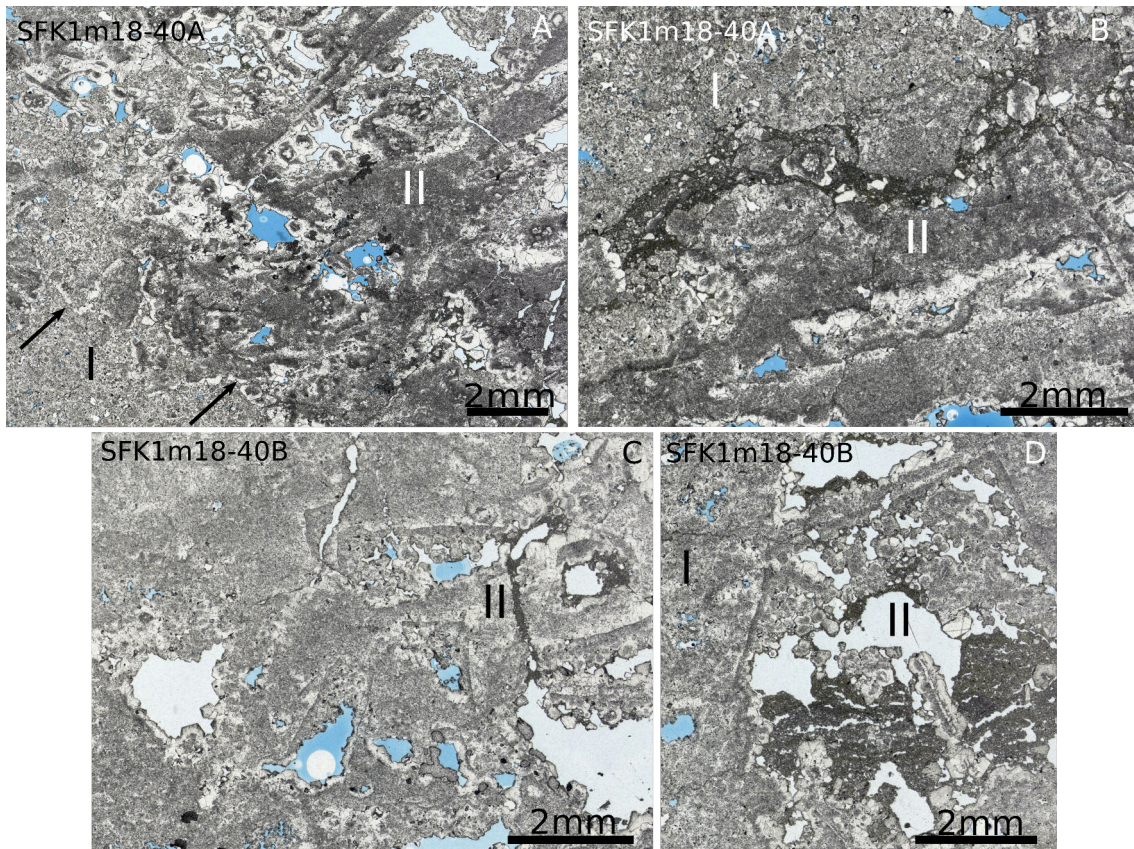


Figure 4.21 – SFK1m18-40A and B. A, B: Rom. I. marks compact sections of the rock with low porosity, rom. II the cavernous sections. Arrows mark the contact between the sections. B: Pressure solution seam with concentrated rock flour deriving from the same carbonatic clasts. C, D: Sample 18-40B is less porous and more compact than 18-40A. Here, dol-particles are more evenly distributed in cc-cement. D: Arrows indicate pressure solution seams that deform the cells' walls. Rom. II: Pore with fractured cc-septae or cell walls, encrusted with cc.

Cathodoluminescence The luminescence-signal is weak at exposure lengths of > 10 seconds. When comparing the samples, following statements can be made:

- Shattered dol in the cavernous parts of the cellular dolomite luminesces in subtle brownish-reddish colours. Dol-particles of rock flour are again too fine-grained for optical resolution (Fig. 4.22F, G, Fig. 4.23D).
- Cc-cement that grows in *cells* luminesces in bright colours, is zoned and develops euhedral crystal faces. The cement-sequence is complex: 1) black 2) bright orange 3) broad, brown seams. 4) Non-luminescing cement terminates the succession (Fig. 4.22E).
- Cc in *densily cemented sections* grows in multiple phases. Nuclei of cc-crystals consist of rock flour. The cement-sequence is as follows: 1) Non-luminescing cement 2) multiple broad, brownish seams. The succession is terminated by 3) non-luminescing black cc-cement. In the last cementation event, cc-single crystals are encrusted by cc-cement and cc-aggregates develop (Fig. 4.23B).
- Weakly-luminescing shattered dol in the densily cemented section of the rock is evenly distributed. Here, the dol particles are optically resolvable (Fig. 4.22D). Zoned cc-fragments could originate from earlier cementation events (Fig. 4.22D).
- Rock flour (20 - 50µm) in the rocks' cells luminesces in bright, orange- and reddish colours. In cemented cells, the dol-rock flour sinks to the bottom of cells and geopetalaggregates develop (Fig. 4.22D).

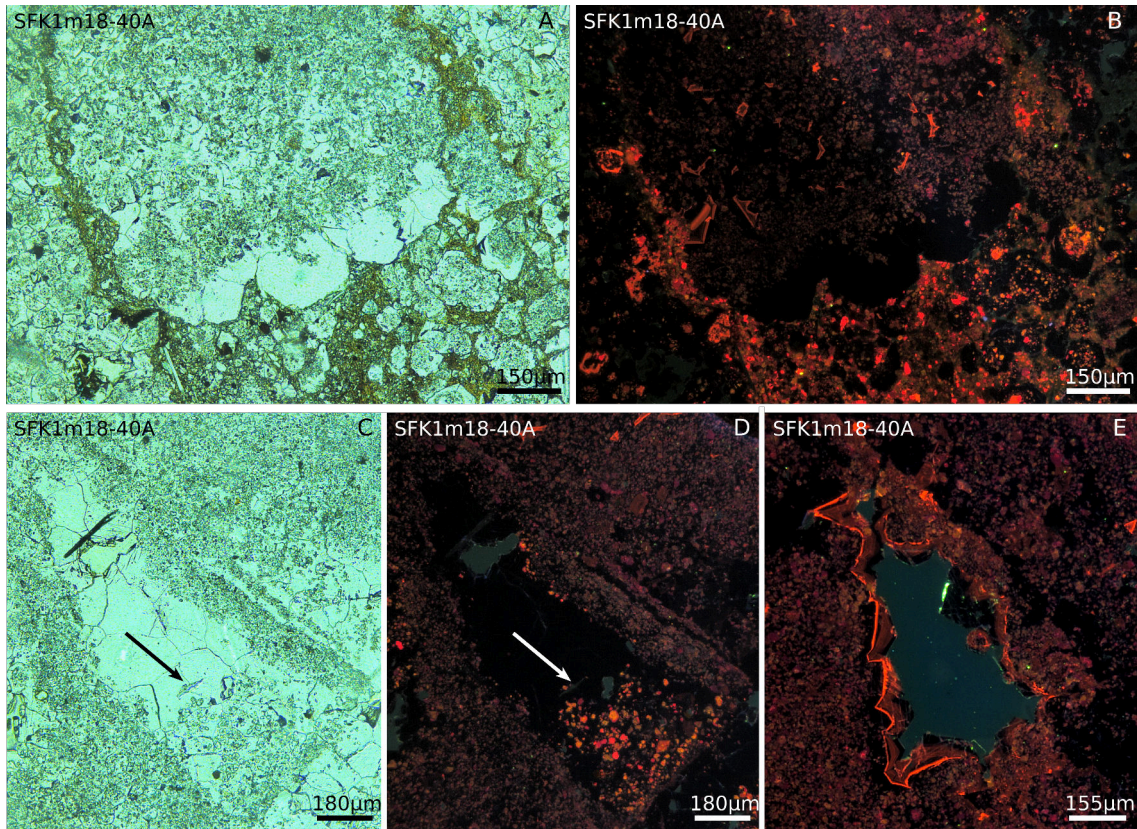


Figure 4.22 – SFK1m18-40A. A, B: Clast of a recemented carbonatic-rock in a stylolite. Non-luminescing cc-cement encrusts one side of the clast. In the stylolite, brightly luminescing rock flour is concentrated. The particles give a different chemical signal than dol in the recemented carbonatic clasts. C, D: ?Geopetal aggregate in a cell, encrusted by non-luminescing cement. E: Exemplary succession of cements. Only the walls of the breccia clast are preserved. The main volume of the component is dissolved. In the empty cell, cc-cement with perfect crystal faces can encrust its walls. Five seams are observable. The cement seams are comparable to seams in SFK1m20-40.

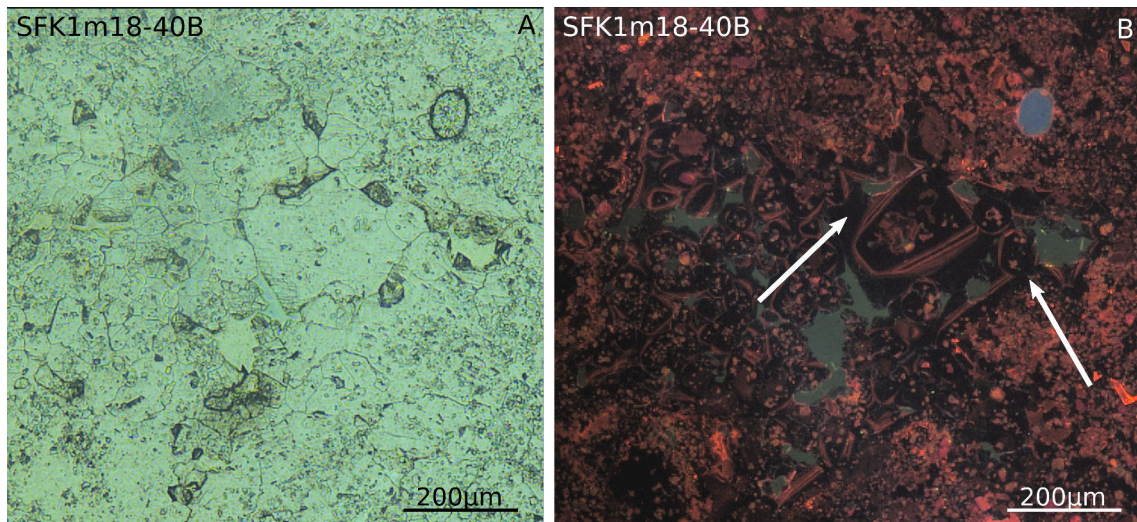


Figure 4.23 – SFK1m18-40B. A, B: Cc-crystals of max. 300µm show multiphase growth. Where single crystals grow large and develop grain-contacts, a new, non-luminescing cement-seam grows and cc-aggregates result. White arrows indicate grain-contacts.

Cc-cement encrusting cells in Rom II. grows multiple cement-seams. Five cement-seams can be distinguished. (Fig. 4.22E, Fig. 4.23B):

1. Non-luminescing cement encrusts the breccia clasts' walls, but does further grow into the shattered breccia-components.
2. Where cement cannot encrust the shattered clasts' infill, the non-solidified dol rock flour is dissolved.
3. Bright-red luminescent cc-seams grow.
4. Growth of brownish luminescing cement seams (Fig. 4.22E).
5. Growth of non-luminescing cement (Fig. 4.23E).

The non-cavernous parts of the rock develop following cement-seams (Fig. 4.23B):

1. Rock flour in suspension is encrusted by non-luminescing cement.
2. Brown, broad euhedral seams overgrow the crystals.

3. Non-luminescing cc-cement of seemingly different crystallographic-orientation terminates the succession under development of euhedral crystal faces. Eventually, point contacts develop between these crystals.

Interpretation The rock consists of two types of recemented carbonatic-rocks with supposedly different genetic history, with Rom. II being seemingly better preserved. Rom. II strongly resembles the fabric as in samples SFK1m22-90 and SFK1m23-10. Angular cells of a shattered, then dilated dol-?protolith, are encrusted in several cementation-events but the cell-walls are still recognisable. Rom. II is in contact with another type of recemented carbonatic rock: The densely cemented type Rom. I.

It is obvious that despite strong influence of fluid flow and pressure solution, fragments of the cellular dolomite are well preserved. The former protolith-dol-clasts are - in almost all cases - completely dissolved by mentioned fluid flow. Where cc-cement completely encrusts dol-clasts, they are protected against further dissolution (see. Fig. 4.3). Otherwise, the characteristic cells develop. As in sample SFK1m22-90 and SFK1m23-10, preserved clasts, cells and septae of this sample are differently well preserved (comp. Fig. 4.21A, C).

The succession of cementation in the cells of greater diameter in Rom. II is characteristic for all cellular developed samples of this study and can be observed in several samples.

4.5 SFK1m19-50A, B

The sample is a greyish-ochre cellular dolomite with pressure solution seams penetrating the rock. The walls of the cells in the rock are uneven. There are no protruding septae (comp. SFK1m22-90) and the cells are arranged randomly. Cc-crystals in the pores are observable as euhedral with the naked eye, but not as well developed like these in samples SFK1m23-10 or SFK1m18-40 (Fig. 4.25).



Figure 4.24 – SFK1m19-50. Dissolved dol creates cells with uneven walls, encrusted with cc-crystals. Brownish spots derive from weathering and pressure solution.

Optical microscopy The distribution of rock flour in cc-cement is heterogeneous. Cells in the rock, with few exceptions, are enclosed by cc-cement. Well preserved cell-walls like in SFK1m18-40A, B are not abundant. Instead, the walls of dissolved clasts are diffuse and appear "ghostly" (Fig. 4.25A, B).

Euhedral cc-cement encrusts rock flour. Concentric rims of dol particles are incorporated in cc-single crystals and prove multiple-phase growth of cement (Fig. 4.25). The cc-single crystals in cells are encrusted to clusters of approx. 100 μ m-diameter. These clusters' boundaries are irregular.

Isolated qtz-grains are incorporated between cc-single crystals. Qtz is monocrystalline and shows dulose extinction. One grain has conjugated en-echelon veins in it and therefore is of metamorphically overprinted. Cc grows at the expense of qtz

grains and dissolves their grain boundaries (Fig. 4.25). The growing cc develops perfect crystal faces.

The cells' walls are partly encrusted with cc-crystals. The porosity in the cells is > 50%. Densely packed portions of the rock show relatively low porosity < 20

Cathodoluminescence Various cc-cement-types in the compact sections of the rock give following CL-signals:

1. Cc-dol-rock flour luminesces in bright orange-red. Non-luminescing cc-cement agglutinates these dol-cc-fragments (Fig. 4.26A).
2. Occasionally, pale-brownish luminescing seams follow. These seams are few μm broad (Fig. 4.26A).
3. Non-luminescing cement overgrows cc-single crystals, and aggregates with uneven boundaries develop. After this event, almost all cc-crystals are in contact via point-contacts.
4. Where pore space between crystals is left, broad, diffuse and pale-luminescing brown cement seams can grow (Fig. 4.26B).
5. Bright red-orange, 10s of μm broad cement seams terminate the cementation events. The aggregates are restricted by crystal faces with nooked angles (Fig. 4.26A).

The luminescence signal of cc-cement in the more porous section of the sampled rock developed differently (Fig. 4.25A, B): Isometric cc-crystals show no luminescing cc-seams, but are encrusted by rims of rock flour particles that attach to idiomorphic cc-crystals. (Fig. 4.25C, D, Fig. 4.27). In the core of cc-crystals, both cc- and dol rock flour is concentrated. The particle sizes are too small for resolution via optical methods, but their different CL-signals indicate varied sources (Fig. 4.25).

"Hidden" dol-cc-aggregates that are not observable in TL appear in CL as "relict" or "ghostly" grains (Fig. 4.27). These relict grains have two rims of cc-dol-particles that are incorporated in the cc-crystal. The intersections of the cc-crystals in thin section correspond with the shape of the cc-rhomboeder or bipyramid of calcite.

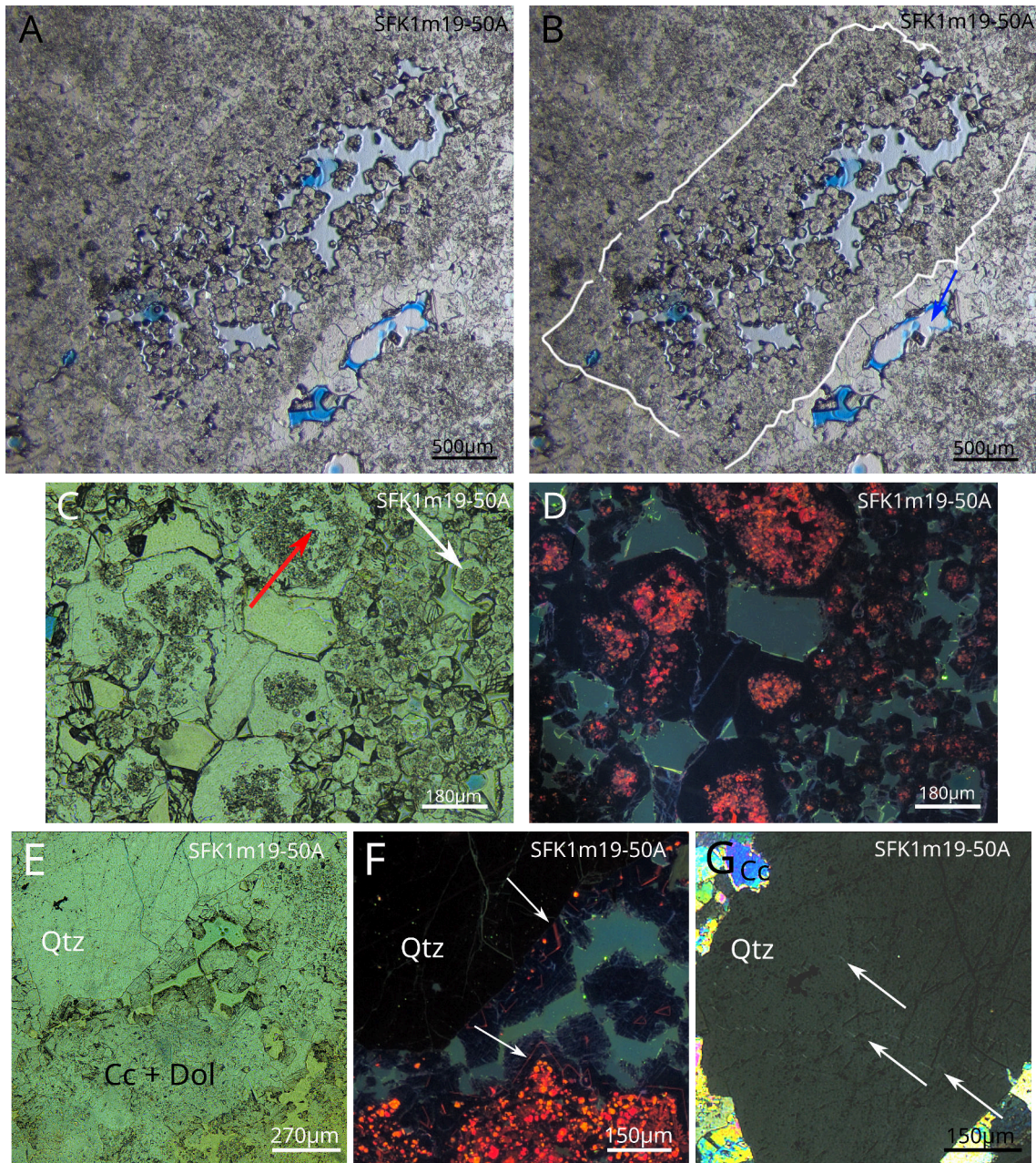


Figure 4.25 – SFK1m19-50A. A, B: Walls of a ?former breccia-clast are encrusted by cc-crystals. The boundary of the cell appears diffuse. Inside the cell grow isometric, euhedral cc-crystals with concentrated rock flour in their cores. Multiphase-growth of cement creates cc-crystal-aggregates. E-G: Picture of qtz-grain with dolose extinction in TL, CL, PL. Away from the qtz-grain, cc is growing in open pore space. Cement is zoned with euhedral seams of cc. G: En-echelon veins in deformed qtz.

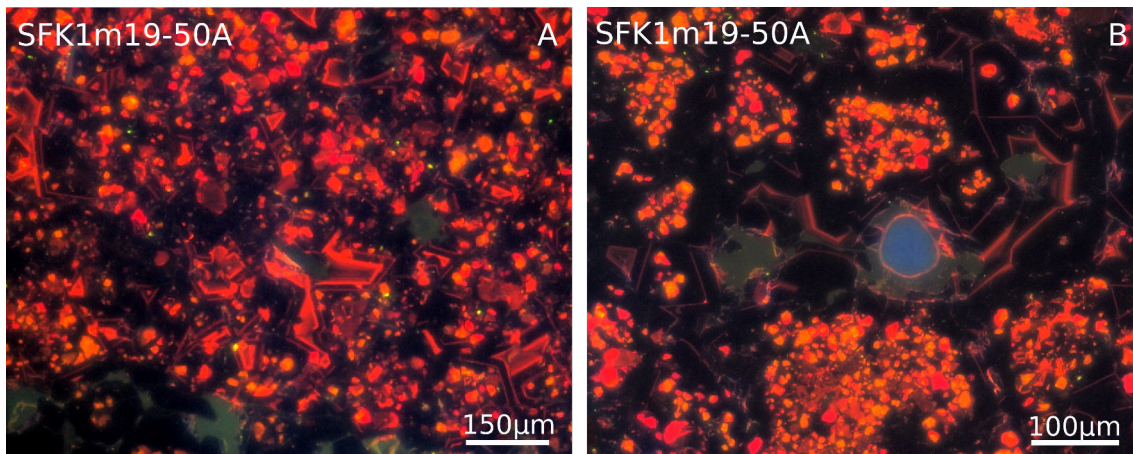


Figure 4.26 – SFK1m19-50A. Various cement-types. A, B: Black cement encrusts cc-single-crystals. A, B: Black cement encrusts cc-single-crystals. A: Note the hooked angles of bright-red cement, encrusting and closing relict pores in the dense portion of the rock. B: Broad, pale-brown seams terminate the cement growth. The pore is protected against further cementation.

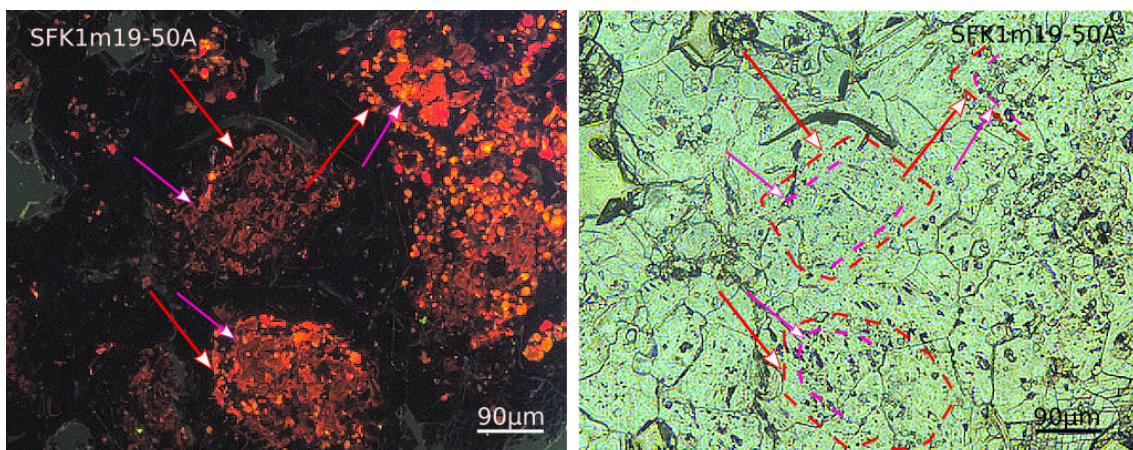


Figure 4.27 – SFK1m19-50A. Concentric rims of cc-dol-particles that only appear in CL. Here, particles encrusted by cc-cement are evenly distributed.

EBSD-Analysis It is impossible to differentiate between cc-rock flour particles in the cc-crystals' cores and the encrusting cc-cement: Cc-particles in the single crystals do not appear on EBSD. Concentric rims of dol-rock flour that are encrusted by generations of cc-cement are visible (Fig. 4.28). Here, the distribution of dol particles is uneven and therefore their portion in the recemented carbonate clasts hard to determine: Cc-cement contributes approx. >80% of the samples main mass.

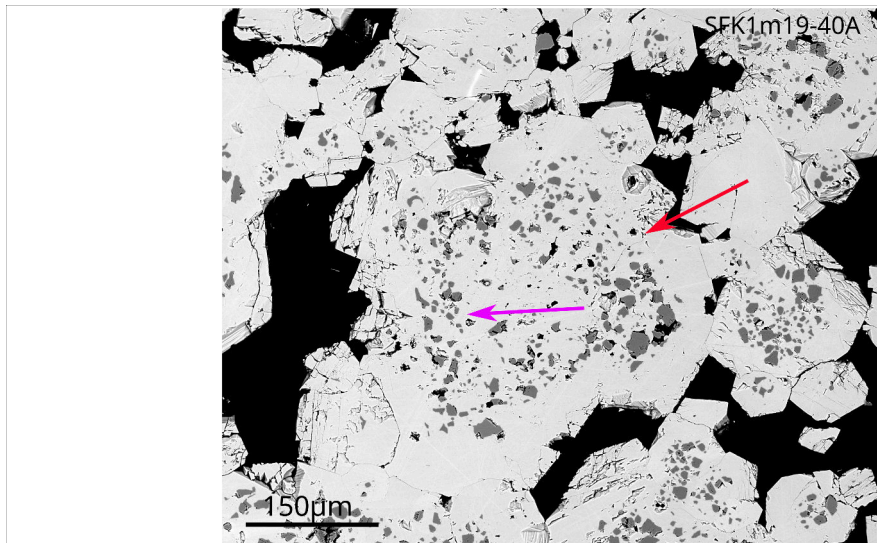


Figure 4.28 – SFK1m19-50A. Rock flour is encrusted by cc-cement. Two concentric rings of dol rock flour particles are indicated by arrows (lilac - inner ring, red: outer ring). Note the fractures at the boundaries of the cc-single crystals. It is unsure, if the fracturing is a artefact of sampling, or caused by a new breakage event.

Interpretation Sample SFK1m19-50 developed in several dissolution-cementation events, following brittle deformation that produced a dilation breccia/tectonic breccia. The main mass of the rock constitutes of different types of cc-cement that encrusts (cc-)dol rock flour. The particles seem to derive from shattered dol-protolith and following dilation of said protolith (for example, comp. with samples SFK1m22-90, SFK1m23-10). The dissolution of shattered dol-clasts creates cells in the breccia, that in turn are encrusted by precipitated cc from passing fluids. The fluids provide further dol-rock flour, that constitutes the cores of the euhedral cc-crystals in cells. Several rims of incorporated rock flour strongly indicate reoccurring fluid-flux events, which in turn can explain the different types of cc-cement, also seen in other samples of this study (comp. SFK1m23-10, Fig. 4.11).

The unsharp, "ghostly" walls of the rocks' cells are interpreted to be the product of repeated fluid flow and dissolution. During continuous fluid flow, the euhedral cc-crystals in cells can grow undisturbed. The concentrically attached rims of rock flour in cc-crystals resemble cockades that supposedly grow in faults and fractures, where great amounts of saturated fluids of different chemical compositions can pass.

4.6 SFK1m18-30

Hand specimen Angular dol-clasts < 5mm protrude out of the matrix. The clasts are incohesive and easily disintegrate when exerting pressure. The matrix is heavily weathered, wet, and according to the HCl test, contains only little cc. In this case, the differentiation between a sedimentary or fault rock is ambiguous. Considering the origin of the rock from a fault zone, it will still be termed as fault breccia with gougy sections.



Figure 4.29 – Hand specimen. Angular dolomite clasts in an ochre-coloured matrix.

Optical microscopy The components in the poorly cemented rock are heterogeneous. Dol-clasts are highly porous and disintegrated into few μm -sized particles that cannot be optically resolved.

The portion of non-carbonatic material is high. The rock comprises qtz-grains (polycrystalline and dulose single-grains) with sutured grain boundaries as well as acicular qtz-grains (Fig. 4.32) and intact to heavily weathered mica-grains. Qtz- and mica-grains are max. $500\mu\text{m}$ in size. Lithic fragments preserving metamorphic foliation are chloritized and < 2mm in size.

Accessory minerals are weathered and cannot be determined by optical methods.

Rare, euhedral cc-crystals with a maximum size of $300\mu\text{m}$ incorporate particles of rock flour (Fig. 4.32A, B). Cc-crystals can be lath-shaped, too. It is unclear whether cc-crystals and carbonate-aggregates grow *in* the breccia or are a breccia-component, deriving from another source rock or cementation event.

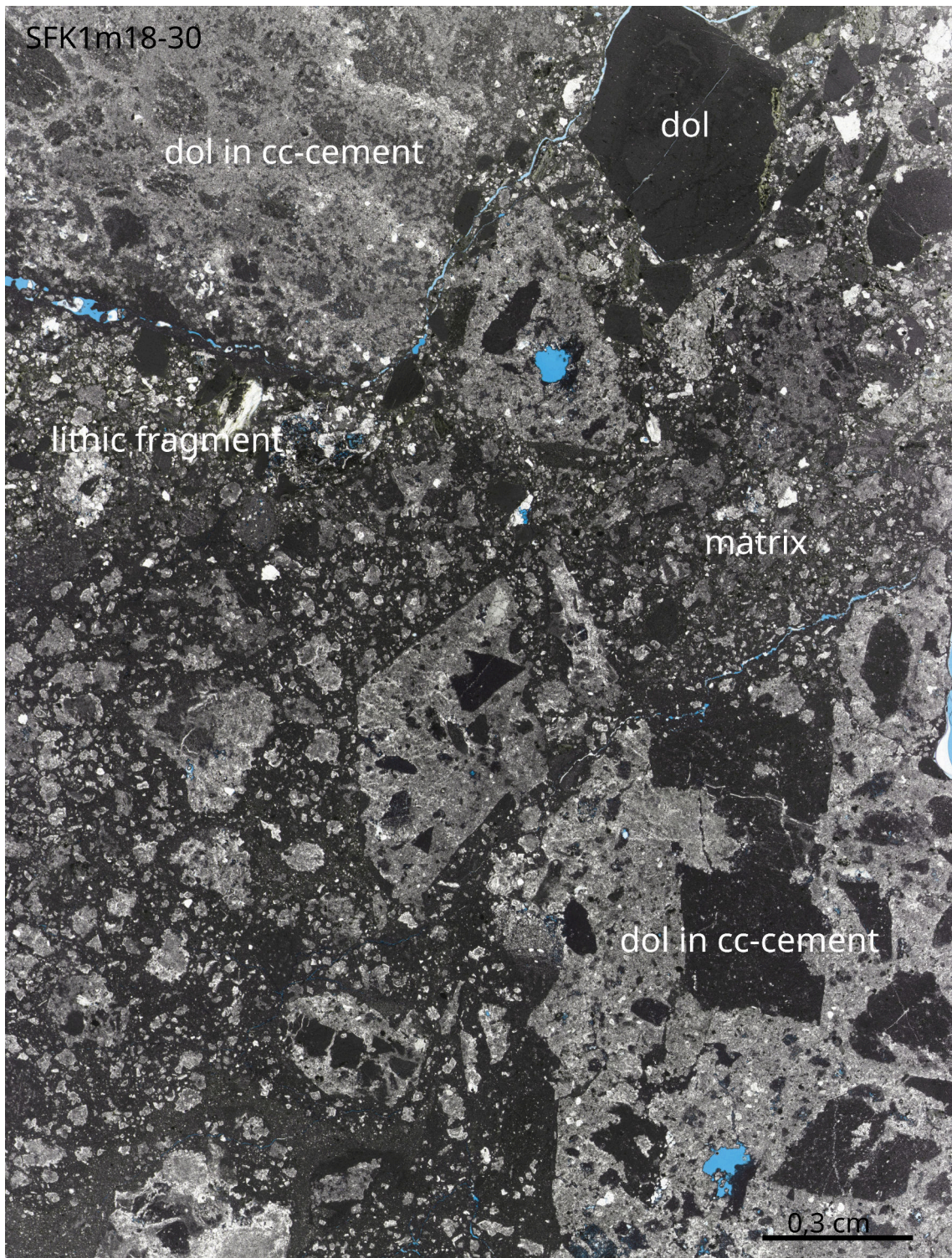


Figure 4.30 – Thinsection scan. Lithic fragments, dol-clasts, dol rock-flour and fragments of ?cellular dol, heavily encrusted by cc, are chaotically arranged. No shear indicators are observable.

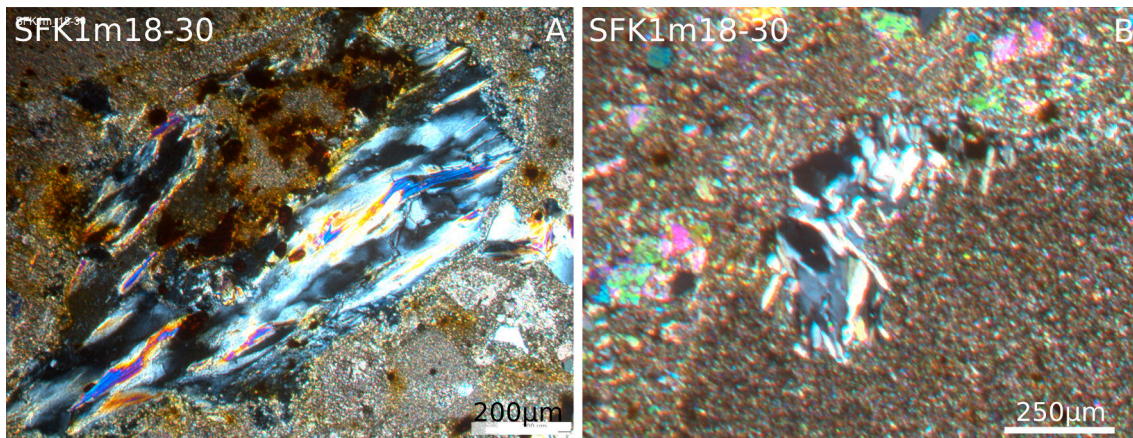


Figure 4.31 – SFK1m18-30. Pictures in PL. A: Lithic fragment from a metamorphic host rock. Between elongated qtz-grains, mica-grains are oriented. Heavy minerals are weathered and produce red spots and cannot be further determined. The matrix is not cemented. B: Needle-shaped qtz-subgrains seem to be replaced by carbonate, which produces irregular grain boundaries.

Cathodoluminescence Dol-clasts and dol-rock flour produce the same bright-red CL-signal. Rhombohedral cc-crystals show polyphase-growth and can be found in fractures as well as in the dol-clasts. The CL-signal of 2 - 3 cc-rims is weak and luminesces in brownish colours (Fig. 4.32A).

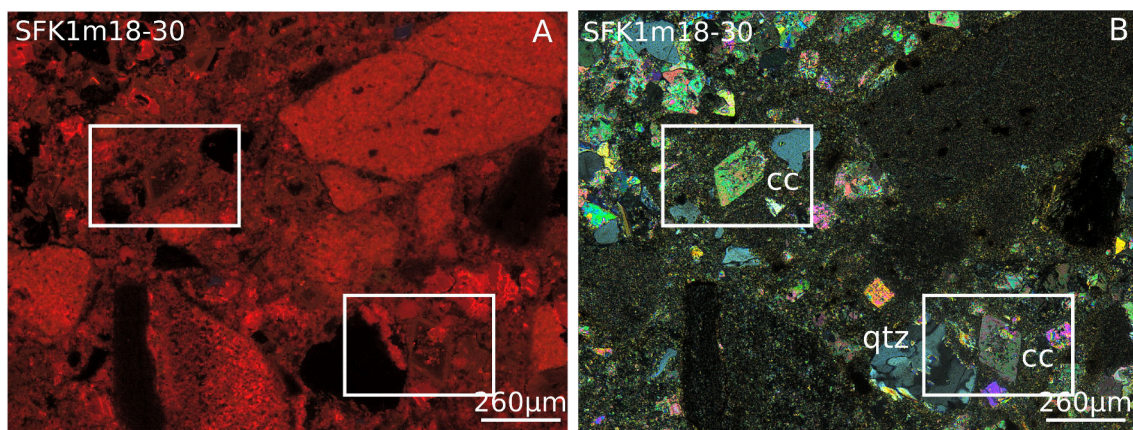


Figure 4.32 – SFK1m18-30. A: Bright-red luminescence signal of dol-clasts. B: Zonated cc-crystals with dol-rock flour in cores (rectangles).

Interpretation Euhedral intact cc-crystals grow at the expense of qtz-grains and lithic fragments in the otherwise uncemented matrix. Neither hand specimen nor

thin section show shear indicators. This, and the heterogeneity of the samples' mineralogy composition would speak for a sedimentary origin of the rock. Still, I want to refer to this rock as fault breccia, considering it to originate from near the core of the fault zone, mapped in the cavern plan (comp. to cavern plan, Fig. 1.2).

4.7 SFK1m17-80

Hand specimen The rock is classified as a tectonic breccia. The sorting of the clasts is better than in sample SFK1m18-30. Grey, angular dol clasts protrude from an incohesive, weathered matrix. The clasts are arranged into a chaotic fabric and range between 1 to max. 7mm. At first glance they seem to be cohesive, but disintegrate when slight pressure is exerted. The newly formed fragments have uneven surfaces. The matrix is ochre-coloured which indicates the existence of Fe-minerals in the protolith or Fe-rich altering fluids.

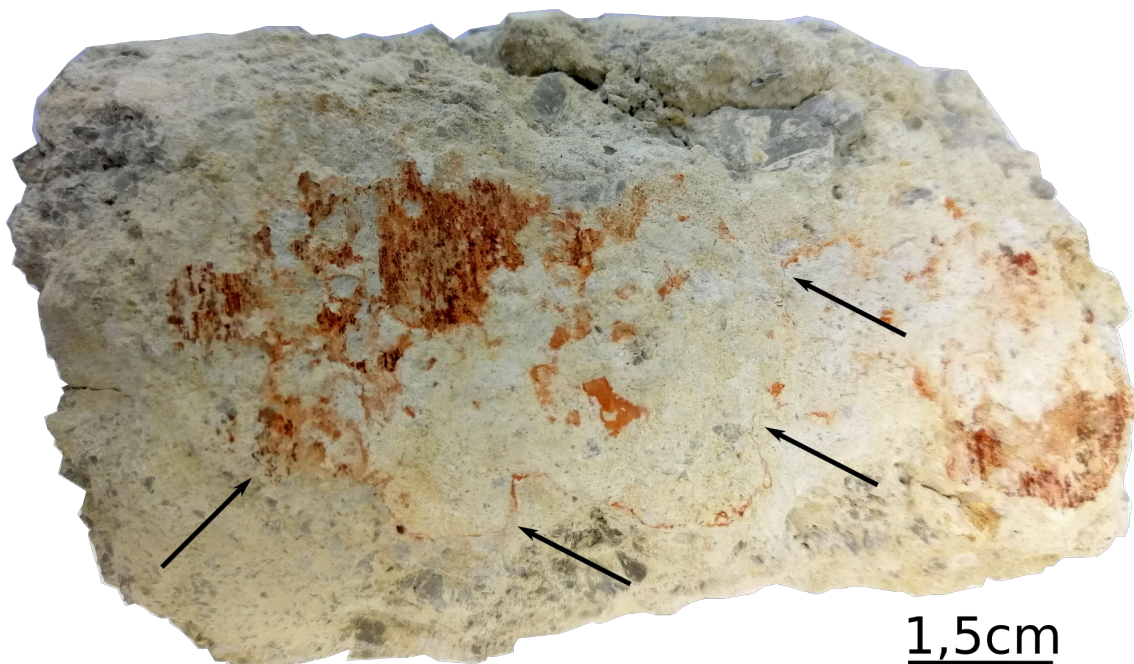


Figure 4.33 – SFK1m17-80. Grey clasts in an ochre-coloured, weathered matrix. Reddish slickensides penetrate the rock; on the striated planes, pressure solution takes place (black arrows): The stylolites are seemingly linked to the slickensides.

The HCl-test confirms small amounts of cc in the ochre matrix (cc).

Slickensides penetrate the breccia. Polished stria are black, even, and are parallel-subparallel. They only penetrate the matrix, but not the clasts.

Optical Microscopy Subparallel veins cut through the shattered dol protolith: The rock is brecciated into subangular clasts, that show no rotation or offset and pre-

serve a fitting fabric (Fig. 4.34). The clasts developed secondary porosity (?through dissolution mechanisms) and are comminuted into optically not resolvable fragments.

No primary sedimentary features are recognizable (Fig. 4.34).

The border between matrix and breccia clasts is not clearly defined and blurry.

Recrystallized quartz grains (qtz) in fractures include poly- and monocrystalline qtz-grains. Grains show dulose extinction and their sizes range up to 1 mm. Only little cementation takes place. Even so, carbonate-bearing fluid led to chemical alteration of the grain boundaries.

The sample can be characterized as clast-supported dilation breccia or fault breccia with puzzle/mosaic fabric.

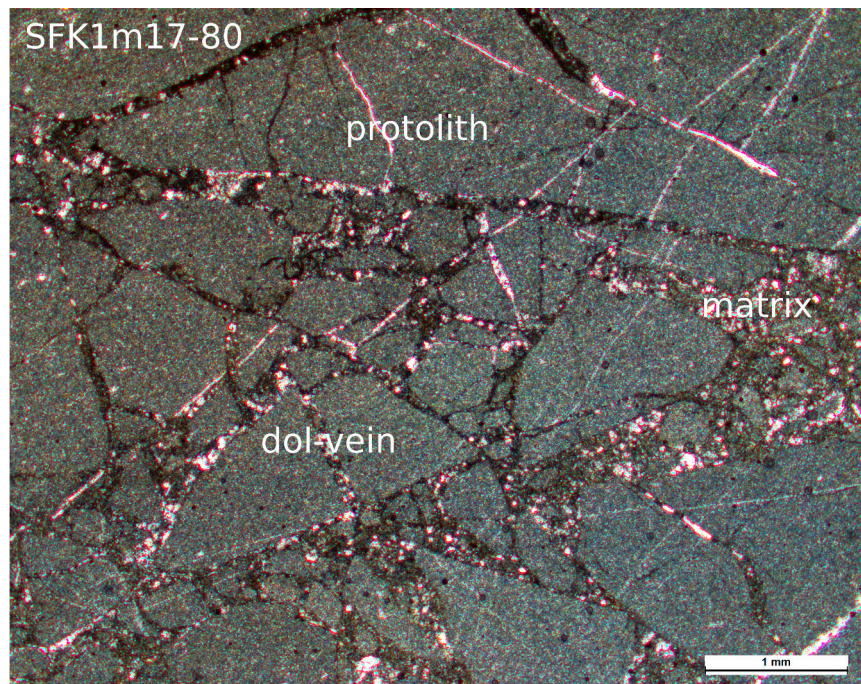


Figure 4.34 – SFK1m17-80. PL-Picture. Fine-grained protolith is penetrated by bright, subparallel- to parallel dol veins. The boundary protolith-fractures is not clearly defined. The brecciated clasts experience little rotation and offset. The fine-grained matrix contains few qtz- and mica-grains, but its main constituents cannot be determined by optical methods.

Cathodoluminescence The dol clasts produce a bright-red luminescence signal. The penetrating veins produce the exact same signal and consist of dol, too. Qtz-grains partly are replaced by the same bright-red dol-cement. Only qtz-grains show solution of its boundaries by dol.

Euhedral cc-crystals grow in the protolith clasts with sizes up to 120 μm (Fig. 4.35). These cc-crystals are zoned and grow in three phases:

1. Non-luminescent cement grows in pores of the dol clasts.
2. Euhedral, brownish cc-seams follow that are several 10's of μm wide.
3. Cementation is terminated by non-luminescing, euhedral black cc-cement seams (Fig. 4.35B).

The euhedral cc-cement type never grows in fractures between the dol clasts, but grows under development of anhedral crystal faces without exceptions.

The main constituent of the matrix luminesces in the same colour as dol clasts. The border matrix-clast, observable in TL, disappears in the CL-picture. It can be reasoned that the shattered dol-protolith clasts progressively disintegrate to form matrix.

Mica and qtz give no luminescence signal (Fig. 4.35D).

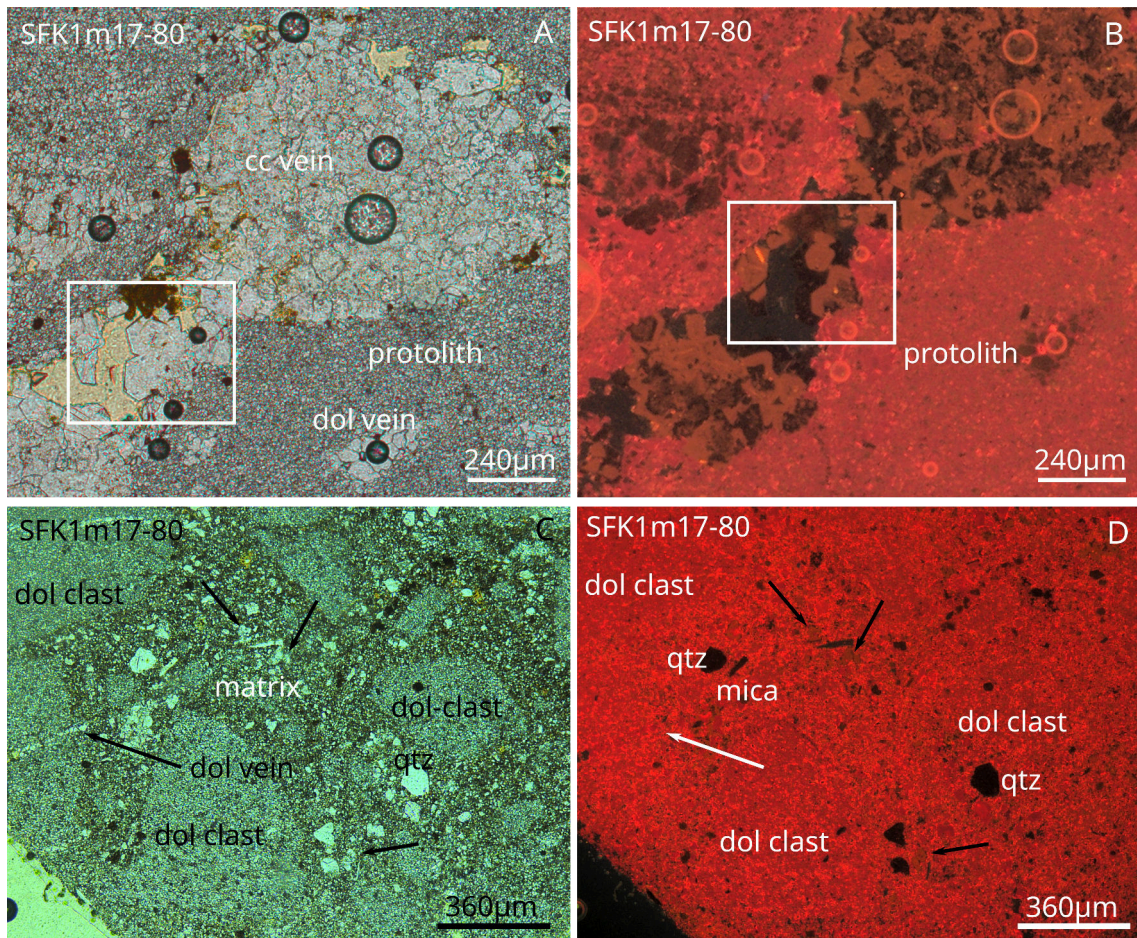


Figure 4.35 – SFK1m17-80. A, B: Cc-veins penetrate host rock, where pores are wide enough, well developed crystal faces grow. In contrast to other samples, cc-crystals do not grow around rock flour. Additionally, clast-penetrating dol-veins are indistinguishable from the clasts' main material (B). C, D: Dol-vein and dol-rock flour in fractures cannot be distinguished from the breccia clasts in CL. The white arrow marks one of the dol-veins, that disappears in CL. Black arrows point towards the rare zoned cc-cement. Qtz and mica produce no luminescence signal.

EBSD Analysis Subparallel veins penetrating the dol protolith are confirmed to be dolomitic, too. Cc-veins in the breccia clasts grow in open pores and develop euhedral crystal shape.

The porosity in the fractures averages up to 50% (Shvetsov, 1954).

The whole rock contains qtz-grains and cc-cement (Fig. 4.36). Dol particles that replace qtz-grains have identical grain sizes and chemistry as the rock flour filling

the fractures between clasts (Fig. 4.36B). Cc-cement partly grows in situ and partly consolidates shattered dol-particles in fractures. Cementation takes place only in a minor degree (Fig. 4.36A, C, D).

Qtz-grains are fractured in situ, particles deriving from the shattering preserve a fitting fabric.

The dol-clasts contain accessory minerals and mica-grains of few μm in size that disintegrate into the fractures, too (Fig. 4.36C). Clasts and qtz-grains disintegrate transitionally into the matrix, explaining the missing colour-differences in CL between clasts and matrix.

Dol-rock flour particles in fractures are slightly rounded and unevenly distributed in cc-cement clusters (Fig. 4.36A, E). In Fig. 4.36E, a thin rim of dol rock flour is concentrated in a layer overgrown by cc-cement. This structure could be the result of gravitational sinking or accumulating of dol-rock flour at the bottom of a pore. Estimates on the porosity of the disintegrated dol clasts yield approx. 10-15%, the porosity of the matrix approx. is 50%.

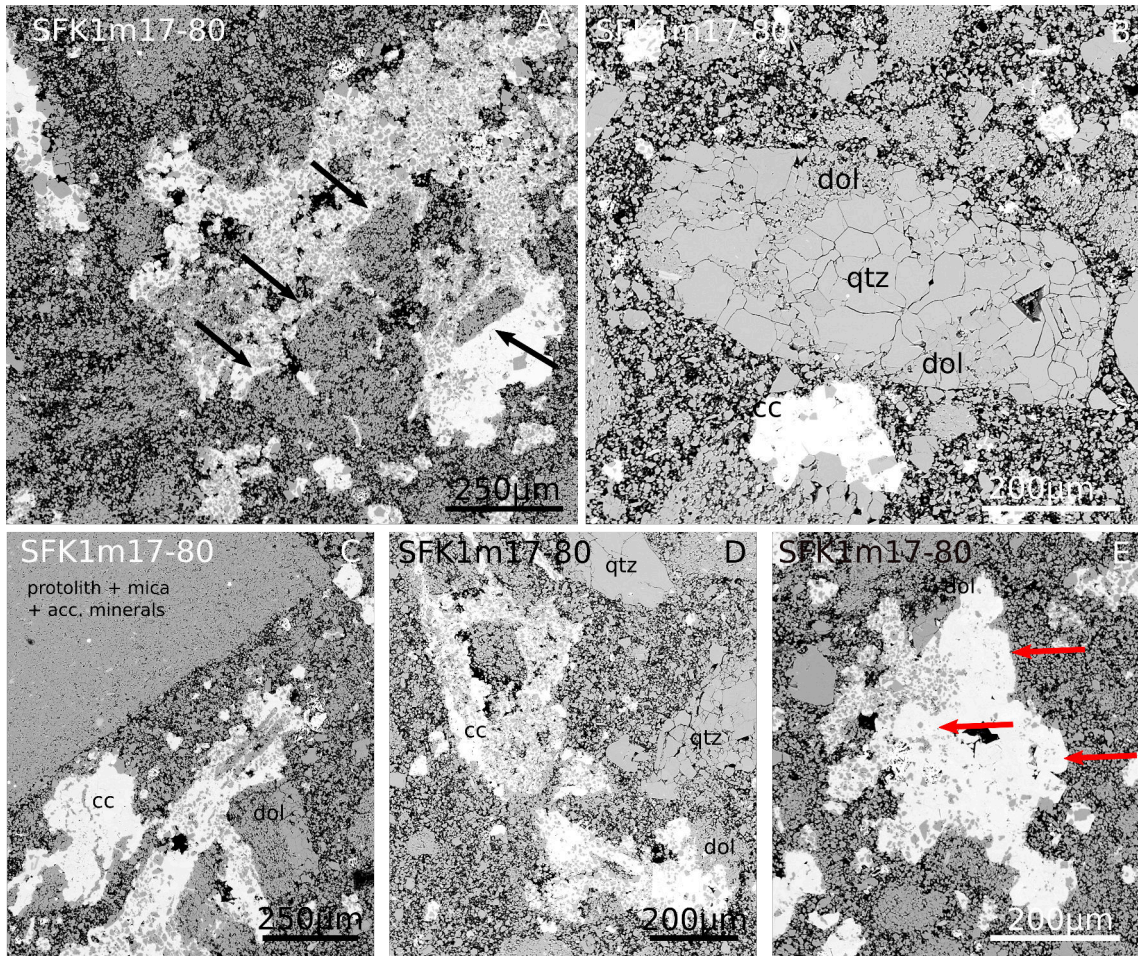


Figure 4.36 – SFK1m17-80. A, D: Shattered clasts of the brecciated rock are partially solidified by anhedral-growing cc-cement. A: Arrows pointing towards shattered dol clasts. B: Polycrystalline qtz-grain is replaced by ?dol-cement. C, D: The dol-protolith clasts are slightly rounded and consolidated by cc. E: Pieces of cc-cement overgrowing rock flour particles that accumulated in the open pore prior to cementation. A rim of rock flour is consolidated by cc-cement (red arrows).

Interpretation The dolostone ?protolith is penetrated by undeformed dol-veins with a similar CL-signal as the protolith's. The event of fluidization took place after the shattering that led to the internal comminution of the rock.

Brecciation and following dilation occur. The breccia clasts experience only little rotation and offset (Fig. 4.33). In the next event, allochthonous mica- and qtz-grains are transported into the fractures. The further evolution of the rock is inconclusive. Qtz-grains partly get replaced by dol-cement of identical chemistry

as the dol-protolith and dol-veins, penetrating the protolith. Only qtz-grains are affected of dissolution by dol and thus were eventually altered before being transported into the fractures. Qtz-grains are shattered into rock flour, too. Why clasts of dolostone-protolith and qtz-grains in fractures are penetrated by the same cement (Fig. 4.35C, D, Fig. 4.36B), but not dol-rock flour *in* the fractures is hardly explainable. The dolostone protolith does not contain any qtz-grains, so the qtz must derive from another source.

Mica grains are not chemically altered.

Euhedral cc-cement with dark-brownish luminescing rims occur in other samples, to a lesser extent.

Cc-cement growing in the dol-clasts differs from cc-cement in fractures. An analogous cement cannot be found in other samples.

Macroscopically, one can observe striated surfaces of the rock. This does not fit with the unnoteworthy rotation and relative offset of clasts that is observable in thin section.

4.8 SFK1m23-70A, B

The fault breccia is clast-supported, with weathered brownish matrix and protruding clasts. The cm- dm-sized carbonate-rich components are compact and cohesive. Mm-sized pores in the clasts are well rounded without visible cc crystals encrusting the walls. Pressure solution seams penetrate the rock in different orientations. Matrix and clasts react to HCl.

Short <50mm slickensides confirm shear deformation. Black, shiny striae appear on the slickensided surfaces as well.



Figure 4.37 – SFK1m23-70. The author paid attention to select a part of the sample containing matrix as well as breccia clasts. The sample is incohesive and the matrix weak. It contains slickensides which are not resolvable on the photograph.

The matrix consists of clay minerals and is easily grindable by the fingers. Its colour indicates weathering of Fe-oxides.

This stained sample was prepared with epoxy resin and sections were chosen, that contain clasts as well as matrix.

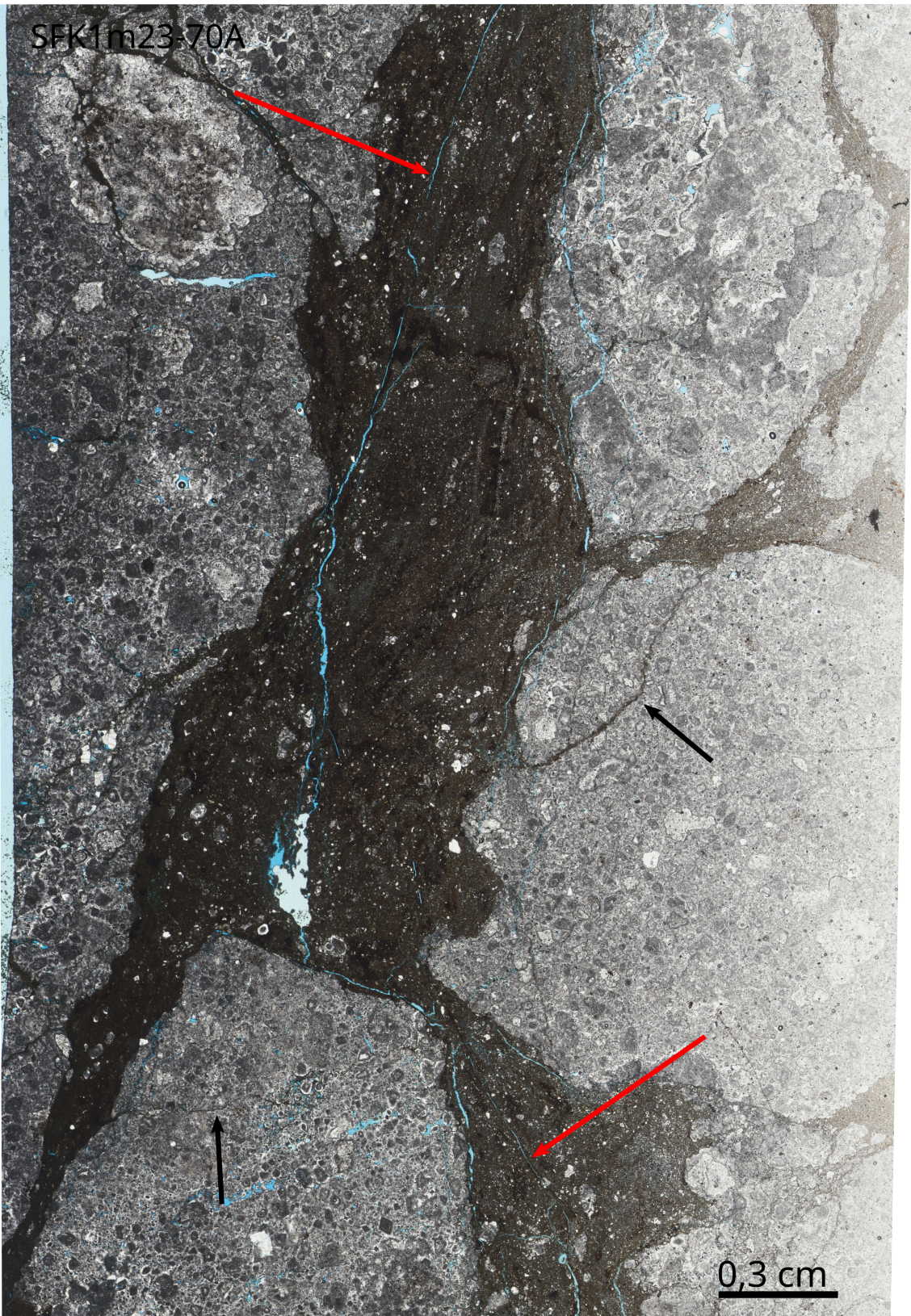


Figure 4.38 – SFK1m23-70A. Thinsection scan. Subangular clasts of recemented carbonatic rock in fine-grained clay-cc matrix. Red arrows mark fractures in the matrix, their arrangement possibly indicates sinistral shear sense. Blue colour indicates pores in the macroscopically dense clasts and matrix. Black arrows: Note dark pressure solution seams, crossing clasts.

Optical microscopy Surfaces at the boundary clast-matrix are uneven due to abrasion.

The clasts consist of cc-cement, encrusting dol-rock flour $< 30\mu\text{m}$ in size. Cc-dol aggregates accumulate, preserving the cc's euhedral crystal faces, but do not follow the habit of cc, thus creating irregular cc-crystal shapes (Fig. 4.39A). Cc-crystals incorporate weakly developed concentric rims of particles of dol rock flour during ongoing crystal-growth (Fig. 4.38). The porosity in the clasts is indicated by blue stain and, compared to other samples, relatively low at max. 20%.

The matrix consists of mica grains, clay minerals, cc-cement- and dol-fragments. The average grain sizes of matrix particles are too small to identify them via optical methods. Sheet-silicates form a foliation. Along the boundary clast-matrix, cc-grains are fragmented and chipping as well as abrasion lead to incipient rounding of the components.

Contrasting to other samples of the study, cc-crystals without cores of rock flour particles partially form recemented carbonatic clasts, but are still overgrown by a rim of dol particles, with the rim not following the crystal habit of cc (Fig. 4.39A).

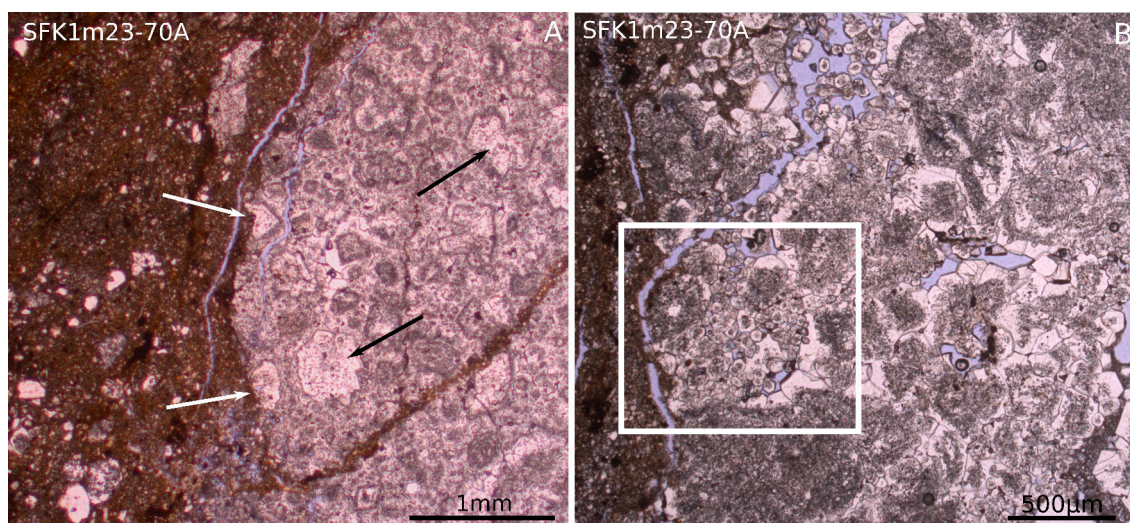


Figure 4.39 – SFK1m23-70A. The boundary clast-matrix. A: White arrows point towards grinded cc-crystals where the carbonatic clast is bordered towards the matrix due to shear deformation. Black arrows: Cc forms euhedral crystal faces, but its shape does not follow the crystal habit of cc. B: A fracture divides clasts from the matrix. Fractures cross the breccia components as well. The rectangle marks pressure dissolution along clasts, cc-grains are partly dissolved.

After the fragmentation of matrix and clasts occurs, no cementation event proceeds. The matrix is entirely uncemented.

Cathodoluminescence Dol clasts in the matrix and dol particles deriving from degraded recemented carbonate-clasts apparently originate from different source rocks. Rock flour particles that act as nuclei to the cc-single crystals in breccia clasts faintly luminesce brown. In contrast, shattered dol incorporated in the matrix intensely luminesces red. This points towards different source areas of the types of shattered dol.

The shattered dol-fragments differ in size, too: Portions of rock flour in the matrix are large enough to be optically resolved, with diameters up to 2 mm. Cc-dol-rock flour incorporated in the porous breccia clasts are fine-grained with diameters of 5-30µm and appear blurry. Mica and clay-grains as well as qtz-grains produce no luminescence signal (Fig. 4.40B).

Neither cc-cement of the clasts nor the cement-fragments in the matrix show luminescing seams. The multiphase-crystal-growth can only be proven by faint concen-

tric rings of rock flour in only some of the cc-single crystals (Fig. 4.39 B).

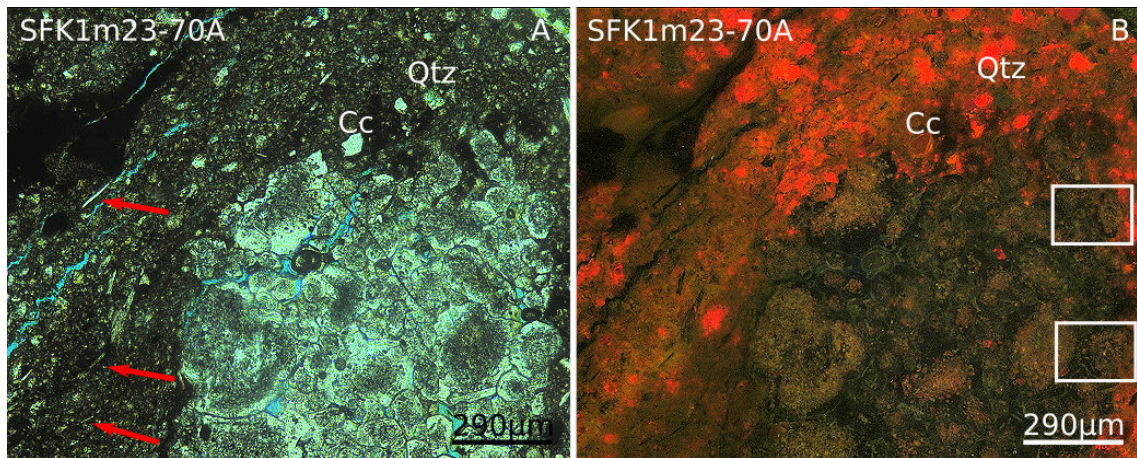


Figure 4.40 – SFK1m23-70A. Image in TL and CL. A: Red arrows point towards the non-luminescent mica grains. B: The luminescence signal of dol fragments in the matrix is bright red. Dol rock flour that is encrusted by non-luminescent cc cement faintly luminesces brown. The matrix is poorly foliated. Rectangles mark abraded cc-crystals at the clast fracture-surfaces.

EBSD-analysis Roughly isometric rock flour particles function as cores of cc-crystals. The fragmented material probably derives from an earlier deformation event. Scarcely, mica grains are incorporated in the recemented carbonatic rock clasts.

Cc crystals in the matrix are fragmented and rounded (Fig. 4.41A, B). Diameters of rock flour particles range from $<1\mu\text{m}$ to $100\mu\text{m}$. Fractures cutting through the comparatively larger dol-clasts follow the cleavage of dol.

In pressure solution seams (Fig. 4.41E), rock flour with grain sizes $< 1\mu\text{m}$, heavy-mineral accessories (mainly FeS_2 , Fe_2O_3 , Fe_3O_4 , TiO_2), mica, or clay minerals in the sub- μm range, are enriched (Fig. 4.41C, D, E). Accessory minerals mainly derive from the shattered dol-protolith, but examples of in situ-growth of Fe-minerals exist, too (Fig. 4.41D).

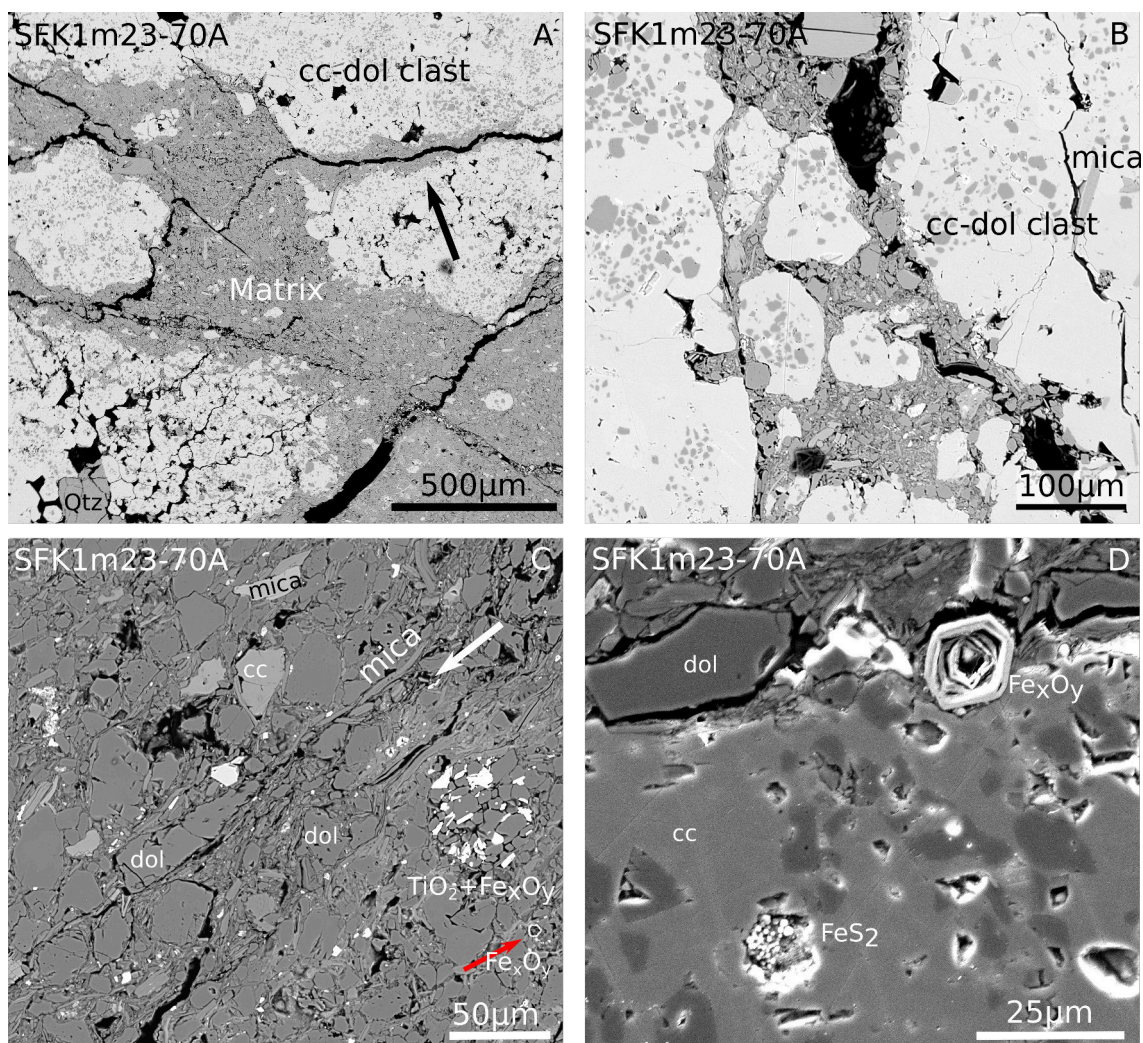


Figure 4.41 – SFK1m23-70A. A: The rock consists of clasts of recemented carbonatic rock and a fine-grained (particles < 50µm) matrix, mainly consisting of clay minerals. Fractures and pressure solution affect both clasts and matrix (black arrow). Sheet-silicates in the matrix are visually aligned. B: (Sub)rounded clasts in matrix. Carbonatic rock clasts contain subordinate cemented mica grains. C: Mica grains degrade to clay, supposedly by a combination of shear and chemical weathering. The white arrow traces likely shear planes. Red arrow: Hematite/magnetite grain. D: Carbonatic rock clast in matrix. In situ grown Fe-Oxide. Pyrite-fromboids grow.

Interpretation The rock consists of cm-dm sized clasts of recemented carbonatic-rock, subordinately, they contain mica. The type of rock occurs in all breccias of this study (comp. SFK1m20-40, SFK1m27-80, Fig. 4.12, Fig. 4.42). The clasts are

affected of fracturing and pressure solution and comparing to other samples, heavily weathered. In the stylolites, mica deriving from the dissolving clasts is enriched (Fig. 4.41A).

An substantial amount of dol-clasts, from 10-100 μ m, and mica of presumably surrounding source rock is sheared into the main rock mass. The dol-clasts show a different CL-signal than dol that partly constitutes the recemented carbonatic rock (comp. Fig. 4.40).

Mica grains in the matrix are poorly aligned and their portions in the matrix unevenly distributed: Parts consisting solely of dol alternate with mica-rich parts (Figure 4.41C).

Following statements can be made:

1. Clasts in the rock consist of recemented carbonatic rock. This rocktype is interpreted to be a fault rock, with the rock flour encrusted by cc-cement (comp. SFK1m20-40, SFK1m18-40, SFK1m19-50, Fig. 4.20, Fig. 4.23, Fig. 4.26). This is indicated by different types of cement and cc-single crystals with dol-rock flour incorporated.
2. The clasts break in a breakage event.
3. Shear deformation causes rounding of the clasts of carbonatic rock and the smearing-into of mica- and clay-minerals.

As a consequence, SFK1m23-70 can be referred to as fault rock (fault breccia with a component of pressure solution), containing clasts of recemented carbonatic rock deriving an earlier deformation event.

4.9 SFK1m27-40A, B; SFK1m27-50A, B

Samples SFK1m27-40 A, B and SFK1m27-50 A, B can be referred to as tectonic breccia or cohesive cataclasite, stylolites indicate a component of pressure solution. The samples are characterized by greyish rounded clasts of recemented carbonatic rock (comp. Fig 4.39), ranging from approx. 10mm - 5cm in an ochre-coloured matrix.

Even though the matrix is heavily weathered and can be scratched by a fingernail, the sample is cohesive when examined in hand.

Sub-parallel, brown pressure-solution seams penetrate the rock. The boundary matrix-clast is sutured.

Along slickensides with a reddish, metallic appearance, the drill core is broken into two pieces. Lithic fragments cannot be macroscopically further determined. Conclusive indicators of shear direction are not present.



Figure 4.42 – SFK1m27-40 and SFK1m27-50. Sutured, greyish carbonatic clasts in a intensely weathered matrix. Arrows tracing the orientation of reddish, metallic appearing slickensides. Unidentifiable lithic fragments are visible.

Optical microscopy The breccia clasts resemble clasts of recemented carbonatic rock in SFK1m20-40 and SFK1m23-70, but are less porous and contain more detrital mica grains in cc-cement.

The matrix is composed of dol-clasts $> 100 \mu\text{m}$ in size and qtz-grains deriving from different source rocks (poly- or monocrystalline fragments, dulose or undulose extinction). Examples of high-strained qtz with abnormal interference colours are abundant (Fig. 4.43A). Additionally, mica grains, crystalline lithic fragments and weathered accessory minerals occur (Fig. 4.43B).

The matrix contains mm-sized euhedral cc-crystals with rings of incorporated dol-rock flour (Fig. 4.43B). Considering the rest of the matrix being completely unce-mented, it is strungly suggested that the crystals are recycled components.

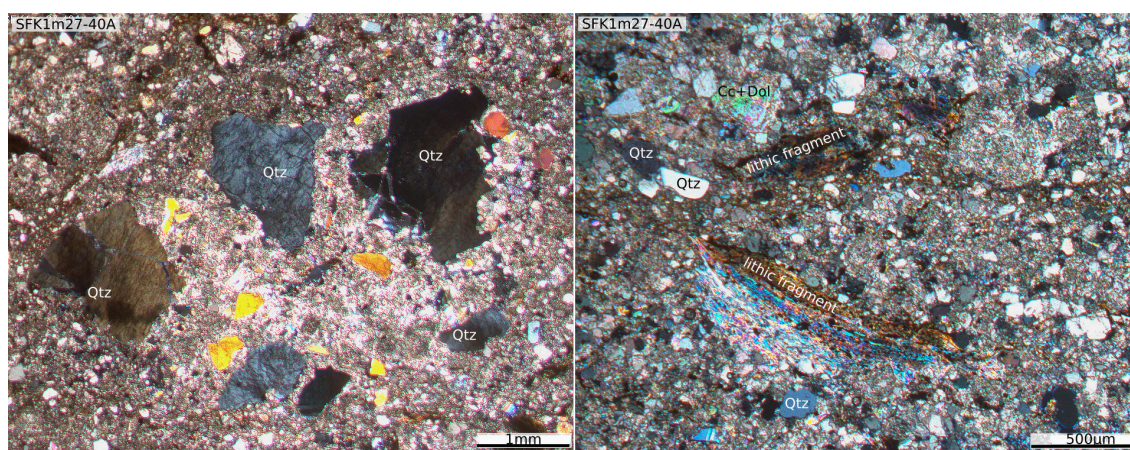


Figure 4.43 – SFK1m27-40A. A: Qtz with ?abnormal (grey-brown-yellow) interference colors. The crystal lattice of the qtz grains is heavily strained. B: Deformed lithic fragments with visible metamorphic foliation. Qtz grains show a dulose extinction pattern. Rectangle: Cc-single-crystal with high interference colours and two rings of shattered dol.

Cathodoluminescence It can be distinguished between two types of dol:

1. Weakly luminescing dol rock flour $< 50\mu\text{m}$ in dark-red colours. The rock flour is chemically altered by supposedly cc-rich fluids (Fig. 4.44B).
2. Intensely luminescing dol $> 50\mu\text{m}$ fragments, colours ranging from orange to bright red (Fig. 4.44B).

Mica grains and dol clasts are poorly aligned in shear bands (Fig. 4.44).

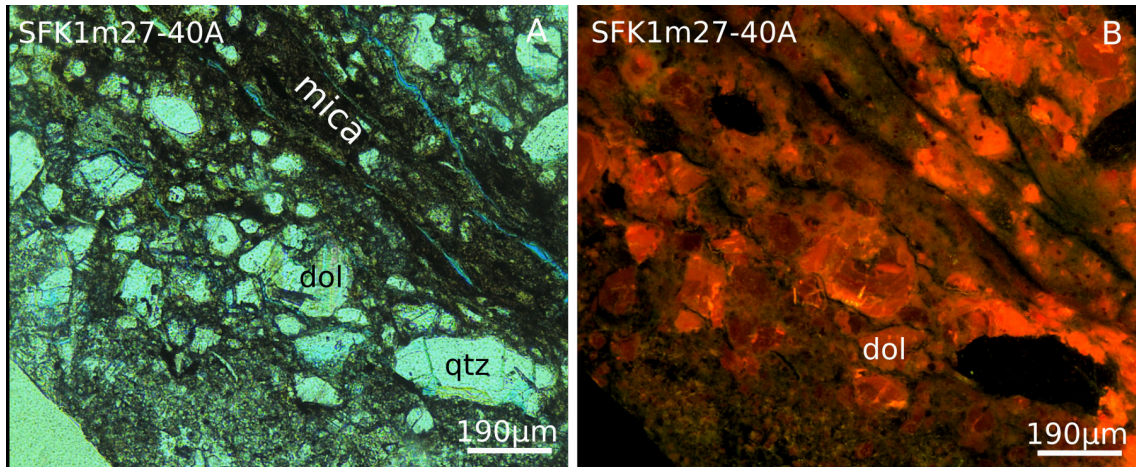


Figure 4.44 – SFK1m27-40A. TL and CL images. A: Clay-minerals and dol are poorly aligned. B: Brownish-luminescing rock flour. Note the heavily altered, orange-luminescing dol fragments.

Mica, clay minerals in altered lithic fragments, and quartz grains do not give any luminescence signal.

EBSD-Analysis Phyllosilicates in the matrix follow a preferred direction. Clasts of recemented carbonate are exceptionally smooth (Fig. 4.45A, B). Subangular dol clasts as well as accessory minerals (Ti-oxides, Fe-oxides) are embedded between weathered mica-grains and clay mineral-grains. Micaceous fragments from weathered carbonate and crystalline lithic fragments are released into the matrix (Fig. 4.45B, C). The porosity of the matrix is low despite the missing cementation of its particles. Sub- μm -sized clay grains manage to fill open space between dol-fragments, cc-crystals, lithic fragments and carbonatic rock-fragments. The porosity is approx. $< 5\%$ and notably less high than porosities noticed in the other samples of this study.

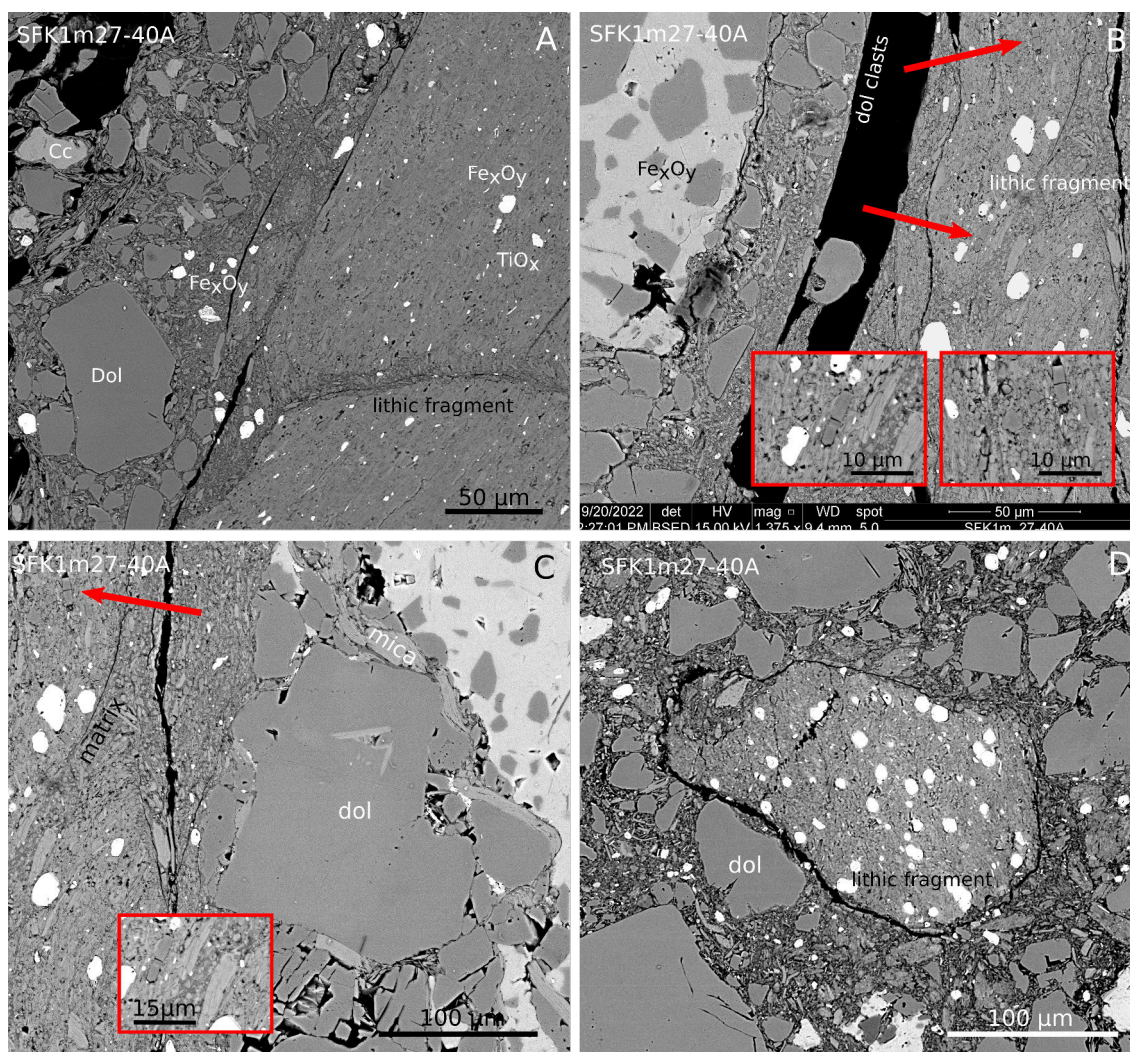


Figure 4.45 – SFK1m27-40A. A: Mica is broken down to sub- μm sized clay grains. Compared to clasts in other samples, the lithic fragment is relatively dense (porosity $< 5\%$). B, left: Accessory minerals in in a carbonatic-rock clast. Rectangles: Dol clasts are aligned parallel to the foliation. Fractures in the dol grains are oriented perpendicular to the foliation plane. C: Mica grains in a breccia clast are gradually released into the matrix. The carbonatic clast contains approx. 20% bright grey dol-particles. D: A lithic fragment with abundant accessory minerals (Fe-oxides, Ti-oxides). The ?metamorphic foliation of the source rock is still recognizable. B, C, D: Note the low porosity of the matrix, caused by sub- μm sized clay-grains being densely packed.

Mica grains do not exclusively derive from ambient sedimentary rocks: Carbonatic breccia clasts and dol-clasts contain little amounts of mica that are progressively

released into the matrix as the clasts are dissolved or broken down. Apparently, deformation leads to the degradation of mica grains into clay minerals (Fig. 4.45C). Altered phyllosilicates are enriched in pressure solution seams. It can be assumed that intense pressure solution must have occurred to achieve the high portions of mica in the stylolites.

Lithic fragments are heavily altered and mainly consist of chloritized phyllosilicates, as well as 10s of μm -sized qtz grains (Fig. 4.43B, Fig. 4.45D).

Samples SFK1m27-40 and SFK1m27-50 are the samples with the most indicative shear indicators and slip planes and best-developed foliation in the matrix and therefore different from all other samples of this study. The samples' deformation history is similar to SFK1m23-70. Following statements can be made:

- Breakage of recrystallized carbonatic rocks to dm-sized fragments.
- Carbonatic- and crystalline lithic fragments from surrounding source rocks are sheared together. Rounding of the clasts occurs.
- Dissolved/weathered fragments of recrystallized carbonatic rocks release mica grains into pressure solution seams and fractures and matrix, where they are partially degraded to clay grains. The weathering of phyllosilicates eventually causes the low porosity in the rock.
- Shearing of the rock allows the formation of well-developed foliation in the mica and clay grains in the matrix.
- No final cementation occurs.

Chapter 5

Discussion

5.1 Grain size reduction via pore fluid pressure or mechanical processes?

Several springs in the Auebachtal confirm large amounts of mountain-water that flow in the area of the Grasberg-Schlagl-fault zone (Göstritz spring, Auebach springs, Hirsch spring, Palka spring) (SBT-Baulos, 2010). In the Semmering-tunnel, high fluid flow requires constant drainage. In the samples, recementation of particles deriving from shattered dol-protolith by cc-cement took place. The cc presumably precipitated from the mountain water.

It is possible to raise objections that the admittedly complicated and heterogeneous appearance of e.g. SFK1m23-70 does not result from mechanical fragmentation processes but the deposition of detritus deriving from different source areas and source rocks. Strain markers, if abundant, are ambiguous, the samples are very heterogeneous in terms of mineralogy, and lithic fragments such as quartz originate from many different source rocks. In hand specimen, the matrix appears brownish-ochre, and in thin section one can observe the alteration from mica to clay- and chlorite-grains. It cannot be denied that to some extent, weathering caused alteration, accompanied with the disintegration of the rock. Still, we reason that in the area of the mountain Semmering, mechanical processes were the main contributor to the comminution of rocks into μm -sized particles ("rock flour"), instead of hydraulic processes, where pore fluid pressure exceeds the tensile strength of the rock.

Key characteristics of dol in fault zones are:

1. Dolostone is a more brittle rock than limestone, and can accommodate less strain before breakage. Strain in dolomite preferably creates a network of interconnected, small fractures instead a major plane of failure as in limestone (Schröckenfuchs et al., 2015). Fractures exhibit a preferred orientation that is linked to the master fault. Faulting in dolostone creates smaller fragments than in limestone.
2. Dolostone is less soluble than limestone (Liu et al., 2005) and less susceptible to twinning and pressure solution. Dolostone accommodates strain without being able to release it through intracrystalline deformation. Eventually, this leads to easier shattering of the rock (Passchier and Trouw, 2005).
3. Dolomite remains longer in the brittle regime than cc. Recrystallization of cc can start at near surface conditions with the development of twins, whereas dolostone requires temperatures $> 300^{\circ}\text{C}$ (Passchier and Trouw, 2005).

Tarasewicz et al., 2005 and Schröckenfuchs et al., 2015 describe that mechanical fracturing causes fragments in breccias to be arranged into a configuration that corresponds to the overall deformation orientation observable in the outcrop. They conversely conclude:

1. Hydraulic fracturing does not cause fragmentation of protolith into smaller clasts, that are arranged in preferred orientation. Further evidence of hydraulic fracturing would be:
2. Cementation of in-situ fragmented rock, as fluids penetrate microscopic cracks in the protolith and cement them.

In this study, the orientation of fractures in the rock mass where the drill cores were obtained could not be measured. Therefore, it cannot be verified whether the first statement also applies to the samples of this study.

Indisputably, the partial recementation of fractured rock is evidence of the presence of cc-saturated fluids that penetrated the rock volume (comp. Fig. 4.2). But did

these fluids penetrate the rock and cause the intense fragmentation? Or are the fractures product of an deformation event before the infiltration of fluids?

Samples SFK1m17-80 and SFK1m22-90 may be suitable for discussing this question.

The samples share following features:

- Both samples are brecciated, but their matrices' are re-cemented to different extents (comp. Fig. 4.34, Fig. 4.2).
- The protolith consists of dol.
- The breccia clasts are shattered into μm -sized particles and incohesive.
- Breccia clasts preserve a fitting-mosaic fabric, and in the case of SFK1m22-90, sedimentary features are preserved (see Fig. 4.2).
- No cement-growth is observable in the initial microscopic fractures. Subordinately, the tiny fractures are cemented with cc.
- Portions of rock flour deriving from protolith clasts are encrusted by vein-cement and therefore must descend from a breakage event *prior* to fluid influx.

Missing calcite cement in the initial fractures points to mechanical breakage of the main rock volume.

The fractures get filled with calcite cement, but the extent of cementation is very low. While the first basic assumption of Schröckenfuchs et al., 2015 cannot either be confirmed or ruled out, it is certain that brecciation of the rock occurred first, and was *then* followed by fluid flow and precipitation of calcite cement. So hydraulic fracturing as a mechanism for the genesis of the finest-grained dolomite portions can be ruled out.

Therefore, we prefer mechanical fragmentation as an explanation for the existence of rock flour in the sampled rocks (Gibowicz, 2009). I suppose that initially, fractures in host rock were rapidly opened. Dilation was then succeeded by fluids penetrating the rock and precipitation of cement.

For further reading, several studies by different authors address the topic of comminution of rocks into smaller grain size fractions and discuss mechanical versus hydraulic fracturing in detail (comp. Schröckenfuchs et al., 2015, Bauer et al., 2016, Kaminskaite et al., 2020).

5.2 Did rock pulverization occur along the Grasberg-Schlagl-fault zone?

The samples SFK1m17-80, SFK1m22-90, and SFK1m23-10 display some features, that eventually could be associated with being the product of rock pulverization (in the strict sense after Dor et al., 2006 (comp. Section 2.6 Pulverized rocks):

- The rock is comminuted into μm -sized fragments, arranged in a crackle- or fitting fabric, that attest in-situ fragmentation of the protolith. Partially, the primordial fabric is reduced into a mosaic-fabric and chaotic fabric.
- Clasts on the macro-scale display a fitting fabric too, as seen in SFK1m22-90 (comp. Fig. 4.1). Here, the lamination of the dolostone-protolith is preserved, despite the rock being entirely disintegrated into mm - μm -sized clasts.
- In hand specimen, most samples neither show considerable rotation or translation. Presumably, only fluid flow or rock load/overburden of the mountain range can act as an explanation for the small amounts of disordering the fitting breccia clasts, considering pressure solution and the missing shear indicators (comp. sample SFK1m23-70A, B).
- The drill core shows a multitude of (e.g. SFK1m27-40, SFK1m27-50, and SFK1m17-80) small, subparallel and partly oxidized slickensides that penetrate the rock. This indicates ?late shear deformation that the otherwise uncemented rock has experienced.
- On the surface, outcrops of cohesive rocks that yet easily crumble when exerting slight pressure are recorded. Even mm-sized clasts break into μm -sized, angular polyhedral particles with even fracture surfaces ("pulverized rock", more generic "rock flour").
- Evidence for tectonic activity in the area is documented extensively. Examples for tectonic movement are horizontal slickensides in the Adlitzgraben area along the contact zone between Rauchwacke and Muschelkalk (signatures 104

and 101) or sheared-into fragments of lower-triassic Muschelkalk in the stratigraphically overlying Rauwacke-strata (see Tollmann, 1957). Unfortunately, Tollmann interpreted the genesis of the cellular dolomites incorrectly).

Nonetheless, I prefer to use the more general terms "shattering" or "rock burst" when discussing the process accountable for the genesis of rock flour. Although the intense fragmentation into polyhedral particles, the fitting fabric of the clasts and particles of rock flour, and the complete lack of cohesion of the rock in hand specimen are present, and thus the studied samples share some characteristics with rocks proven to be actual pulverized rocks, here none of the processes necessary for pulverization can be definitively proven.

I will argue this as follows. The process of "rock pulverization" was introduced in Brune, 2001's paper and is now accurately defined (comp. Section 2.6). Today, there is consensus in the seismotectonic community regarding three possible ways to create this rock type: rock burst, dynamic unloading, and impact crater shattering. As mentioned in the Fault rock chapter, I exclude an impact event as the cause of the intense fragmentation in the analyzed samples for self-evident reasons.

In a bachelor's thesis from the University of Vienna (Mohideen, 2020), pulverized rocks were described in an outcrop at Göstritzgraben. Outcrop investigation and microscopy confirmed that pulverization in the strict sense had definitely overprinted the crystalline rocks of Mohideen, 2020's study.

It is tempting to assume that the samples in this study were deformed in pulverization as well. However, the merely examination of hand specimens and EBSD images is not sufficient to prove that the other two processes did take place. If carbonate rocks from surface outcrops, which are comparable to actual pulverized rocks (i.e. similar microscopic properties) and these in the drill core-samples are studied, one can confidently argue that subsurface slivers of pulverized carbonate have been preserved in the Grasberg-Schlagl-fault zone as well.

Additionally, some of the observations do not align with the theory of pulverization. Sample SFK1m17-80, which most closely resembles pulverized rock from a microscopic perspective, exhibits slickensided surfaces indicating slip displacement. The sample is so contradictory that it would not be legitimate to argue for pulverization of the rocks.

5.3 Growth of calcite-dolomite-aggregates as initial cockade-cores?

Euhedral calcite crystals with rock flour particles in the cores exhibit single or multiphase growth. Frenzel and Woodcock, 2014 and Berger and Herwegh, 2019 propose that rapidly flowing fluids can provide enough energy for particles in the μm -size range to float in suspension. The authors assume cockade breccias to be the result of crystal growth during seismic and interseismic phases; some cockades growing to up several cm in diameter. There are only few studies on cockade growth (comp. the extensive work of Masoch et al., 2019), and the described examples in the literature are usually over > 1 cm in size and have been rarely investigated microscopically.

Dill and Weber, 2010 postulate that in cockade breccias, high concentrations of fine-grained sediments and particles (at least 20%) should be visibly present. In existing literature, such high concentrations are usually not observable.

I would like to note that the samples examined in this study do indeed contain the required fine grained particle portions, according to Frenzel and Woodcock, 2014.

Dill and Weber, 2010 postulate that high concentrations of fine-grained sediments and particles should be visibly present in the cockade breccias, but this is typically not observable. Here, I would like to note that the samples examined in this study do indeed contain fine-grained material, ranging from approximately 20-50 μm , in the proportions required by Frenzel and Woodcock, 2014.

Gaskell, 1992 derived equations for the minimum velocities of low-viscosity fluids needed to bring cubic, roughly isometric, bodies into suspension. Eichhubl and Boles, 2000 use these equations to calculate the minimum velocities of approx. 10^{-3} m/s at 100°C needed for fluidization of particles in the size range of 62 μm . Considering the average width of cc-twins observed in the veins of sample SFK1m22-90 (approx. 35 μm , bent twins, see Fig. 4.4) I assume the temperature of the cc-bearing fluid that caused the precipitation of the twinned cc-cement to have been $> 100^\circ\text{C}$, so the necessary fluid velocity for the fluidization of rock flour particles in the sample could be even less than Eichhubl and Boles, 2000' estimates.

These rough estimates cover the fluid-velocities that are necessary to bring densely packed sediment particles in suspension and therefore apply for high-viscosity fluids

that Dill and Weber, 2010 deem necessary for the genesis of cockades structures. Once fine-grained particles are no longer in dense suspension and therefore no longer interfere with each other through friction, Gaskell, 1992' equations cannot be longer used. In the case of a fluid bearing only little amounts of rock flour particles, it would be more appropriate to apply Stokes' law to calculate the minimum fluid flow velocities that are required to keep *single* particles in suspension (Demtröder, 2014).

$$\bar{v} = \frac{2}{9} \frac{\rho_p - \rho_f}{\mu} g R^2 \quad \begin{cases} \rho_p > \rho_f & \implies \vec{v} \text{ vertically downwards} \\ \rho_p < \rho_f & \implies \vec{v} \text{ vertically upwards} \end{cases}$$

Where \bar{v} = vector quantity of fluid velocity in [m/s]

ρ_p = mass density of the particle [kg/m³]

ρ_f = mass density of the fluid [kg/m³]

μ = dynamic viscosity of the fluid [kg/m³]

g = gravitational field strength [m/s²]

R^2 = radius of the spherical particle [m]

The settling velocity again represents the lower limit of the necessary velocities for suspended particles.

But the problematic aspect in calculating the required conditions of the fluids is to find the dynamic viscosity μ of calcite-saturated mountain water. The saturation of cc in water can either be proportional or invers to increasing temperature of the solvens (Barrier, 2022), depending on additional chemicals in the fluid. Therefore, the density of said fluid that depends on the cc saturation of the water, is hardly predictable (Loos et al., 2004). With already two uncertain factors, it is impossible to give more accurate estimates about any fluid flow velocities: Except for the fact that flow velocities do not need to be *high* in order to keep the particles in suspension, no further statements on actual velocities can be made.

According to Eichhubl and Boles, 2000, the fluid flow velocity required to fluidize particle sizes in that size range, i.e., to bring them into suspension, is only 10–2 m/s, and according to Gaskell, 1992, even lower velocities are required to keep them in suspension.

In contrast, Frenzel and Woodcock, 2014 exclude that continuous fluid flow is able to provide enough energy for cockades to grow in steady suspension. Instead, they suggest that pulses of fluid, caused by seismic activity, can only temporarily bring cockades into suspension but not long enough for the cement growth rings to form. Instead, they consider the rotation-accretion hypothesis as an explanation for the genesis of cockades.

Observations made in this study support the following statements. The euhedral cc-single crystals observed in almost all samples exhibit growth rims of calcite cement and rings of fine rock flour particles, which concentrically attach to those crystals, indicating growth in multiple stages (see samples SFK1m18-40, SFK1m19-50, SFK1m22-90, and SFK1m23-10). The crystals, with diameters as small as 300 μm , show up to two rings of rock flour and additional euhedral cc-cement growth rims of different chemistry. The cockade structures in Frenzel and Woodcock, 2014s' publication comprised several cm, as opposed to the μm -sized cc-single crystals with several cement seams and incorporated rock flour of this study. I propose that the observed structures are cockade structures in an early growth stage as well, for the following reasons:

- Observed cement seams grow isometrically-euhedral after the habit of calcite. They are even, and overgrow cores of rock flour particles on all sides and build complete crystal faces.
- The cores of rock flour are isometric as well and show nowhere just one-sided overgrowth of cc cement.
- Rock flour particles in the calcite single crystals exhibit uniform thickness on all sides and show no signs of preferential deposition on the crystals due to gravity. If rotation of the cc-dol-aggregates had occurred, one would expect to observe rings with differently oriented thicknesses (comp. with Frenzel and Woodcock, 2014 and Masoch, 2018).

Indications of gravitational settling are only observable in veins in fractures (see sample SFK1m22-90 and SFK1m23-10) and in cc-single-crystal aggregates (that build the recemented carbonatic rock, another type of fault rock. See sample SFK1m20-40). These aggregates consist of μm -sized cc-dol-single crystals that are enveloped

and encrusted by "terminating" calcite cement. These aggregates are several cm in size and actually exhibit one-sided rings of incorporated rock flour particles, which I interpret to have settled during low fluid flow velocities in interseismic periods (after Berger and Herwegh, 2019).

Interestingly, the best-developed cockade-"crystals" appear in cells of the former dilation breccias, now cellular dolomites (comp. Fig. 4.10, Fig. 4.11), making the deformation history of the cellular dolomites once again more complex (see Fig. 5.4).

5.4 The problem with „cellular dolomite“ in the area of the intermediate access Göstritz

As mentioned in the introduction, the scientific community is not in agreement on how to distinguish cellular dolomite; a fault rock type, from sedimentary "Rauhacken", with extreme positions of some geologists denying the existence of sedimentary Rauhacken altogether. Based on the new analysis of this studies' samples, the author aims to contribute to the discussion:

In the past, it was tempting to classify Rauhacke, which is admittedly conspicuously common in Triassic evaporite horizons throughout Europe (Swiss and Austrian Alps, Jura Mountains, Carpathians, and many more), as sedimentary rocks (Tollmann, 1963).

Leine, 1969 distinguishes between Rauhacke of pseudoconglomeratic structure, in which rounded components are present in a (recrystallized) matrix, and the breccia-like type, in which polygonal rock fragments fit "puzzle-like" between thin, calcitic septae and whose original dolomitic chemistry remains intact. The author was able to make similar observations in the samples SFK1m22-90 as well as SFK1m23-10, possibly SFK1m19-50 and SFK1m18-40.

Thus, Leine's work describes as early as the 1960s a rock type that is identical to cellular dol in carbonatic units in the Semmering area. Tollmann, 1963 does not consider the tectonic origin of cellular dolomite, even though he recognized this rock type as the tectonic base of the Adlitzschuppe (Tollmann, 1987). Still, he regards cellular dol as sedimentary rock and places it stratigraphically in the Lower- (or

Middle-) Alpine Trias (the concept of a Middle-Austroalpine is outdated today, see Schmid et al., 2004). This assumption can be quickly dismissed, as there are known horizons of cellular dolomite crosscutting sedimentary strata (Kellermann, 2008 speculates about this). In the 105 Neunkirchen map, these horizons can be traced well along known fault planes (Herrmann et al., 1992). Therefore, we follow Leine, and exclude the sedimentary nature of the investigated rocks found in the Grasberg-Schlagl-fault zone of the Semmering area. This master's thesis presents new microscopic investigations that describe the evolution from tectonic- or dilation breccia to cellular dolomite. The sequence of events can be summarized as follows:

1. Intense fragmentation or shattering of dolostone due to seismic activity along the Grasberg-Schlagl-fault zone with the protoliths' sedimentary features remaining intact. The product of this disruption is the rock flour common in the samples (Fig. 5.4).
2. Brecciation and dilation of the shattered rock. The amount of dilation and volume expansion is low and the degree of breccia clast-rotation varies (Fig. 5.4).
3. Influx of calcareous mountain water (Fig. 5.4).
4. Clasts get either enclosed by cc-cement and therefore protected of dissolution or are completely dissolved, the dissolution creating the characteristic angular cells. Rock flour of the shattered breccia clasts gets elevated in suspension (Fig. 5.4).
5. Rock flour particles are encrusted by cc-vein cement at elevated temperatures, indicated by broad twin lamellae (Fig. 5.4). The decelerating fluids do not provide enough energy anymore to keep the particles in suspension and geopetal aggregates form.

In Fig. 5.4, "cockades" that grow in a cell are displayed. CL revealed, that the calcareous mountain water is both responsible for the growth of cockades with rock flour particle cores as well as the growth of wall-encrusting cc-cement.

The cellular dolomite appears to have undergone later brittle deformation as well, with occasionally observed fragments of cement being re-cemented elsewhere (indicated in Fig. 4.11C, D).

In Fig. 5.4, the proposed deformation steps are illustrated:

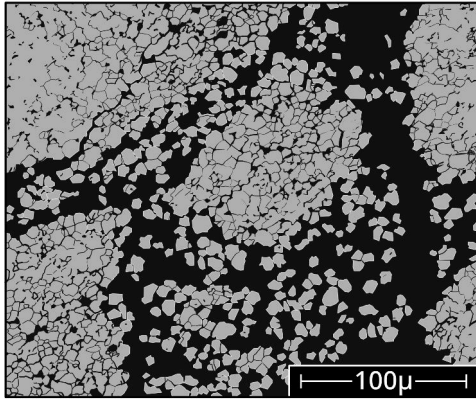


Figure 5.1 – A rock comminuting process creates micron-sized polyhedral particles of dolostone-protolith that display a fitting- to mosaic-fabric.

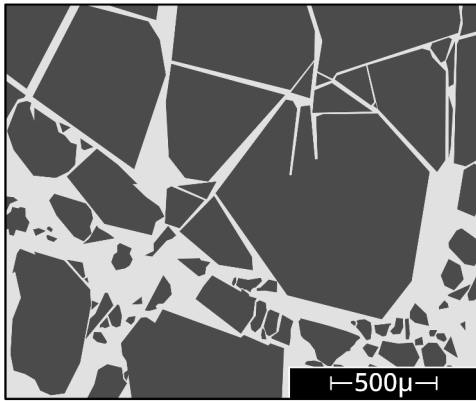


Figure 5.2 – The disintegrated rock gets dilated into angular breccia clasts. Fractures open. Only little clast rotation or transport occur.

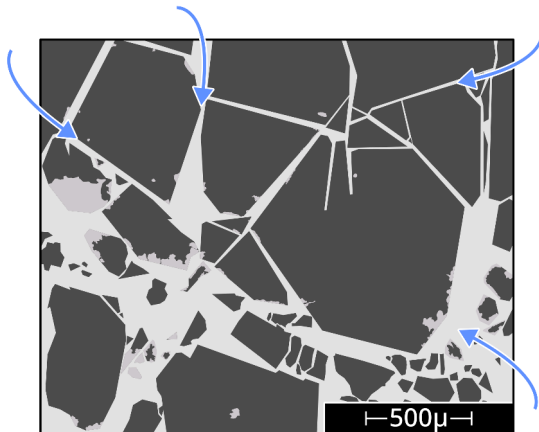


Figure 5.3 – After brecciation, fluids penetrate the rock volume via the newly formed fractures. Fluids are enriched in cc and penetrate the breccia clasts where precipitated cc in the shattered rock clasts takes on "cloudy" forms.

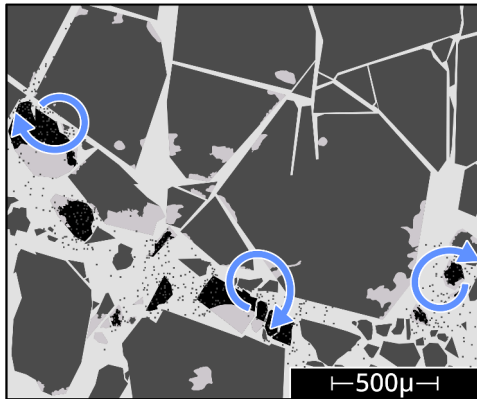


Figure 5.4 – Passing fluids dissolve rock particles and create angular cells. Precipitated cc from the fluid partly encrusts breccia clasts and fractures. Shattered rock particles are transported into the fractures.

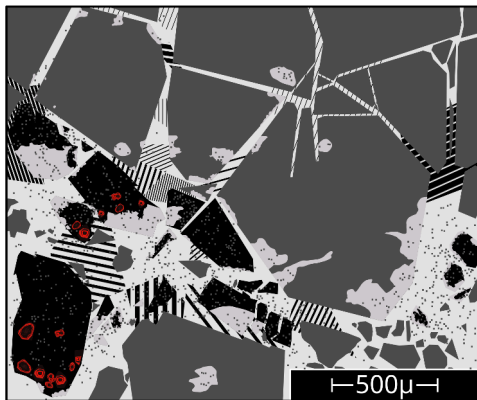


Figure 5.5 – Partly, former clasts are completely dissolved and only their remnants as cells observable. Rock flour particles are incorporated into the vein-cement and form geopetal aggregates. The twinned vein-cement hints towards elevated crystallization temperatures. In red: Euhedrally grown cc-single crystals, close-up in Fig. 5.6.



Figure 5.6 – On the walls of a former breccia clast, euhedral cc-cement grows. "Cockades" in the cell grow euhedral, too, and are zoned as well with a core of rock flour particles incorporated. Note the gravity-driven settling of cockades in the cell and of rock flour particles, incorporated in the vein cement.

5.5 Fault rocks of the Grasberg-Schlagl-fault zone

The samples of this study no longer contain protolith fragments $> 500 \mu\text{m}$. The source rocks of the components found in the drill cores are completely disintegrated. Some mineral grains allow for the identification of their source rocks as either magmatic or metamorphic-crystalline.

The carbonatic-rock samples (SFK1m18-40, SFK1m19-50, SFK1m20-40, SFK1m22-90, SFK1m23-10) were identified as dilation breccias/cellular dolomite in different states of preservation. The formation of this type of fault rock is illustrated in the chapter on cockade growth and on the formation of cellular breccias. Samples SFK1m18-30, SFK1m23-70, and SFK1m27-40 and SFK1m27-50 have a more diverse composition and contain not only mineral grains originating from crystalline rock, but also (non-carbonatic) lithic fragments $> 1\text{mm}$.

The four samples mostly consist of well-rounded clasts of recemented carbonatic rock that is composed of rock flour particles and calcite cement, as well as a matrix rich in mica and clay minerals (comp. Fig. 4.37).

Except rare slickensides on the surfaces of breccia clasts, there are no conclusive macroscopic indicators of shear deformation visible (comp. Fig. 4.8). Samples SFK1m27-40 SFK1m27-50 and SFK1m23-70 are the only samples providing useful evidence of shear deformation and prove that these rocks are not siliciclastic sedimentary rocks, but rather fault breccias slightly overprinted by dissolution-precipitation. The crystalline lithic fragments in the foliated matrices of these rocks are not surprising, as the potential source rocks can be found on the cavern plan (see Fig. 1.2). I interpret the recemented carbonatic material to derive from fault rocks and the three samples therefore to give testimony of earlier deformation events.

The matrix of the younger „generation“ of fault breccias is fine-grained (grain sizes $< 10\mu\text{m}$) and contains fragments of dolomite ($> 100\mu\text{m}$) that are not identical to the dolomite of the rock flour (with particle sizes $< 100\mu\text{m}$) and is not cemented. Matrix components are visibly aligned and suggest a stretching direction. Fractures in lath-shaped dolomite fragments are oriented perpendicular to the stretching axis, which I also interpret as an indicator of shear deformation (comp. Fig. 4.45).

Chapter 6

Conclusion

The samples derive from the active Grasberg-Schlagl-fault zone. Macroscopic shear indicators (slickensides) are only minorly visible. Over the course of investigation, it became apparent that the microscopic properties of the rock cannot be inferred from its macroscopic appearance. None of the samples contain protolith fragments $> 0,5$ cm and the samples are almost completely consist of clasts of recemented carbonatic rock, that itself consists of rock flour particles from an earlier deformation/shattering event and is encrusted by cc-cement. These recemented carbonatic fault rock fragments overall consist of $> 80\%$ calcite cement and hint at immense amounts of calcite-bearing fluids, from which the calcite was precipitated.

This study presents a microstructural analysis that traces the evolution from carbonatic-fault breccia to cellular dolomite. A multi-stage process involves the fragmentation of protolith, fluid influx, solution processes, and precipitation of calcite cement, giving the rock its characteristic porous appearance.

All samples contain varying amounts of μm -sized dol particles, here referred to as "rock flour". Brittle deformation contributed the most to the fragmentation.

Calcite-dolomite structures resembling cockade structures were also observed. These structures consist of a core of rock flour particles surrounded by overgrowing euhe-dral calcite cement and additional incorporated rings of rock flour, the structures being primarily $< 300\mu\text{m}$ in size. Not only the rings of dolomite particles, but also chemically distinct rims of calcite cement demonstrate that the genesis of the "cockade"-bearing rocks occurred in multiple stages, too. The observed structures

are smaller than described examples in the by now existing literature.

Six major stages of evolution are determined:

1. Dolostone-protolith is comminuted by a not determined process into micron-sized polyhedral particles of rock flour. The particles display a fitting-mosaic fabric.
2. Dilation of the disintegrated rock volume into angular breccia clasts creates a dilation breccia.
3. The newly formed fractures are pathways for passing mountain water, enriched in cc. The fluid manages to penetrate breccia clasts. Precipitated cc grows under development of irregular crystal faces.
4. Passing fluids dissolve or elutriate rock particles of the shattered breccia clasts. Precipitated cc on cell-walls develops euhedral crystal faces. Particles of shattered rock are transported into the cells.
5. Partly, the former breccia clasts are dissolved completely. As remnants, only their encrusted walls are observable. Rock flour particles are incorporated into the vein cement and form geopetal aggregates.
6. In cells, cockades with rock flour particles as cores grow. The cockades are zoned, indicated by different cc-cement seams. The settling of the cockades is gravity-driven, too.

Neither the conditions of cement precipitation in the recemented carbonatic fault rocks, nor these of the growth of the cockade structures can be easily determined. The results of this study strongly suggest that the growth of these structures occurred in suspension. Temperature, chemistry, and fluid flow velocities of this suspension stay unclear and reconstructing these conditions was beyond the scope of this study, but may be of interest for future research works.

Bibliography

- Aben, F., Doan, M.-L., Mitchell, T., Toussaint, R., Reuschlé, T., Fondriest, M., Gratier, J.-P. and Renard, F. (2016), ‘Dynamic fracturing by successive coseismic loadings leads to pulverization in active fault zones’, *Journal of Geophysical Research: Solid Earth* **121**, 1–23.
- Agosta, F. and Aydin, A. (2006), ‘Architecture and deformation mechanism of a basin-bounding normal fault in Mesozoic platform carbonates, central Italy’, *Journal of Structural Geology* **28**, 1445–1467.
- Agosta, F., Prasad, M. and Aydin, A. (2007), ‘Physical properties of carbonate fault rocks, Fucino Basin (central Italy): implications for fault seal in platform carbonates’, *Geofluids* **7**(1), 19–32.
- Barrier, J. (2022), Controls on Solubility and Deposition of Quartz, Calcite, Fluorite and Anhydrite in Boiling Saline Hydrothermal Systems, Diplomarbeit, University of Alberta.
- Bauer, H., Schröckenfuchs, T. and Decker, K. (2016), ‘Hydrogeological properties of fault zones in a karstified carbonate aquifer (Northern Calcareous Alps, Austria)’, *Hydrogeology Journal* **24**, 1147–1170.
- Berger, A. and Herwegh, M. (2019), ‘Cockade structures as a paleo-earthquake proxy in upper crustal hydrothermal systems’, *Scientific reports* **9**(1), 9209.
- Billi, A. (2010), ‘Microtectonics of low-P low-T carbonate fault rocks’, *Journal of Structural Geology* **32**(9), 1392–1402.
- Blattmann, S. (1937), ‘Deformationstypus der Radstädter Tauern’, *Jahrbuch der geologischen Bundesanstalt* **87**, 208–233.

- Boggs, S. and Krinsley, D. (2009), *Application of Cathodoluminescence Imaging to the Study of Sedimentary Rocks*, Cambridge University Press.
- Brune, J. (2001), ‘Shattered Rock and Precarious Rock Evidence for Strong Asymmetry in Ground Motions during Thrust Faulting’, *Bulletin of the Seismological Society of America* **91**, 1937–1940.
- Brückner, W. (1941), ‘Über die entstehung der rauhacken und zellendolomite’, *Eclogae Geologicae Helvetiae* **34** 1.
- Cornelius, H. (1936), ‘Geologische Karte von Österreich Blatt Mürzzuschlag 1:75000’.
- Decker, K., Peresson, H. and Faupl, P. (1994), ‘Die miozäne Tektonik der östlichen Kalkalpen: Kinematik, Paläospannungen und Deformationsaufteilung während der lateralen Extrusion der Zentralalpen’, *Jahrbuch der Geologischen Bundesanstalt* **137**(1), 5–18.
- Decker, K., Peresson, H. and Hinsch, R. (2005), ‘Active tectonics and Quaternary basin formation along the Vienna Basin Transform fault’, *Quaternary Science Reviews* **24**(3-4), 307–322.
- Demtröder, W. (2014), *Experimentalphysik 1*, Springer-Verlag Berlin Heidelberg.
- Dill, H. G. and Weber, B. (2010), ‘Variation of color, structure and morphology of fluorite and the origin of the hydrothermal F-Ba deposits at Nabburg-Wolsendorf, SE Germany’, *Neues Jahrbuch für Mineralogie, Abhandlungen* **187**(2), 113–132.
- Doan, M. and Gary, G. (2009), ‘Rock pulverization at high strain rate near the San Andreas fault’, *Nature Geoscience* **2** 10, 709–712.
- Doan, M.-L. and d’Hour, V. (2012), ‘Effect of initial damage on rock pulverization along faults’, *Journal of Structural Geology* **45**, 113–124.
- Dor, O., Ben-Zion, Y., Rockwell, T. and Brune, J. (2006), ‘Pulverized rocks in the Mojave section of the San Andreas Fault Zone’, *Earth and Planetary Science Letters* **245** 3-4, 642–654.

- Dor, O., Reches, Z. and van Aswegen, G. (2001), 'Earthquake Rupture at the Focal Depth of M=5.1 and M=3.7 Earthquakes in Gold Mines, South Africa', *South African Institute of Mining and Metallurgy* p. 109–112.
- Dor, O., Yildirim, C., Rockwell, T., Ben-Zion, Y., Emre, O., Sisk, M. and Duman, T. (2008), 'Geological and geomorphologic asymmetry across the rupture zones of the 1943 and 1944 earthquakes on the North Anatolian Fault: possible signals for preferred earthquake propagation direction.', *Geophysical Journal International* **173**, 483–504.
- Eichhubl, P. and Boles, J. (2000), 'Rates of fluid flow in fault systems - evidence for episodic rapid fluid flow in the miocene Monterey formation, Coastal California', *American Journal of Science* **300**, 571–600.
- Fossen, H. (2016), *Structural geology*, Cambridge University Press.
- Frenzel, M. and Woodcock, N. (2014), 'Cockade breccia: product of mineralisation along dilational faults', *Journal of Structural Geology* **68**, 194–206.
- Frisch, W., Dunkl, I. and Kuhleemann, J. (2000), 'Post-collisional orogen-parallel large-scale extension in the Eastern Alps', *Tectonophysics* **327**(3-4), 239–265.
- Gaskell, D. R. (1992), *An Introduction to Transport Phenomena in Materials Engineering*, second edn, Momentum Press.
- Genna, A., Jébrak, M., Marcoux, E. and Milési, J. P. (1996), 'Genesis of cockade breccias in the tectonic evolution of the Cirotan epithermal gold system, West Java', *Canadian Journal of Earth Sciences* **33**(1), 93–102.
- Gibowicz, S. J. (2009), Chapter 1 - Seismicity Induced by Mining: Recent Research, in 'Advances in Geophysics', Vol. 51 of *Advances in Geophysics*, Elsevier, pp. 1–53.
- Handy, M., Schmid, S., Bousquet, R. and Bernoulli, D. (2010), 'Reconciling plate-tectonic reconstructions of Alpine Tethys with the geological–geophysical record of spreading and subduction in the Alps', *Earth-Science Reviews* **102**, 121–158.

- Herrmann, P., Mandl, G. W., Matura, A., Neubauer, F. R., Riedmüller, G. and Tollmann, A. (1992), ‘Neunkirchen 1:50000’, Geologische Karte der Republik Österreich 1:50000, Wien.
- Häusler, H., Plasienska, D. and Polak, M. (1993), ‘Comparison of Mesozoic Successions of the Central Eastern Alps and the Central Western Carpathians’, *Jahrbuch der Geologischen Bundesanstalt* **136**(4), 715–739.
- Jobson, D. H., Boulter, C. A. and Foster, R. (1994), ‘Structural controls and genesis of epithermal gold-bearing breccias at the Lebong Tandai mine, Western Sumatra, Indonesia’, *Journal of Geochemical Exploration* **50**, 409–428.
- Kaminskaite, I., Fischer, Q. and Michie, E. (2020), ‘Faults in tight limestones and dolostones in San Vito lo Capo, Sicily, Italy: Internal architecture and petrophysical properties’, *Journal of Structural Geology* **132**, 103970.
- Kellermann, H. (2008), Petrographie und Geotechnik von Kataklasiten am Semmering, Diplomarbeit, Universität Wien.
- Key, W. and Schultz, R. (2011), ‘Fault formation in porous sedimentary rocks at high strain rates: First results from the Upheaval Dome impact structure, Utah, USA’, *GSA Bulletin* **123** 5-6, 1161–1170.
- Kober, L. (1912), ‘Der Deckenbau der östlichen Nordalpen’, *Denkschriften der Kaiserlichen Akademie der Wissenschaften. Math. Natw. Kl.* **88**.
- Kober, L. (1923), ‘Der Deckenbau der östlichen Nordalpen.’, *Denkschriften der kaiserlichen Akademie der Wissenschaften. Math. Natw. Kl.* **88**.
- Kober, L. (1925), ‘Die tektonische Stellung des Semmering-Wechsel-Gebietes’, *Tschermaks mineralogisch-petrographische Mitteilungen* **38**, 268–276.
- Kristan-Tollmann, E. and Tollmann, A. (1963), ‘Das mittelostalpine Rhät-Standardprofil aus dem Stangalm-Mesozoikum (Kärnten) Mit Vergleich zum unter- und oberostalpinen Rhät’, *Mitteilungen der Österreichischen Geologischen Gesellschaft* **56** 2, 539–589.

- Leine, R. (1969), 'Rauhacken und ihre Entstehung', *Geologische Rundschau* **60**, 488–525.
- Linzer, H.-G., Decker, K., Peresson, H., Dell'Mour, R. and Frisch, W. (2002), 'Balancing lateral orogenic float of the Eastern Alps', *Tectonophysics* **354**(3-4), 211–237.
- Liu, Y., Genser, J., Handler, R., Friedl, G. and Neubauer, F. (2001), '40Ar/39Ar muscovite ages from the Penninic-Austroalpine plate boundary, Eastern Alps', *Tectonics* **20**, 526–547.
- Liu, Z., Yuan, D. and Dreybrodt, W. (2005), 'Comparative study of dissolution rate-determining mechanisms of limestone and dolomite', *Environmental Geology* **49**(2), 274–279.
- Loos, D., Pasel, C., Luckas, M., Schmidt, K. G. and Herbell, J. D. (2004), 'Experimental Investigation and Modelling of the Solubility of Calcite and Gypsum in Aqueous Systems at Higher Ionic Strength', *Fluid Phase Equilibria* **219**(2), 219–229.
- Masoch, S. (2018), Formation of cockade breccias in extensional brittle faults (Col de Teghime, Alpine Corsica), Diplomarbeit, Università degli Studi di Padova.
- Masoch, S., Fondriest, M., Preto, N., Secco, M. and Di Toro, G. (2019), 'Seismic cycle recorded in cockade-bearing faults (Col de Teghime, Alpine Corsica)', *Journal of Structural Geology* **129**, 103889.
- Mitchell, T. M., Ben-Zion, Y. and Shimamoto, T. (2011), 'Pulverized fault rocks and damage asymmetry along the Arima-Takatsuki Tectonic Line, Japan', *Earth and Planetary Science Letters* **308**, 284–297.
- Mohideen, A. (2020), Pulverisierte Störungsgesteine der seismisch aktiven Mürz-Mürz-Störung SW des Semmerings, Bachelor's thesis, Universität Wien.
- Mohr, H. (1910), 'Zur Tektonik und Stratigraphie der Grauwackenzone zwischen Schneeberg und Wechsel (Niederösterreich)', *Mitteilungen der Österreichischen Geologischen Gesellschaft* **3**, 104–213.

- Mohr, H. (1912), ‘Versuch einer tektonischen Auflösung des NE-Spornes der Zentralalpen’, *Denkschriften der Akademie der Wissenschaften. Math. Natw. Kl.* **88**, 633–652.
- Mohr, H. (1950), ‘Erster Bericht über die Verfolgung der geologischen Aufschlüsse im Semmering-Tunnel II’, *Akademie der Wissenschaften* **3**, 51–55.
- Mohr, H. (1951), ‘Zweiter Bericht über die Verfolgung der geologischen Aufschlüsse im Semmering-Tunnel II’, *Denkschriften der Akademie der Wissenschaften. Math. Natw. Kl.* **7**, 191–199.
- Mort, K. and Woodcock, N. (2008), ‘Quantifying fault breccia geometry: Dent Fault, NW England’, *Journal of Structural Geology* **30**, 701–709.
- Oberhauser, R. (1980), Das Unterengadiner Fenster, in ‘Der geologische Aufbau Österreichs’, Springer, Wien, pp. 291–299.
- Passchier, C. and Trouw, R. (2005), *Microtectonics*, Springer, Berlin-Heidelberg.
- Peresson, H. and Decker, K. (1997), ‘The Tertiary dynamics of the northern Eastern Alps (Austria): changing palaeostresses in a collisional plate boundary’, *Tectonophysics* **272**(2-4), 125–157.
- Piller, W., Egger, H., Erhart, C., Gross, M., Harzhauser, M., Hubmann, B., van Husen, D., H.-G., K., Krystyn, L., Lein, R., Lukeneder, A., Mandl, G., Rögl, F., Roetzel, R., Rupp, C., Schnabel, W., Schönlaub, H. P., Summesberger, H., Wagneich, M. and Wessely, G. (2004), ‘Stratigraphische Tabelle von Österreich 2004 (sedimentäre Schichtfolgen)’, Pangeo Austria, 2004.
- Ratschbacher, L., Frisch, W. and Linzer, H.-G. (1991), ‘Lateral extrusion in the eastern Alps, Part 2: Structural analysis’, *Tectonics* **10**(2), 257–271.
- Ratschbacher, L., Merle, O., Davy, P. and Cobbold, P. (1991), ‘Lateral extrusion in the eastern Alps, Part 1: Boundary conditions and experiments scaled for gravity’, *Tectonics* **10**(2), 245–256.
- Reches, Z. and Dewers, T. (2005), ‘Gouge formation by dynamic pulverization during earthquake rupture’, *Earth and Planetary Science Letters* **235**, 361–374.

- Rempe, M., Mitchell, T. M., Renner, J., Nippres, S., Ben-Zion, Y. and K., R. T. (2013), ‘Damage and seismic velocity structure of pulverized rocks near the San Andreas Fault’, *Journal of Geophysical Research: Solid Earth* **235**, 2813–2831.
- Richter, D. K., Götte, T., J., G. and Neuser, R. D. (2003), ‘Progress in application of cathodoluminescence (CL) in sedimentary petrology’, *Mineralogy and Petrology* **79**, 127–166.
- Rockenschaub, M. (2003), Innsbrucker-Quarzphyllit, Tarntaler Mesozoikum, Patscherkofelkristallin, in M. Rockenschaub, B. Kolenprat and A. Nowotny, eds, ‘Arbeitstagung 2003 Blatt 148 Brenner’, Vol. 10, Geologische Bundesanstalt, pp. 41–58.
- Rockwell, T., Sisk, M., Girty, G., Dor, O., Wechsler, N. and Ben-Zion, Y. (2009), ‘Chemical and physical characteristics of pulverized tejon lookout granite adjacent to the San Andreas and garlock faults: implications for earthquake physics’, *Pure and Applied Geophysics* **166 10-11**, 1725–1746.
- SBT-Baulos (2010), ‘Semmering-Basistunnel Neu. Einreichoperat für das eisenbahrechtliche Baugenehmigungsverfahren einschließlich wasserrechtlicher Belange’, fragezeichen.
- Schmid, S., , Fügenschuh, B., Kissling, E. and Schuster, R. (2004), ‘Tectonic map and overall architecture of the Alpine orogen’, *Eclogae Geologicae Helveticae* **97**, 93–117.
- Schmid, S., Scharf, A., Handy, M. and Rosenberg, C. (2013), ‘The Tauern Window (Eastern Alps, Austria): a new tectonic map, with cross-sections and a tectonometamorphic synthesis’, *Swiss Journal of Geosciences* **106**, 1–32.
- Schröckenfuchs, T., Bauer, H., Grasemann, B. and Decker, K. (2015), ‘Rock pulverization and localization of a strike-slip fault zone in dolomite rocks (Salzach–Ennstal–Mariazell–Puchberg fault, Austria)’, *Journal of Structural Geology* **78**, 67–85.
- Schuster, R. (2022), ‘Regionale Geologie Österreich’, Lecture.

- Schuster, R., Scharbert, S., Abart, R. and Frank, W. (2001), 'Permo-Triassic extension and related HT/LP metamorphism in the Austroalpine-Southalpine realm', *Mitteilungen der Geologie- und Bergbaustudenten Österreichs* **44**, 111–141.
- Schuster, R. and Stüwe, K. (2008), 'Permian metamorphic event in the Alps', *Geology* **36**, 603–606.
- Shvetsov, M. (1954), 'Concerning some additional aids in studying sedimentary formations', *Moscow University Geology Bulletin* **29**, 61–66.
- Sibson, R. (1977), 'Fault rocks and fault mechanisms', *Journal of the Geological Society* **133**(3), 191–213.
- Sibson, R. H. (1986a), 'Brecciation processes in fault zones: Inferences from earthquake rupturing', *Pure and Applied Geophysics* **124**, 159–175.
- Sibson, R. H. (1986b), 'Earthquakes and rock deformation in crustal fault zones', *Annual Review of Earth and Planetary Sciences* **14**(1), 149–175.
- Tarasewicz, J., Woodcock, N. H. and Dickson, J. A. (2005), 'Carbonate dilation breccias: Examples from the damage zone to the Dent Fault, northwest England', *Geological Society of America Bulletin* **117**(5-6), 736–745.
- Termier, P. (1904), 'Sur quelques analogies de faciès géologique entre la zone centrale des Alpes orientales et la zone interne des Alpes occidentales.', *Comptes rendus de l'Académie des sciences* **1903**, 807–808.
- Tollmann, A. (1957), 'Semmering und Radstädter Tauern. Ein Vergleich in Schichtfolge und Bau', *Mitteilungen der Geologischen Gesellschaft in Wien* **50**, 325–354.
- Tollmann, A. (1959), 'Der Deckenbau der Ostalpen aufgrund der Neuuntersuchung des zentralalpiner Mesozoikums', *Mitteilungen der Gesellschaft der Geologie- und Bergbaustudenten in Österreich* **10**, 3–63.
- Tollmann, A. (1963), *Ostalpensynthese*, Franz Deuticke, Wien.
- Tollmann, A. (1977), *Geologie von Österreich Band I Die Zentralalpen*, Franz Deuticke, Wien.

- Tollmann, A. (1987), Bericht 1985 über geologische Aufnahmen auf Blatt 105 Neunkirchen, in 'Jahrbuch der Geologischen Bundesanstalt', Vol. 130, Geologische Bundesanstalt, p. 306.
- Toula, F. (1876), 'Ein Beitrag zur Kenntnis des Semmeringgebirges', *Verhandlungen der k.u.k geologischen Reichsanstalt* pp. 334–341.
- Toula, F. (1877), 'Beiträge zur Kenntnis der „Grauwackenzone“ der nördlichen Kalkalpen', *Verhandlungen der k.u.k geologischen Reichsanstalt* p. 240–244.
- Wilson, B., Dewers, T., Reches, Z. and Brune, J. (2005), 'Particle size and energetics of gouge from earthquake rupture', *Nature* **434**, 749–752.
- Woodcock, N. and Mort, K. (2008), 'Classification of fault breccias and related fault rocks', *Geological Magazine* **145**(3), 435–440.
- Yuan, F., Prakash, V. and Tullis, T. (2011), 'Origin of pulverized rocks during earthquake fault rupture', *Journal of Geophysical Research* **116**, B06309.

List of Figures

1.1	A tectonic map of the study area. In the NE, one can see the Vienna Basin, in the SW Styrian basin, bordered by the Lavanttal fault and MU-fault. The rectangle marks the area of Göstritz, where the intermediate access Göstritz of the Semmering-tunnel is located. After Decker et al., 2005.	14
1.2	Sample site. The samples derive from a drillcore in the course of an exploratory drilling. The green line marks the borehole of RKB2-SFK1, the red line the studied segment between meters 14-30. Modified figure from Robert Holzer, pers. communication.	16
2.1	The classification scheme of Woodcock and Mort, 2008. Despite the weaknesses concerning the differentiation between mylonite and catclasite, the classification allows great differentiation possibilities of fault breccias.	20
2.2	The classification of fault breccias of Mort and Woodcock, 2008. From left to right: Increase of the rocks' net volume due to dilation of the rock. From top to bottom: Increase of the clasts' rotation produces a chaotic fabric of the rock.	21
2.3	Schematic scetch of a cellular dolomite. Dol clasts in grey, cells in black. The septum consist of cc-vein cement that is intensily twinned. The red colour indicates euhedral cc-crystals that encrust the cells' walls.	24
4.1	SFK1m22-90. Sample preparation included treatment with resin due to the incohesiveness of dol-clasts that could be easily destroyed by performing slight pressure or simply holding it under water. Dol-breccia clasts are arranged to a fitting fabric.	33

- 4.2 SFK1m22-90. Thinsection-scan. Sedimentary bedding (S0) is still recognizable. Geopetalaggregates are deposited in cc-veins (red arrows). Dilation of the protolith and partial solution of dol-clasts create the "Rauhacken"-resembling appearance. Clasts are angular. From top to bottom, the fabric disintegrates towards a progressively more chaotic fabric. 36
- 4.3 SFK1m22-90 A: Twinned cc grows in fractures. Gravitational sinking of the rock flour in suspension creates geopetalaggregates (in the picture recognizable as grey spots, deposited in sub-horizontal direction). Cc-bearing fluid penetrates protolith and encrusts its clast so the rock is protected of further dissolution (black arrow). B: No protolith in cells is left. Cc in cells develops euhedral crystal faces. Note the perfectly preserved shape of former breccia clasts, now only indicated by attached rock flour. Arrow pointing to a cavity, through which fluids could infiltrate the clasts. . . . 36
- 4.4 SFK1m22-90. Cc in fractures is intensely twinned. Twins are up to 35µm wide and bent. This indicates elevated temperatures during crystal growth. Note fractured cc crystals, fractures in the crystal follow cc-cleavage. . . . 37
- 4.5 SFK1m22-90: Cementation succession. A: Shattered protolith (orange) is penetrated by dol-vein. Dol-veins are subsequently fractured by non-luminescing cc-cement. Cc-bearing fluid creeps into the clasts, growth of anhedral crystal faces follows (rectangles). Orange-luminescing cement seams follow. B: Non-luminescing cc-cement partially encrusts clasts and preserves their former shape. Where cc-saturated fluid enters the cells, protolith is dissolved and euhedral cc-crystals can grow. A succession of broad, diffuse brown cement seams grow into cells. C: Brightly-luminescing crystals grow in a cell with little preserved protolith. A fragment of zoned cc-cement is overgrown by cc-cement that cannot be definitely subsumed into the cement-growth succession (arrow). D: Vein intruding the porous protolith, zoned cc-cement manages to grow from the vein into open cells (arrow). 40

4.6	SFK1m22-90. Protolith, comminuted into rock flour, disintegrates into μm -sized fragments. Fractures tend to follow the cleavage planes of dol. Partly, porous breccia clasts get dissolved, the secondary porosity reaches $> 50\%$. Rock flour particles are encrusted in vein cement between clasts. The particles start to sink and geopetal aggregates accumulate (red arrow).	41
4.7	SFK1m22-90. A, B: Arrows pointing towards the upper surface of geopetal aggregates. The disintegrated dol is highly porous and clasts are arranged in a fitting fabric. Remains of protolith-clasts are not cemented, only the walls of the clast are solidified by vein cement. Vein-cc has anhedral crystal faces. The solidified surfaces of the former clasts serve as a plane, where the aggregates can be deposited. B: Note the almost completely decomposed protolith clasts, with porosities $> 50\%$.	42
4.8	SFK1m23-10. Cell-diameters range from mm - cm are and angular to subrounded. Euhedral cc-crystals encrust the cells. No protruding clasts between the septae are preserved.	44
4.9	SFK1m23-10. Thinsection scan. The rectangles mark the spots of the CL pictures. Note the missing protolith in former clasts and high amounts of young cc-cement in cells and along septae. The septae break easily and get recemented.	46
4.10	SFK1m23-10. The left rim of the cell is overprinted by pressure solution seams. A: Cement-seams of two different generations next to each other. B: Supposedly older cement-piece luminesces brownish (rectangle). The single cc-crystals in the cell incorporate particles of rock flour. Two bright seams surround non-luminescing cc-cement. The inner seam is irregular, the outer one is broad and diffuse and follows the habit of cc. The CL-signal of cc in the cell and the cement encrusting the cell-walls is identical.	47

4.11	SFK1m23-10. A, B: Cell encrusted with brightly luminescing cc and filled with euhedral cc-crystals. Note the brownish cement next to the specific cell. C, D: A piece of the same, brightly luminescing cement is incorporated elsewhere in the rock. The arrow points towards the wall of the cement-fragment. In TL, the clast is barely visible. E, F: Supposedly the oldest cement types. Rom. I and rom. II are marked with question marks, since it is non-excludible that these cements were formed prior to the main cementation forming the main current rock volume.	48
4.12	SFK1m20-40A. Clasts in the matrix range between mm-dm in size. Cells in the greyish-blueish components are rounded and chaotically arranged. Cell-diameters range from few mm to > 1.5 cm. Towards the matrix, clasts are bordered by thin pressure solution seams (black arrow). Even though the sample is heavily weathered, it is cohesive.	50
4.13	SFK1m20-40A. Porous clast in even more highly porous matrix. Pressure-solution seams with lithic fragments and qtz-grains (red arrows) are enriched in weathered mica-grains. The clast is pressed into the matrix, but cc-crystals do not break or develop pressure-induced twins. instead, they are dissolved. The lithic fragments are altered by weathering (black arrow) and develop porosity.	52
4.14	SFK1m20-40A. A, B: Lithic fragment, replaced by cc. Cc grows into grains, creating sutured grain boundaries. Red spots are weathered accessory-minerals. C: Polycrystalline qtz-grain with undulose extinction. Arrows point towards areas of advanced chemical alteration.	53
4.15	SFK1m20-40A. A fragment of heavily overprinted dilation breccia/cellular dolomite. A: Arrows pointing towards perfectly planar veins. Cc-crystals with euhedral crystal faces encrust the septae of fragments of cellular dolomite (black arrows). Note the concentrated particles of rock flour in the cc-crystals. B: Close-up view of a cellular dol-fragment. C: Close-up view of euhedral cc-crystals growing into a pore, their cores eventually consisting of rock flour.	55

- 4.16 SFK1m20-40B. I: Clasts in matrix. Cc encrusts the heterogeneously distributed dol particles. The porosity in the clasts is low. Pores in the clast are round and scarce. Pressure solution seams cross the densely packed clast. II: Euhedral cc-crystals with dol particles as nuclei. Note the high porosity between the single-crystals. 57
- 4.17 SFK1m20-40D. A: Right hand side: A rounded clast is overgrown by a white seam of cc-cement, that contain a thin line of rock flour. The clast is dense with little left porosity (black arrows). The heterogeneous matrix consists of carbonate- as well as crystalline rock components. B: Polycrystalline qtz, highly recrystallized. Cc-single crystals grew in several phases, indicated by rings of rock flour in them. White arrow: A undeformed, unaltered mica-grain. C: Examples of euhedral cc-crystals with a core and concentric rings of dol particles. This type of cc-crystals is interpreted to have grown in suspension with enough supply of rock flour. D, E: Dissolved, deformed and poorly recrystallized qtz-grain in TL and PL. Fsp in lithic fragments is altered (ochre-colours). The needle-shaped qtz-grains in the fragments point towards a magmatic origin of the source rock. . . 60
- 4.18 SFK1m20-40E. A: Clast-type I: Black arrow pointing towards the cc-cement-seam, encrusting the clast. Here, the cement-seam contains thin rims of rock flour. White arrows point to lithic fragments in matrix. Brownish colour: A pressure solution seam; poorly solvable lithic fragments are concentrated. B: The highly porous matrix mainly consists from euhedral multiphase-grown cc-crystals. Clast-type II has pores with irregular boundaries. 61
- 4.19 SFK1m20-40E. Material in the matrix. A, B: Lithic fragment with metamorphic foliation and weathered accessory minerals. Black arrows pointing towards qtz-grains, red arrows pointing towards strongly altered lithic fragments with sutured boundaries. Rectangle: See C, D: Qtz-grain is dissolved by fluids and a secondary porosity develops. Lithic fragment consisting of qtz and fsp, but without any accessories. E: Dulose single-grain qtz with fluid inclusions (black spots). Cc dissolves this grain, too. Pores between euhedral cc-crystals remain. 63

4.20	SFK1m20-40B, D, E. Particles of rock flour incorporated in the clast-overgrowing rims of cc-cement. A: Cc-single crystal is encrusted on a carbonate clast by euhedral cc-cement and a rim of rock flour (red arrow). B, C, D: Cc-rims around clasts (black arrows). Heavy minerals are part of the aggregates, too (white arrows).	65
4.21	SFK1m18-40A and B. A, B: Rom I. marks compact sections of the rock with low porosity, rom. II the cavernous sections. Arrows mark the contact between the sections. B: Pressure solution seam with concentrated rock flour deriving from the same carbonatic clasts. C, D: Sample 18-40B is less porous and more compact than 18-40A. Here, dol-particles are more evenly distributed in cc-cement. D: Arrows indicate pressure solution seams that deform the cells' walls. Rom. II: Pore with fractured cc-septae or cell walls, encrusted with cc.	68
4.22	SFK1m18-40A. A, B: Clast of a recemented carbonatic-rock in a stylolite. Non-luminescing cc-cement encrusts one side of the clast. In the stylolite, brightly luminescing rock flour is concentrated. The particles give a different chemical signal than dol in the recemented carbonatic clasts. C, D: ?Geopetal aggregate in a cell, encrusted by non-luminescing cement. E: Exemplary succession of cements. Only the walls of the breccia clast are preserved. The main volume of the component is dissolved. In the empty cell, cc-cement with perfect crystal faces can encrust its walls. Five seams are observable. The cement seams are comparable to seams in SFK1m20-40.	70
4.23	SFK1m18-40B. A, B: Cc-crystals of max. 300µm show multiphase growth. Where single crystals grow large and develop grain-contacts, a new, non-luminescing cement-seam grows and cc-aggregates result. White arrows indicate grain-contacts.	71
4.24	SFK1m19-50. Dissolved dol creates cells with uneven walls, encrusted with cc-crystals. Brownish spots derive from weathering and pressure solution. .	73

4.25	SFK1m19-50A. A, B: Walls of a ?former breccia-clast are encrusted by cc-crystals. The boundary of the cell appears diffuse. Inside the cell grow isometric, euhedral cc-crystals with concentrated rock flour in their cores. Multiphase-growth of cement creates cc-crystal-aggregates. E-G: Picture of qtz-grain with dulose extinction in TL, CL, PL. Away from the qtz-grain, cc is growing in open pore space. Cement is zonated with euhedral seams of cc. G: En-echelon veins in deformed qtz.	75
4.26	SFK1m19-50A. Various cement-types. A, B: Black cement encrusts cc-single-crystals. A: Note the nooked angles of bright-red cement, encrusting and closing relict pores in the dense portion of the rock. B: Broad, pale-brown seams terminate the cement growth. The pore is protected against further cementation.	76
4.27	SFK1m19-50A. Concentric rims of cc-dol-particles that only appear in CL. Here, particles encrusted by cc-cement are evenly distributed.	76
4.28	SFK1m19-50A. Rock flour is encrusted by cc-cement. Two concentric rings of dol rock flour particles are indicated by arrows (lilac - inner ring, red: outer ring). Note the fractures at the boundaries of the cc-single crystals. It is unsure, if the fracturing is a artefact of sampling, or caused by a new breakage event.	77
4.29	Hand specimen. Angular dolomite clasts in an ochre-coloured matrix.	78
4.30	Thinsection scan. Lithic fragments, dol-clasts, dol rock-flour and fragments of ?cellular dol, heavily encrusted by cc, are chaotically arranged. No shear indicators are observable.	79
4.31	SFK1m18-30. Pictures in PL. A: Lithic fragment from a metamorphic host rock. Between elongated qtz-grains, mica-grains are oriented. Heavy minerals are weathered and produce red spots and cannot be further determined. The matrix is not cemented. B: Needle-shaped qtz-subgrains seem to be replaced by carbonate, which produces irregular grain boundaries. . .	80
4.32	SFK1m18-30. A: Bright-red luminescence signal of dol-clasts. B: Zonated cc-crystals with dol-rock flour in cores (rectangles).	80

4.33	SFK1m17-80. Grey clasts in an ochre-coloured, weathered matrix. Reddish slickensides penetrate the rock; on the striated planes, pressure solution takes place (black arrows): The stylolites are seemingly linked to the slickensides.	82
4.34	SFK1m17-80. PL-Picture. Fine-grained protolith is penetrated by bright, subparallel- to parallel dol veins. The boundary protolith-fractures is not clearly defined. The brecciated clasts experience little rotation and offset. The fine-grained matrix contains few qtz- and mica-grains, but its main constituents cannot be determined by optical methods.	83
4.35	SFK1m17-80. A, B: Cc-veins penetrate host rock, where pores are wide enough, well developed crystal faces grow. In contrast to other samples, cc-crystals do not grow around rock flour. Additionally, clast-penetrating dol-veins are indistinguishable from the clasts' main material (B). C, D: Dol-vein and dol-rock flour in fractures cannot be distinguished from the breccia clasts in CL. The white arrow marks one of the dol-veins, that disappears in CL. Black arrows point towards the rare zoned cc-cement. Qtz and mica produce no luminescence signal.	85
4.36	SFK1m17-80. A, D: Shattered clasts of the brecciated rock are partially solidified by anhedral-growing cc-cement. A: Arrows pointing towards shattered dol clasts. B: Polycrystalline qtz-grain is replaced by ?dol-cement. C, D: The dol-protolith clasts are slightly rounded and consolidated by cc. E: Pieces of cc-cement overgrowing rock flour particles that accumulated in the open pore prior to cementation. A rim of rock flour is consolidated by cc-cement (red arrows).	87
4.37	SFK1m23-70. The author paid attention to select a part of the sample containing matrix as well as breccia clasts. The sample is incohesive and the matrix weak. It contains slickensides which are not resolvable on the photograph.	89

4.38	SFK1m23-70A. Thinsection scan. Subangular clasts of recemented carbonatic rock in fine-grained clay-cc matrix. Red arrows mark fractures in the matrix, their arrangement possibly indicates ?sinistral shear sense. Blue colour indicates pores in the macroscopically dense clasts and matrix. Black arrows: Note dark pressure solution seams, crossing clasts.	91
4.39	SFK1m23-70A. The boundary clast-matrix. A: White arrows point towards grinded cc-crystals where the carbonatic clast is bordered towards the matrix due to shear deformation. Black arrows: Cc forms euhedral crystal faces, but its shape does not follow the crystal habit of cc. B: A fracture divides clasts from the matrix. Fractures cross the breccia components as well. The rectangle marks pressure dissolution along clasts, cc-grains are partly dissolved.	92
4.40	SFK1m23-70A. Image in TL and CL. A: Red arrows point towards the non-luminescent mica grains. B: The luminescence signal of dol fragments in the matrix is bright red. Dol rock flour that is encrusted by non-luminescent cc cement faintly luminesces brown. The matrix is poorly foliated. Rectangles mark abraded cc-crystals at the clast fracture-surfaces.	93
4.41	SFK1m23-70A. A: The rock consists of clasts of recemented carbonatic rock and a fine-grained (particles < 50µm) matrix, mainly consisting of clay minerals. Fractures and pressure solution affect both clasts and matrix (black arrow). Sheet-silicates in the matrix are visually aligned. B: (Sub)rounded clasts in matrix. Carbonatic rock clasts contain subordinate cemented mica grains. C: Mica grains degrade to clay, supposedly by a combination of shear and chemical weathering. The white arrow traces likely shear planes. Red arrow: Hematite/magnetite grain. D: Carbonatic rock clast in matrix. In situ grown Fe-Oxide. Pyrite-fromboids grow.	94
4.42	SFK1m27-40 and SFK1m27-50. Sutured, greyish carbonatic clasts in a intensely weathered matrix. Arrows tracing the orientation of reddish, metallic appearing slickensides. Unidentifiable lithic fragments are visible.	97

4.43	SFK1m27-40A. A: Qtz with ?abnormal (grey-brown-yellow) interference colors. The crystal lattice of the qtz grains is heavily strained. B: Deformed lithic fragments with visible metamorphic foliation. Qtz grains show a dulose extinction pattern. Rectangle: Cc-single-crystal with high interference colours and two rings of shattered dol.	98
4.44	SFK1m27-40A. TL and CL images. A: Clay-minerals and dol are poorly aligned. B: Brownish-luminescing rock flour. Note the heavily altered, orange-luminescing dol fragments.	99
4.45	SFK1m27-40A. A: Mica is broken down to sub- μm sized clay grains. Compared to clasts in other samples, the lithic fragment is relatively dense (porosity < 5%). B, left: Accessory minerals in in a carbonatic-rock clast. Rectangles: Dol clasts are aligned parallel to the foliation. Fractures in the dol grains are oriented perpendicular to the foliation plane. C: Mica grains in a breccia clast are gradually released into the matrix. The carbonatic clast contains approx. 20% bright grey dol-particles. D: A lithic fragment with abundant accessory minerals (Fe-oxides, Ti-oxides). The ?metamorphic foliation of the source rock is still recognizable. B, C, D: Note the low porosity of the matrix, caused by sub- μm sized clay-grains being densily packed.	100
5.1	A rock comminuting process creates micron-sized polyhedral particles of dolostone-protolith that display a fitting- to mosaic-fabric.	113
5.2	The disintegrated rock gets dilated into angular breccia clasts. Fractures open. Only little clast rotation or transport occur.	113
5.3	After brecciation, fluids penetrate the rock volume via the newly formed fractures. Fluids are enriched in cc and penetrate the breccia clasts where precipitated cc in the shattered rock clasts takes on "cloudy" forms.	113
5.4	Passing fluids dissolve rock particles and create angular cells. Precipitated cc from the fluid partly encrusts breccia clasts and fractures. Shattered rock particles are transported into the fractures.	114

5.5	Partly, former clasts are completely dissolved and only their remnants as cells observable. Rock flour particles are incorporated into the vein-cement and form geopetal aggregates. The twinned vein-cement hints towards elevated crystallization temperatures. In red: Euhedrally grown cc-single crystals, close-up in Fig. 5.6.	114
5.6	On the walls of a former breccia clast, euhedral cc-cement grows. "Cockades" in the cell grow euhedral, too, and are zoned as well with a core of rock flour particles incorporated. Note the gravity-driven settling of cockades in the cell and of rock flour particles, incorporated in the vein cement.	114
A.1	Borelog of meters 14-16 from the drilling RKB-SFK1m.	ii
A.2	Borelog of meters 16-18 from the drilling RKB-SFK1m.	iii
A.3	Borelog of meters 18-20 from the drilling RKB-SFK1m.	iv
A.4	Borelog of meters 20-22 from the drilling RKB-SFK1m.	v
A.5	Borelog of meters 22-24 from the drilling RKB-SFK1m.	vi
A.6	Borelog of meters 24-26 from the drilling RKB-SFK1m.	vii
A.7	Borelog of meters 26-28 from the drilling RKB-SFK1m.	viii
A.8	Borelog of meters 28-30 from the drilling RKB-SFK1m.	ix
A.9	Borelog of meters 30-32 from the drilling RKB-SFK1m.	x
B.1	Drillcores m14-20. The samples are relatively wet, ochre coloured and heavily fractured. One can see tectonic breccias as well as "cellular breccias" (m19-20).	xii
B.2	Drillcores m20-26. Of great interest were the cellular breccias. The rocks are intensely weathered and show many open cells. Denser parts were referred to as carbonatic fault breccia. From m24-25, one can see a fracture containing fine-grained matrix and carbonatic clasts. . .	xiii
B.3	Drillcores m26-30. Pressure solution overprinted the shapes of former fault breccia clasts (m26-27). In the cavern plan, these rocks are referred to as dolostone, dolostone-marble and dolostone breccia. Microscopic analysis revealed, that the main mass of the rocks indeed is calcite, with only little amounts of dol rock-flour as constituents. .	xiv

Dankensworte

Einigen Personen möchte ich aufrichtig für deren Unterstützungen danken:

... meinem Betreuer Kurt Decker, der mein Interesse an diesen vielseitigen und seltsamen Proben schon in Zuge meiner Bachelorarbeit geweckt hat. Danke für die viele Zeit, die die Arbeit in Anspruch genommen hat, die aufmunternden Worte und die Zuversicht, dass dieses Projekt gut gelingen würde!

... Katarina Schöpfer, die mich an so vielen Gelegenheiten von früh bis spät am Elektronenmikroskop unterstützt hat, inhaltlich so viel beigesteuert hat, mit mir gemeinsam den Kopf über nicht funktionierende Geräte geschüttelt hat und mich immer daran erinnert, dass die Masterarbeit ganz sicher fertig werden würde.

... Bernhard Grasemann und Michl Bestmann, die sich die Zeit genommen haben, mit mir meine Beobachtungen zu diskutieren und mich davor bewahrt haben, mich in meinen Interpretationen zu verlaufen.

... Dieter Mader, der mir so viel mit der Kathodenlumineszenzmikroskop geholfen hat.

... Robert Holzer, Chefgeologe am Zwischenangriff Göstritz des Semmeringbasistunnels, der von seinen vor-Ort Beobachtungen erzählt hat.

... meinem Freund Stephan, der mir beim Verfassen dieser Arbeit geholfen hat und ohne dessen Hilfe ich mich noch immer mit Office-Produkten herumschlagen würde...

... und natürlich Richard A. Schultz, der während seiner Gastprofessur viele Stunden mit mir diskutiert und mich auf wichtige Punkte aufmerksam gemacht hat. Ohne seine Hilfe wären die Diskussion und Interpretation meiner Ergebnisse um einiges schwächer geworden.

Zuallerletzt möchte ich meinen lieben Semesterkollegen und Freunden die ich auf der Uni kennenlernen durfte, Danke sagen: Vor allem Sophia, Gloria, Manuel, Aubert

(aber allen anderen natürlich auch). Egal ob es um die ärgerlichen oder um die vielen schönen Erlebnisse; unsere Exkursionen, Feiern, Stammtische und alle anderen Dinge geht, die wir gemeinsam durchgestanden haben - ich habe dabei nicht nur über die Geologie, sondern genauso viel über mich selbst gelernt.

Appendix A

Borelogs

The borelogs of 18m drillcore contain information about the rocktype, the degree of comminution, grain sizes if determinable, colour and mineralogy, and structural features, if available.

When comparing the macroscopical observations with the results from the microscopical studies, it is apparent that the sole investigation of the fault rocks in hand specimen is insufficient to provide information on the true nature of the rocks.

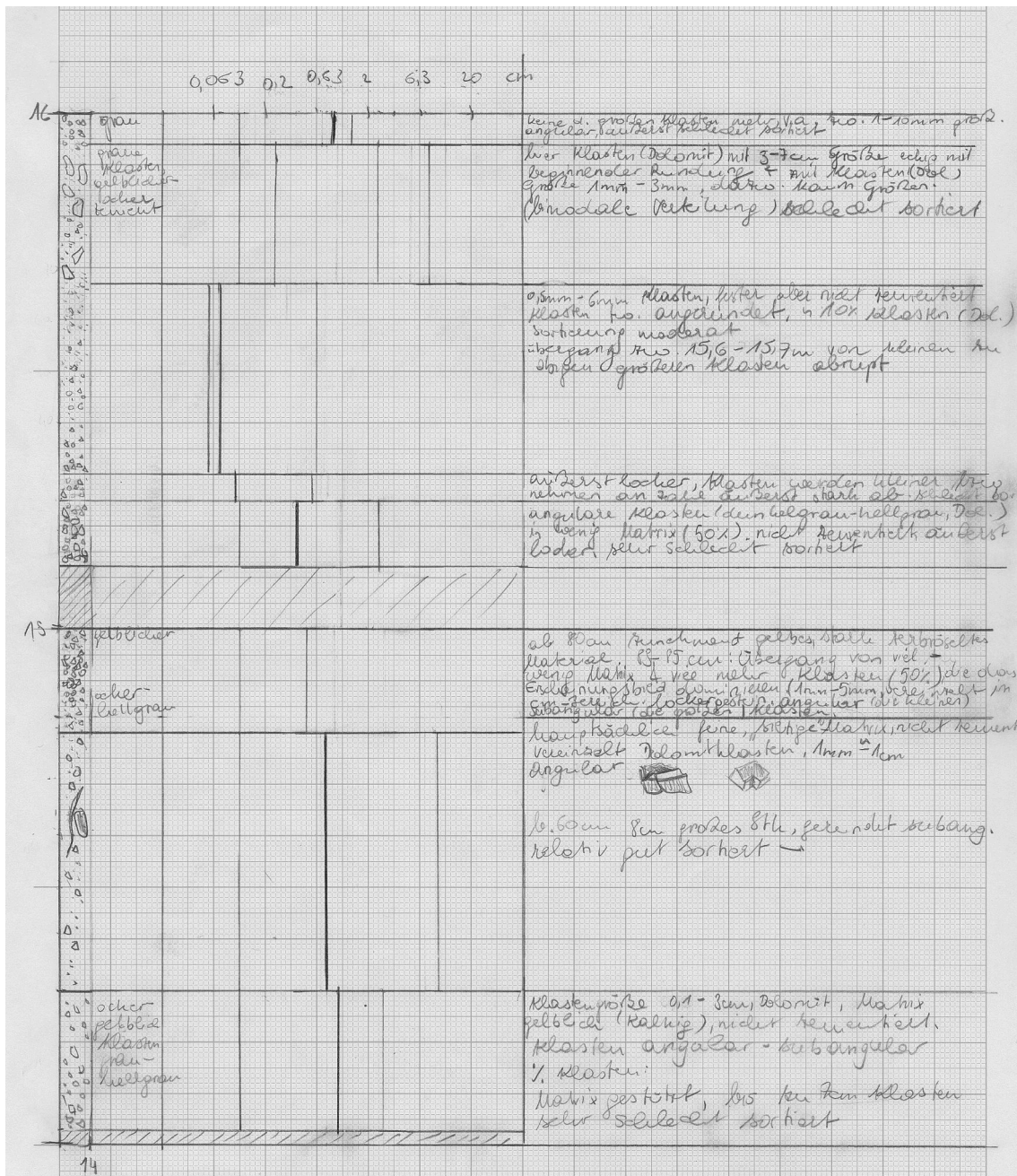


Figure A.1 – Borelog of meters 14-16 from the drilling RKB-SFK1m.

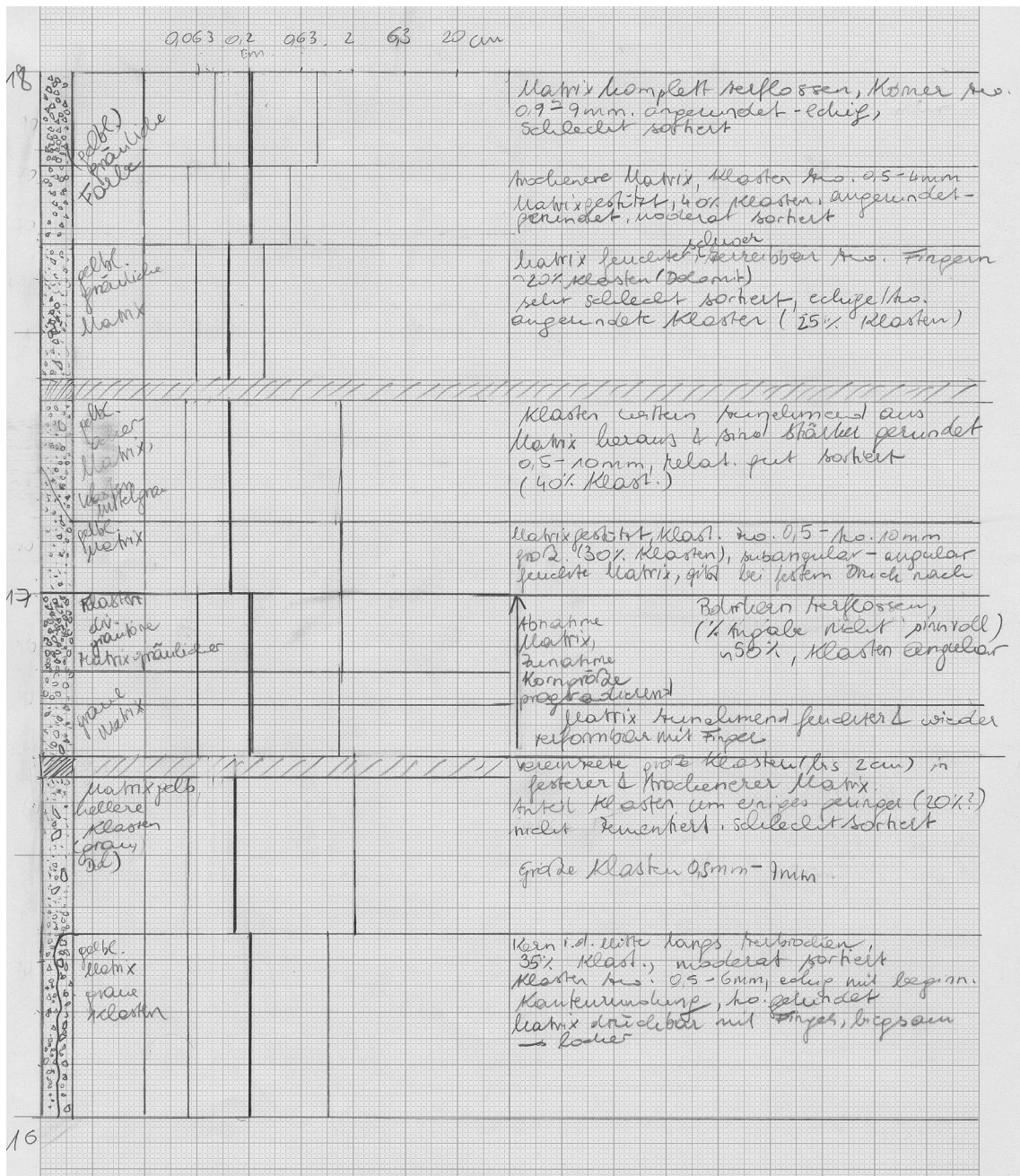


Figure A.2 – Borelog of meters 16-18 from the drilling RKB-SFK1m.

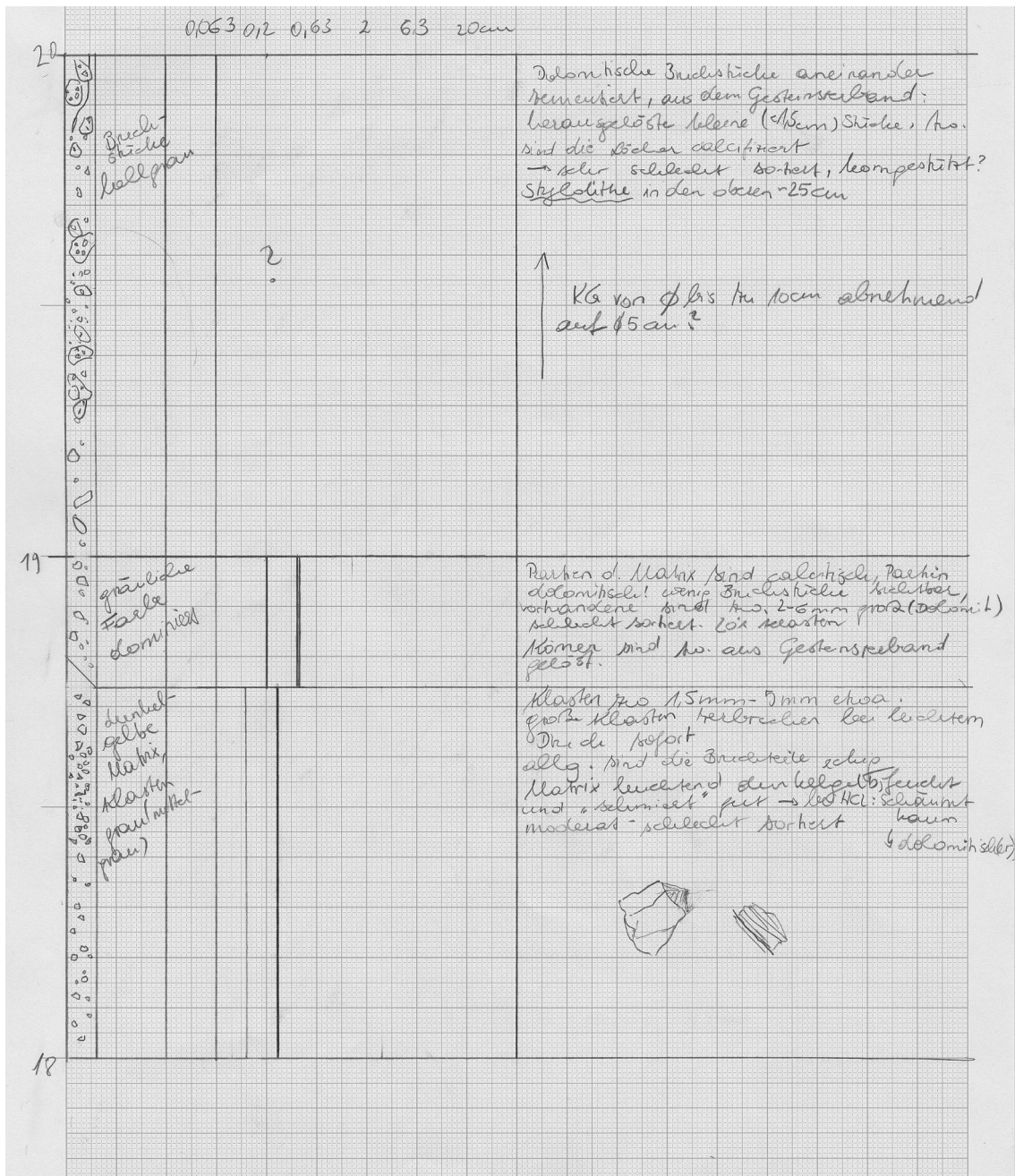


Figure A.3 – Borelog of meters 18-20 from the drilling RKB-SFK1m.

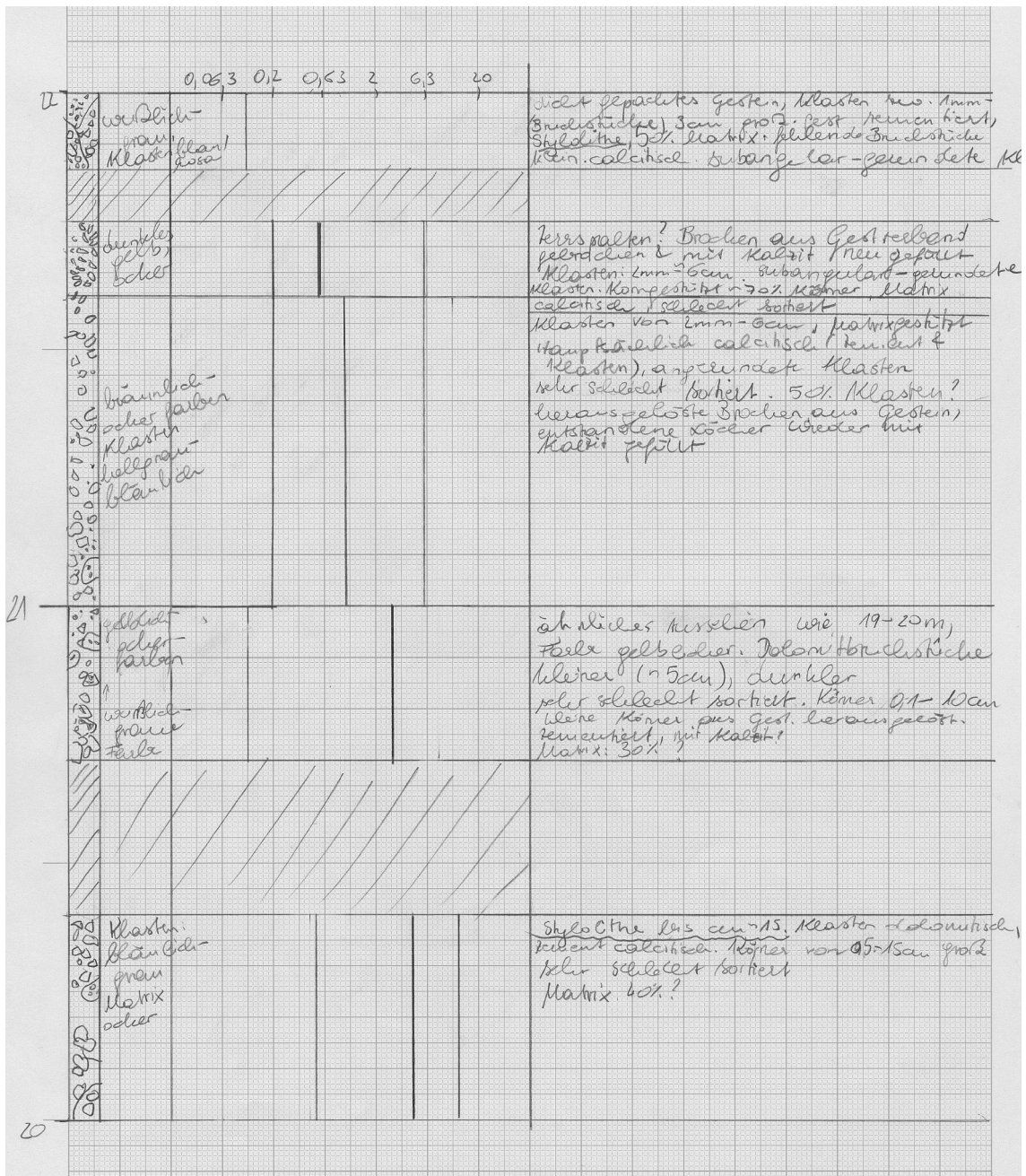


Figure A.4 – Borelog of meters 20-22 from the drilling RKB-SFK1m.

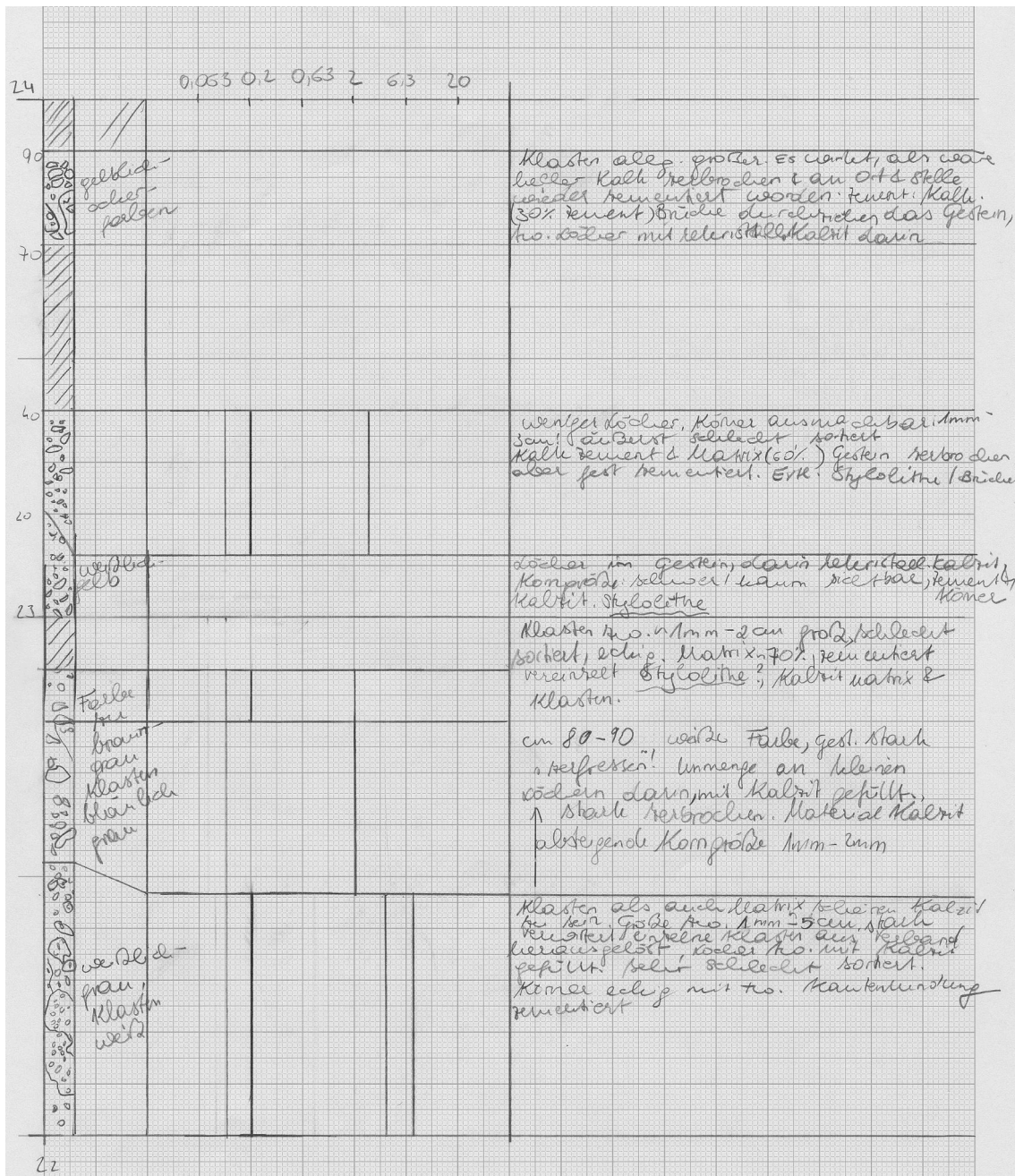


Figure A.5 – Borelog of meters 22-24 from the drilling RKB-SFK1m.

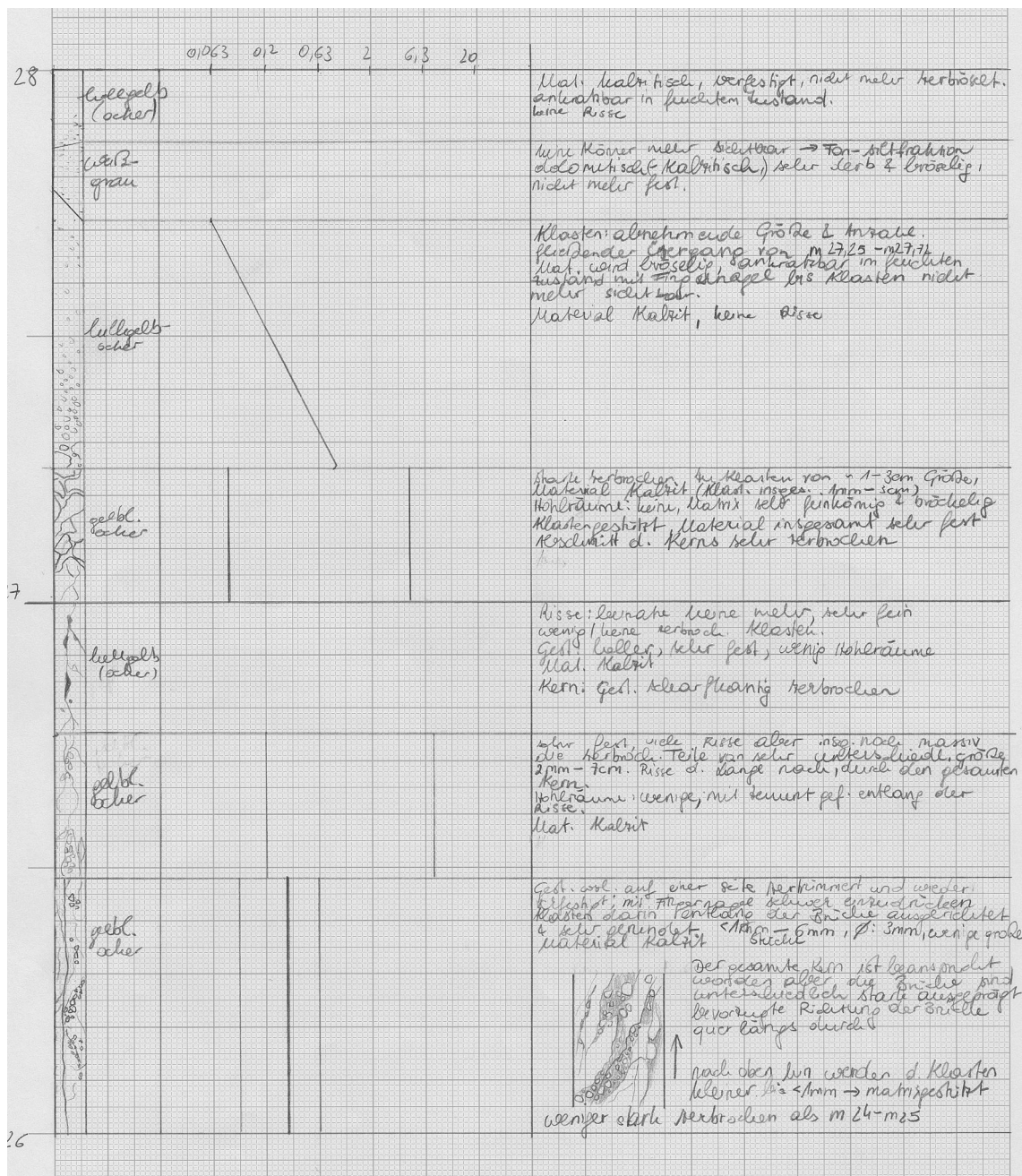


Figure A.7 – Borelog of meters 26-28 from the drilling RKB-SFK1m.

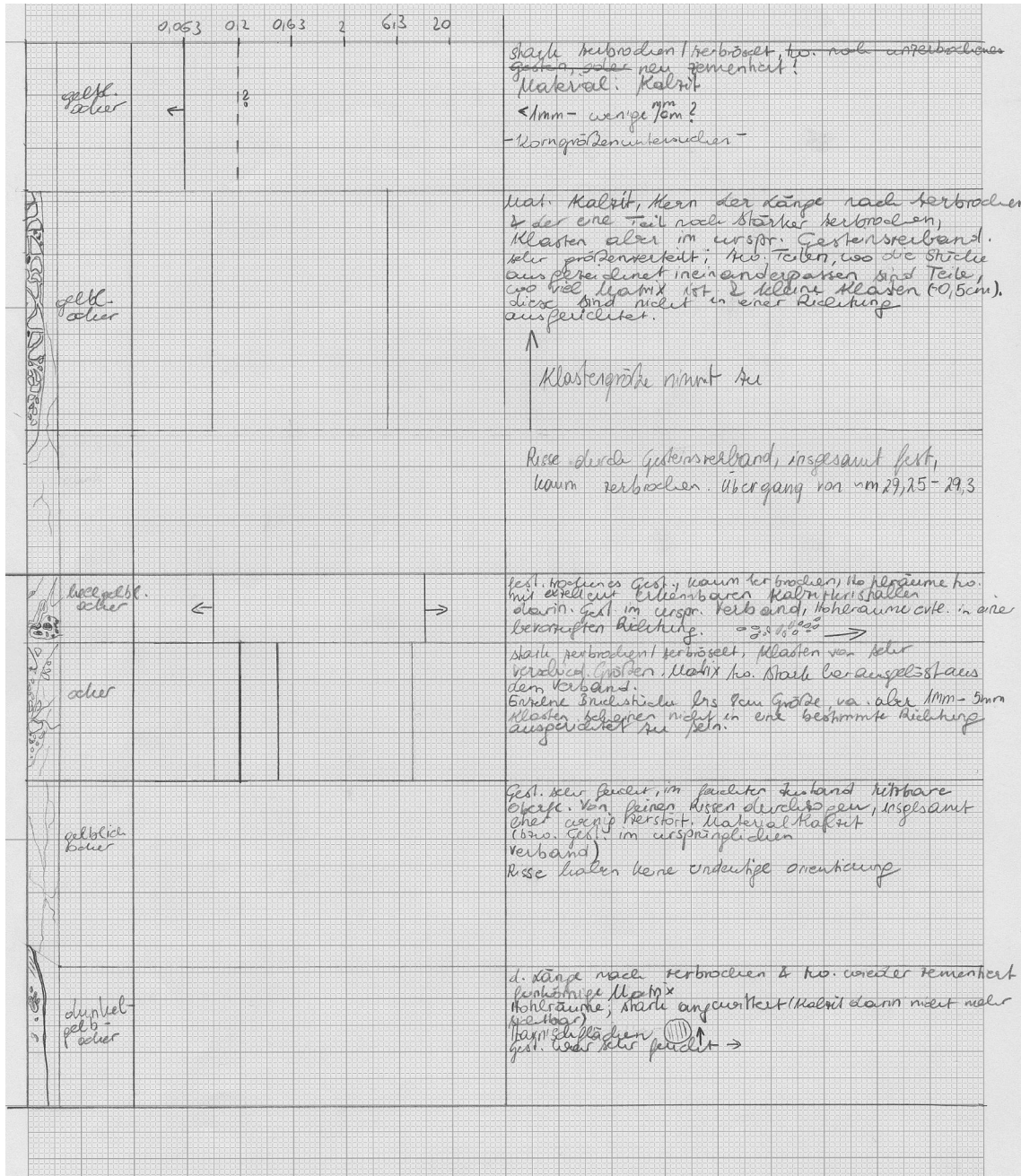


Figure A.8 – Borelog of meters 28-30 from the drilling RKB-SFK1m.

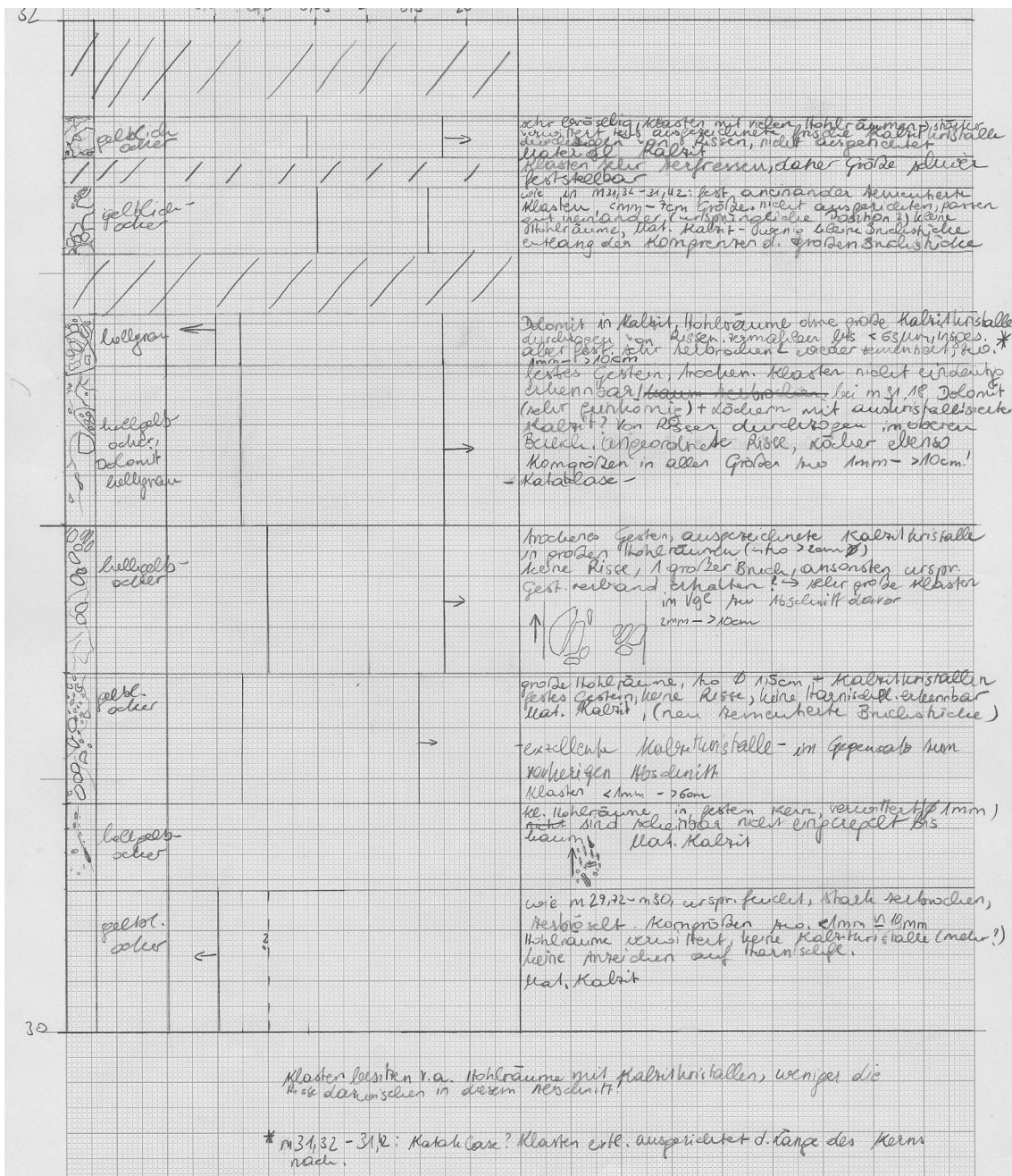


Figure A.9 – Borelog of meters 30-32 from the drilling RKB-SFK1m.

Appendix B

Drillcores

Photographs of the drillcores m14-30.



Figure B.1 – Drillcores m14-20. The samples are relatively wet, ochre coloured and heavily fractured. One can see tectonic breccias as well as "cellular breccias" (m19-20).



Figure B.2 – Drillcores m20-26. Of great interest were the cellular breccias. The rocks are intensely weathered and show many open cells. Denser parts were referred to as carbonatic fault breccia. From m24-25, one can see a fracture containing fine-grained matrix and carbonatic clasts.



Figure B.3 – Drillcores m26-30. Pressure solution overprinted the shapes of former fault breccia clasts (m26-27). In the cavern plan, these rocks are referred to as dolostone, dolostone-marble and dolostone breccia. Microscopic analysis revealed, that the main mass of the rocks indeed is calcite, with only little amounts of dol rock-flour as constituents.